Moisture measurements in concrete and characterization using impedance spectroscopy and RC network circuits

Theophanis Theophanous

Dissertation submitted to the faculty of the Virginia Polytechnic Institute and State University in partial fulfillment of the requirements for the degree of

Doctor of Philosophy
In
Engineering Science and Mechanics

Jack J. Lesko (Chair)
Scott W. Case
Carin L. Roberts-Wollmann
Muhammad R Hajj
Scott L Hendricks

May 20, 2008
Blacksburg, Virginia

Keywords: Cement, concrete, Moisture transport, moisture sensor, Impedance spectroscopy, Dielectric constant, Random R-C networks

Moisture measurements in concrete and characterization using impedance spectroscopy and RC network circuits

Theophanis Theophanous

ABSTRACT

The importance of moisture in concrete is unquestionable. However, quantifying the moisture in concrete is very difficult as concrete microstructure water interactions are not well understood. Concrete is a very complex material spanning the range from the atom to the civil infrastructure. It is the medium that controls moisture at the FRP/concrete interface. Concrete is also a composite material at the level of concrete/rebar, aggregate/sand/cement paste and at the hydration product level.

Water is vital in concrete microstructure development, properties and concrete durability. A moisture sensor based on the dielectric and resistive properties of cement paste was developed. Impedance spectroscopy techniques are used to explore the moisture behavior in relation to dielectric and resistive properties of the sensors. The sensor capacitive response is frequency dependent and it has been described with a multi-linear curve. Resistance values are related to capacitance through a power Law. Both the capacitance/moisture and capacitance/resistance behaviors were observed in all four cement/sand/aggregate mixtures considered.

Although the dielectric constants of water and dry cement paste are not frequency dependent with in the 400 kHz and 10 MHz frequencies considered, the effective dielectric constant of the mixture is frequency dependent
Mixing rules cannot predict the effective dielectric constant of the dielectric medium used in the sensors. Impedance analysis indicated also multiple time constants exist within the cement paste. Using the observation from the experimental results in conjunction to the high conductivity of cement pore solution a random R-C network model was developed to explore the impedance behavior of cement paste.

Acknowledgments

The names below are just a short list of people that participated either directly or indirectly in this work. Each person helped me in their own way to complete this endeavor and lifelong dream and I extend my deepest gratitude to them. The list is not meant to be complete.

Jack and Holly Lesko, Verónica Arroyave, Stephen Ross, Ian Doran, Susie Frasca, Mac McCord, Beverly Williams, Demetris and Yannoulla Theophanous, Maria Theophanous, Costas Theophanous, Rosanne Stoops, Lewis R. Nichols, Heather Switzer, Demetris Georgiou, Loretta Tickle, MRG Group, ESM Staff.

Contents

All images (including graphs and photographs) are the property of the author and were created between January of 2003 and June of 2007

List of Figures

List of Tables

List of Equations

Note to the reader:

Chapters 2 through 4 are written as separate journal papers that will be submitted to an academic journal as noted at the beginning of each chapter.

Chapter 1

Review of Concrete and Fiber Reinforced Polymer reinforcement degradation due to moisture and methods for quantifying moisture in concrete

1.1 Introduction

Moisture in concrete is intricately related to concrete properties and microstructure. The microstructure and chemistry of concrete have an effect on the life of the reinforcement. As a first step, the degradation of FRPs will be explored followed by that of concrete. Both are related to moisture either directly or indirectly.

To understand how moisture affects concrete and FRPs concrete microstructure and properties are investigated next. This will lead to moisture transport which is controlled partially by concrete microstructure. Along with water other elements are migrating in and out of concrete. The presence of water aids not only the transport but also facilities chemical reactions to occur. Modeling of concrete microstructure is considered next to shed some light on the complexity of cement paste. Models are either mimicking the microstructure and/or the behavior of concrete.

Besides modeling, other techniques exist to explore concrete behavior. Electrochemical Impedance Spectroscopy (EIS) or Impedance Spectroscopy (IS) is one such method used in this work to map the response of cement to a sinusoidal signal.

Following IS basics, the main methods to measure moisture will be considered with focus on their applicability in measuring moisture in concrete. Some of the methods have been adapted specifically for concrete but as it will be shown, none of the methods reviewed can perform adequately in the field. The method proposed in this study to measure moisture (i.e. sensor) will be explained and demonstrated next.

The sensor, construction, testing and response are presented. Experimental results will be shown within the IS frame, in addition to the response of the sensors with respect to moisture. Long term monitoring of sensors embedded in

a concrete block are also included. Modeling based or R-C networks and basic principles follows the experimental results in an effort to understand the fundamentals behind the IS behavior of cement paste.

1.2 Degradation of Fiber Reinforced Polymer (FRP) Reinforcement and Degradation of Concrete

1.2.1 FRP degradation due to moisture and alkaline environment

Glass fibers are affected by the alkaline concrete environment. Some protection is offered by the resin; however, this protection is short lived since resins absorb water and consequently the alkaline pore water will reach the fibers. Additionally, water plasticizes, hydrolyzes and degrades polyester and vinyl ester resins over time leading to further degradation of the FRP reinforcement.
Benmokrane et al., studied the creep behavior of FRP reinforcing bars submerged in various alkali environments including simulated pore solution and cast in concrete. Some of the findings include reduction in tensile strength of approximately 15% for one type of rebars. The FRP was immersed in a simulated pore solution and loaded to 30% Ultimate Tensile Strength (UTS). The reduction in strength was recorded at 90 days from the initial loading.

Chen, Davalos and Ray conditioned and tested FRP bars in ordinary cement and high performance cement simulated pore solutions following ASTM D3916-94. Their results showed lower tensile strength, especially on samples conditioned at higher temperatures [1]. Similarly, Tannous and Saadatmanesh examined alkaline resistant glass fiber reinforced polymer (GFRP) conditioned in water, alkaline and acidic environments. Lower strengths between 10% and 30% approximately have been recorded for bars conditioned in the alkaline environments [2].

Bhise tested rebars incased in cement mortar paste and conditioned in a calcium hydroxide at 30°, 45° and 57° C. The solution pH wa s between 8.5 and 9.0. After

180 days, strength loss of approximately 25% was recorded for bars conditioned at 30°and 45°C. Bhise compared his results with t hose of Dejke indicating similar trends [3].

Dejke tested four different FRP rebars conditioned in water, alkaline solution and cast in concrete at 20°, 40°, 60°and 80°C [4]. In all cases, strength degradation was observed. Modulus was also affected; however, in some cases the modulus increased and in some cases decreased.

In another study by Almusallam and Al-Salloum, beams were cast and conditioned in tap water, sea water and wet/dry sea water conditions [5]. The test plan included unloaded and loaded beams in a four point bending configuration to about 25% of ultimate tensile strength (UTS) of the FRP reinforcement used to prepare the specimens. These tests were accelerated by keeping the baths at 40°C. Test results after eight months of exposure indicated reduction in strength of 22% for unstressed wet/dry sea water conditioning. Higher strength reductions were observed in all samples loaded during the conditioning period.

Karbhari et al. investigated the effects of de-ionized water and high alkaline solution obtained by submerging concrete blocks or cement extract in de-ionized water [6]. Composite samples of E-glass/Vinyl Easter resin were manufactured and tested after exposure to the solutions for various lengths of time. A significant drop in tensile strength was observed in all samples exposed to the solutions. A smaller reduction in strength was recorded for samples conditioned in de -ionized water.

Vinyl ester resin samples and glass composites conditioned at room temperature, 20°C, and at 60°C in water, saturate d sodium chloride (NaCl) solution, 5 Molar sodium hydroxide NaOH and 1 M hydrochloric acid (HCl) were tested by Kajorncheappunngam [7]. The results of neat resin indicated small changes in strength and modulus. However, the changes in the composites were more significant with strength reductions after five months of 25% and 28% for

samples conditioned at 20°C in NaOH and water respectively. In addition, it should be pointed out that strength reductions were not monotonically increasing or decreasing. For example, samples in distilled water gain about 0.85% strength at the end of the first month. The samples in NaCl gain strength (about 3%) after five months, while samples tested at one month retain 93% of unconditioned material strength. The increase in strength was attributed to further curing of the resin. Strain to failure was lower for all tests ranging from a fraction of 1% and up to 28% of control sample's strain to failure.

Chu, et al compared strength degradation of pultruted E-glass/ Vinyl ester composites. The samples were conditioned in de-ionized water and in an alkaline solution having a pH of 11.5.[8]. Approximately a 2:1 ratio of $CaCO_3$ and $Ca(OH)_2$ was used to form the alkaline solution. After 75 weeks at 23°C, the residual tensile strengths dropped to 58.2% and 65.2% for samples in alkaline solution and water exposure respectively. The authors also evaluated the effect of drying the samples after exposure in the solutions. Strength increased by 62.3 % for water conditioned samples and 15% for alkaline solution conditioned samples. Tests were also conducted at higher temperatures indicating worse degradation after submersion and lower percentage strength regain after drying the sample. As noted, the level of exposure to moisture in many applications is not constant and evaluating materials on full submersion in a solution may be inaccurate.

Research has shown that FRP reinforcement is vulnerable to water and solutions similar to the concrete pore solution. Strength reductions of FRP conditioned in solutions have been reported by many scientists as shown above. In most cases, accelerated testing was incorporated by conditioning samples in solutions and by elevating temperatures. There are two concerns regarding the accelerated testing. The first is regarding elevated temperature testing and the translation to expected life span. Purnell, in his work on the interpretation of accelerated testing using elevated temperatures, indicates that using typical time-temperature superposition for estimating long life span may give inaccurate predictions due to the difference between average and equivalent service temperatures [9].The

second concern is that the actual moisture level is not known at the vicinity of the reinforcement and submersion in solution may not be representative of actual conditions. Clearly, concrete in hot and dry climates is not likely to be saturated. Andrade measured relative humidity in concrete samples using a hygrometer [10]. The method used is similar to ASTM 2170 which calls for constant temperature for 48 hours before testing [11]. Readings may be inaccurate given that the condition of constant temperature was not met; however the readings do provide an indication of the range of the moisture in the interior of concrete. Relative humidity (RH) between 30 and 100% has been recorded.

1.2.2 Concrete Deterioration Mechanisms

Once concrete is exposed to the elements, deterioration begins. For instance, the two main hydration products, calcium silicate hydrate and especially calcium hydrate, will partially dissolve in water and thus potentially degrade concrete microstructure. This degradation is more pronounced at the surface, and it will change the porosity and permeability of the concrete. Carbonation is another form of deterioration that usually starts at the surface. Carbon dioxide found in the atmosphere penetrates concrete and combines with calcium hydroxide and water to form carbonic acid. This acid etches the concrete by reacting with calcium hydroxide. In reality, any acid will affect concrete including organic and inorganic acids. Water can be considered a very weak acid for concrete. The most common acids that affect concrete are organically formed by microorganisms and degrading vegetation. Acid rain in heavily industrial areas is another source.

Water trapped in cavities contains dissolved ions, especially in the form of calcium hydroxide, which helps to keep the alkalinity (pH) of concrete between 10 and 14. This environment is favorable for steel reinforcement as it creates a passive layer on the reinforcement which prevents further oxidation and is crucial for concrete durability. Reduction in alkalinity will cause the reinforcement to oxidize, expand, and eventually cause the concrete to crack. Steel corrosion

products occupy larger volume than the original un-corroded steel. The increased volume creates tensile stresses in the concrete causing cracks. In the case of FRP reinforcement, the effect of alkalinity levels are not well established since water (lower alkalinity than pore solution) and pore solution have been shown to be damaging to FRP [6, 7].

Similarly, there are other expansive chemical reactions that involve water and will cause tensile stresses. For example, Ferraris et al monitored the expansion of mortars specifically mixed to cause alkali silica reaction [12]. Stress monitoring on confined samples indicates that the tensile strength of the samples was exceeded and thus caused crack formation. The cracks, regardless of origin, become an easy path for water to move which, in turn, accelerates the deterioration. Freeze-thaw cycling either enlarges or creates new microcracks thus creating an easy path for water migration [13].

Many of these deterioration mechanisms take years to occur in properly mixed and cured concrete. Early detection may be a preventative measure to thwart further deterioration. Most deterioration mechanisms (carbonation, expansive reactions, corrosion, etc) require the presence of moisture or the presence of water to accelerate the degradation.

1.3 Concrete properties and characteristics

1.3.1 Concrete Microstructure and Macrostructure

Once water is added to cement /sand /aggregate mixture, hydration starts. Concrete will start to set a few hours after mixing and will gain most of its strength in a few weeks/months depending on the concrete ingredients and cement type. A common measure for concrete is to evaluate the strength at 1, 7, 14 and 28 days with the assumption that at 28 days ordinary Portland cement concrete will typically gain most of it strength [14]. Concrete that contains any

other cementing materials like fly ash and blast furnace slag may take longer to gain strength. It is has been demonstrated that the microstructure evolution will continue past the first month [15, 16]. As the cement hydrates, the microstructure is refined with smaller size crystals that fill pores once occupied by water. Clark, et al, used X-rays to capture the hydration and refinement process in the first 48 hours after mixing [17]. Water trapped in the pores helps the hydration of cement particles to continue. It should be noted that particles of cement may be away from trapped water and may take a long time to fully hydrate. Generally, the filling of pores reduces porosity and permeability. Drying shrinkage has an opposite effect since it causes micro-cracks to form. The degree of this effect depends greatly on the curing conditions. Since most concrete construction occurs outdoors, it is not always possible to have optimum conditions for curing. Mouret, et al. prepared concrete mixtures at 20° C and 50° C [18]. The microstructure was studied using Scanning Electron Microscope (SEM) and Environmental SEM (ESME). Higher porosity and ettringite formation was observed at the cement paste aggregate interface for samples having a higher temperature at mixing. Similar microstructure features were observed on samples cured at 35° C compared to samples cured at 20° C.

A review of the standards for cements and aggregates used in concrete reveals that the proportions of compounds allowed varies considerably. For instance, ASTM C 150 covering Type I and Type II cement powder compositions suggests minimum and maximum content of various compounds and oxides [19]. As an example, Type II may contain up to 6% Aluminium oxide (Al_2O_3), up to 6% Ferric Oxide (Fe_2O_3), and Magnesium Oxide (MgO). Thus, cement powder can vary significantly depending on the source of the raw materials and processing. The products of hydration depend directly on the cement powder composition, and concrete microstructure depends greatly on the hydration products and curing time. The composition variations of cement powder may not have a significant effect on strength, but it affects the microstructure and chemical reactions. The addition of fly ash, blast furnace slag, silica fume and affect the microstructure morphology and development. Jiang and Guan investigated porosity of pastes

derived from various cement/fly ash mixtures [15]. Additionally, different water/(cement+fly ash) ratios were used. Compression tests of samples with ages up to 90 days indicated that pastes with fly ash had higher porosities. In all samples, porosity decreased with curing time. Kjellsen and Atlassi found a more uniform microstructure on pastes with 10% silica fume while containing hollow-shell pores [20].

The proportions of water to cement or water/cement (w/c) ratio is perhaps the most important factor in determining the microstructure of the final product. Lower w/c ratio will produce concrete with higher density and lower porosity. In general, concrete mixtures with low w/c ratio will have higher strength and lower permeability. Work by Roy and Gouda found that by forming samples under pressure, i.e., having very low porosities strength, could be improved significantly [14]. Strengths in excess of 80 kips were measured for porosities values in the 2%-3% range.

From the stoichiometric calculation for type I cement, a w/c ration of 0.36 is required to fully hydrate cement powder (pp 82-83) [21]. In practice, a slightly higher water amount is required to achieve full hydration unless admixtures[1] are used to aid hydration. Other types of cement powder or mixtures with other cementing materials will have different water requirements. For example, silica fume usually increases the required water due to its small particle size which requires more water to wet the increased surface. Silica fume used by Zhao, et al. in their work on concrete permeability had a specific surface area of 190000 cm^2/g while cement and fly ash were measured at 3794 and 5853 cm^2/g respectively [22]. Excess water that does not chemically react with cementing materials will either escape or will be confined within concrete's pore network. The volume occupied by excess water becomes part of the void system of cured concrete. Microcracks or capillaries become escape routes for water and add to any voids formed due to dry shrinkage.

[1] Admixtures are used to mainly to change water to cement ratio, extent or accelerate cure, entrap air and increase workability. Numerous types of admixtures exist in the industry and terminology varies by manufacturer.

Several chemical admixtures exist to lower the w/c ratio required, and to entrap air or change workability and set time. The first two categories of admixtures have the most significant effect on the microstructure. In the case of water reducers, a more uniform microstructure is achieved resulting in lower permeability and higher compressive strengths [21]. Air entrainment agents will, in general, increase the porosity but not necessarily the permeability. The air voids created are mostly closed, thus do not contribute significantly to permeability. Although w/c ratio is defined on a global scale, it is not constant throughout a concrete mixture. Locally, the w/c ratio can be higher or lower, and this affects the microstructure locally. This variability is very pronounced at the aggregate and rebar surface where, due to the wall effect, a higher water to cement ratio exists [23].

The higher w/c ratio produces locally a layer of cement paste with higher porosity and permeability. This layer is termed Interfacial Transition Zone (ITZ), or simply, Transition Zone (TZ), and it could be as much as 40% of the hydrated cement paste [21]. In the ITZ, cement hydration is usually completed at higher percentage than in the bulk paste. Scivener, et al studied the Interfacial Transition Zone (ITZ). Captured images of concrete impregnated with Wood's metal[2] clearly indicated the higher porosity at the paste aggregate interface [23]. In another study, Scivener and Nemati indicate that the ITZ is not a uniformly distributed or a very clearly defined zone [24]. As previously noted, the higher w/c ratio will result in increased permeability, and thus, the ITZ will be important in determining the overall permeability of concrete. A related and very important microstructure feature is the interconnectivity of the pores. Mercury intrusion porosimetry (MIP) measurements indicate that pores become interconnected at a w/c ration of approximately 0.6 water to cement for ordinary Portland cement [25].This may happen locally even if the overall w/c ration is below 0.6 as long as

[2] Woods metal is a low melding alloy (~65°C) with a pproximate composition of 50% bismuth, 25% lead, 12.5% tin and 12.5% cadmium.

the w/c ratio is above this threshold. This condition within the transition zone could become an easy path for water movement.

The hydration process is a chemical reaction where compounds in cement powder or in other cementing materials (e.g. fly ash) come in contact with water. The rate of the reaction is different for each compound and will affect the rate at which concrete strength develops as a consequence of microstructure refinement [15]. Also, the hydration rate affects crystal size and the proportion of hydration products formed. Crystals, at early hydration stages, are large, and they form a network of pores and interconnected cavities. As hydration continues, water trapped in the pores is consumed by the slower hydrating compounds or particles that did not hydrate due to lack of water at the early stages (e.g. isolated due to distance). The crystals formed in the later hydration stages are smaller in size and cause the densification of concrete. Generally, this results in lower porosity and permeability.

Temperature affects hydration. Hydration will slow down significantly at temperatures below 40°F (~ 5°C) and accelerate at higher temperatures [26]. The quality of concrete will be affected at high temperatures where the rate of water loss is high. The stoichiometric hydration reactions for cement are readily available. As mentioned by Mindess, et al. [21] and Lea [27], the actual hydration products vary and depend at least on the stage of hydration, temperature and w/c ratio. Calcium to silicate ratio (C/S) in calcium silicate hydrate (CSH) is between 1.5 and 2.0. Similarly alumina and iron oxide can occur interchangeably in the reaction of tetracalcium aluminoferrite. A possible conclusion one could draw from the above is that concrete macrostructure and consequently, strength, porosity and permeability, varies depending on location influenced by cement, sand, aggregate and water ratios. Other factors affecting the microstructure are curing conditions including temperature, loss of water during the first few days, and also availability of water during later stages of hydration.

1.3.2 Porosity

Porosity is a measure of the volume of the voids, cracks, and pores in relation to the total volume with an indication of distribution with respect to size. During hydration some of the pores will reduce in size or be eliminated completely. Also, salt deposits over the years may influence porosity and permeability while deterioration tends to increase porosity. These empty spaces are available to be occupied by water transporting dissolved ions or facilitating chemical reactions. As mentioned above, mercury intrusion porosimetry (MIP) is often employed to measure porosity [28, 29]. Gases have also been used with success; however, there is controversy as to which fluid gives the best results. For the mercury porosimetry, the pore size and distribution have been measured against the water to cement ratio. The porosity has been modeled using the Washburn equation:

$$P = \frac{\gamma * \sin(\theta)}{d} \qquad \text{Equation 1}$$

where *d* is the pore diameter, γ is the viscosity of the fluid used, and θ is the surface contact angle [30, 31].

Corrections to Equation 1 have been suggested to account for head differences, non spherical pores etc. [28, 32]. There are at least three issues with porosity measurements. The first is the contact angle which is difficult to measure in pores. Adolphs, et al. conditioned samples at various humidity levels and measured contact angles as a function of humidity [33]. For the particular Portland cement used, the contact angle was about 152° at ~ 0% relative humidity. Winslow and Liu measured a value of 116° degrees on the surface of oven dried samples [34]. This value has been used by Leech, et al. in their work on estimating water retention curves from MIP [30]. The second drawback for using MIP is the ink bottle (or bottle neck effect) [35] where two different measurements will be obtained if the fluid is flowing from a small pore to large one (1 to 2 direction) or vice versa (2 to 1 direction) as illustrated in Figure 1.

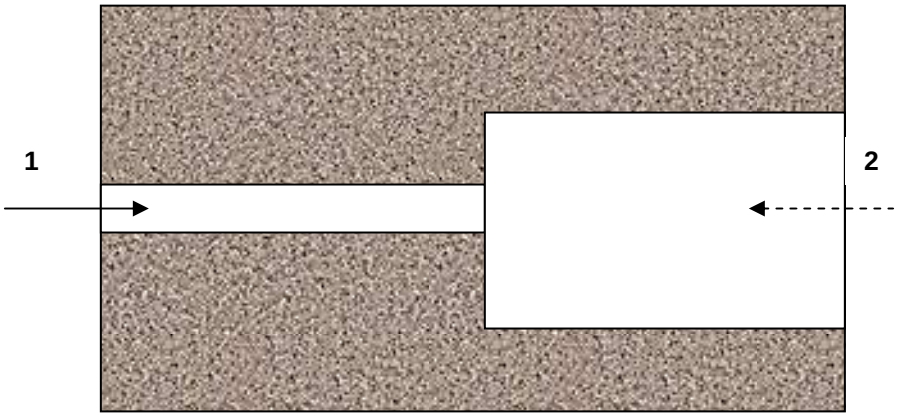

Figure 1. "Ink bottle neck" effect

To infiltrate small diameter pores, large pressure is required to force the fluids into the pores. There is evidence that thin wall pores can collapse, causing changes in the porosity measurements. Moreover, a number of pores may be isolated (closed pores) and will not be represented in the measurements. Diamond's work on MIP mentions numerous reasons why MIP is not the best method to measure porosity including pore geometry and ink bottle effect [35]. Beaudoin compared MIP with helium gas porosity measurements on different cement types [36]. The differences between the two methods are quite large and vary depending on porosity. A maximum difference of 162% was recorded. Clearly helium gas is able to penetrate smaller pores than mercury.

Since the presence of water will interfere with the porosity measurements, the samples must be conditioned by removing moisture before measuring porosity. Popular methods for drying samples include heating at or below 105°C, freeze-drying (sublimation), vacuum drying, and by solvent exchange. Galle measured porosity of cement paste samples and concrete samples dried at 60°C, 105°C, vacuumed and freeze dried [37]. Two different types of cement mixed at 0.3, 0.4 and 0.5 w/c ratios were studied. Porosities were measured with mercury intrusion porosimetry and by monitoring water loss of saturated specimens. Cumulative porosities indicate that the drying methods are not equal. Galle suggested that vacuum drying and heating at 60°C gave similar res ults and are probably less damaging to cement paste microstructure than heating to 105°C. Moukwa and

Atcin also observed that the behavior of samples was affected by the drying method adopted [38]. They dried samples at 105°C, vacuum, and by combination of heating to 105°C and sublimation. I t has been speculated that the CSH sheet-like structure may collapse once the moisture has been removed [39]. Such change will have an effect on the microstructure and consequently on the porosity measurements.

Porosity and mechanical strength are related. Usually, the lower the concrete porosity is, the higher the strength. Beaudoin, et al. analyzed some of the commonly used semi-empirical equations related to porosity and strength [40].

Porosity is not constant with time. As mentioned, concrete microstructure refines over time until hydration is completed resulting in lower porosity. Salts deposits and swelling caused by wetting of the pore surfaces will tend to block pores and capillaries. Degradation of concrete (e.g. carbonation, acid attack) with time will, in general, increase porosity.

Understanding porosity is vital in understanding moisture transport in concrete. This task is more difficult given that sample conditioning and methods used to obtain porosity may affect the measured porosity values obtained.

1.3.3 Permeability, Sorptivity

In measuring porosity, the fluids used have to permeate the microstructure and cannot be used to characterize the permeability of concrete. There are some experimental results indicating that at low w/c ratios, porosity, and permeability may be related. Experimental results by Powers [41] and Khan [26] show that a relationship between porosity and permeability may exist at low w/c. However, the results deviate considerably as the w/c ratio increases beyond 0.35. Permeability is a measure of the how easily a fluid will flow through a porous material. A high porosity concrete may have low permeability as long as the pores are isolated. This is the case for concretes made with air entrainment

agents, which form mostly closed voids. Interconnectivity (tortuosity) and geometry of the pores affect permeability of fluids in hardened cement paste (and in all porous materials in general). Tortuosity is a measure of the ratio of the distance between two points and the length of the actual path a fluid particle travels from one point to the other. The amounts of water, chlorides, carbon dioxide, etc. that will enter concrete highly depends on the permeability of concrete. Both aggregate and cement paste are porous and could provide a path for diffusion. In Power's classic work on cement paste, he has a table comparing porosity of natural stones to that of cement paste at different w/c ratios [41]. Permeability has been long recognized as an important parameter in concrete durability. As early as 1928, Banta and Renz evaluated various w/c ratios, binder/aggregate ratios, and curing conditions on the effect of permeability although w/c ratio used were far higher than the 0.3 to 0.5 commonly used today [42]. Darcy's law is usually used to calculate permeability. It relates the pressure difference between two points, the cross sectional area perpendicular to the flow direction, and the flow rate of the fluid through the permeability constant.

$$q = \frac{-k}{\mu} \nabla P \qquad \text{Equation 2}$$

Where q is the flux of fluid per unit area, k is the diffusivity, μ is the viscosity of the fluid and P is the pressure.

Since the sample must be fully saturated to apply Darcy's law, the diffusivity calculated only represents this particular state of the sample. Many of the concrete structures are not always saturated, and it has been demonstrated that the diffusion coefficient is a function of moisture attributed to chemical reactions and microstructure changes in concrete. Sorption used to characterize permeability of unsaturated cement pastes and concrete as water is absorbed or lost. Dried samples are subjected to one-dimensional moisture difference. Capillary action causes water to infiltrate the sample. One side is in contact with water while the opposite side is at a prescribed relative humidity. The sample weight is monitored to estimate water uptake. Based on Darcy's Law and flow

through cylindrical parallel capillaries, the following equation is used to calculate sorptivity [43, 44].

$$\frac{W}{A} = S\sqrt{t} + S_0 \qquad \text{Equation 3}$$

Where *W* is the weight of the water absorbed, A is the area of the sample exposed to the liquid water, *S* is the sorptivity, *So* is a correction for time zero and *t* is time.

Martys and Ferraris suggested a modified equation that could be used to fit data for two different mortars and two different concrete mixtures cured at various conditions [43]. They note that the equation proposed does not represent experimental data well at the very early stages of adsorption. Similarly, Lampacher and Blight observed different sorption rates at the initial stages of the experiment they conducted on samples obtained from 20 to 30 year old structures [45]. They calculated the thickness of the layer with higher sorption rate to be about 1 to 1.5 mm. They concluded that the higher sorption rate was due to the poor quality of the surface concrete when compared to the interior. Wilson, et al. attribute the initial irregularity in sorption rate to experimental errors like water absorbed from the sides of the sample [44].

Concrete porosity is a three dimensional network of various shapes, dimensions pores and microcracks. A more appropriate approach is to use the diffusion equation with a non constant diffusion coefficient. The diffusion coefficient is at least dependent on moisture and has been modeled using an exponential form [46] or a power law [47]. Nilsso demonstrated that the diffusion coefficient is highly dependent on moisture level for ordinary Portland cement [16]. In addition, after four years the permeability coefficient for the sample made with ordinary Portland cement continued to decrease. Diffusion coefficients of high performance concrete and concrete containing silica fume and/or fly ash were significantly less affected by moisture content.

Carmeliet, et al. used NMR in conjunction with desorption to calculate diffusivities for concrete sample [48]. Liquid dominant diffusion was observed at high moisture levels where the liquid phase is continuous. Once the liquid phase discontinues, the vapor diffusion role increases. At very low moisture levels, an increase in the diffusion observed was attributed mostly to diffusion of vapor.

1.3.4 Pore solution

It is generally accepted that concrete pore solution has a high alkalinity usually between 10 and 14 pH. Although simulated pore solutions have been used, there are questions regarding composition and alkalinity. Calcium hydroxide $Ca(OH)_2$, sodium hydroxide (NaOH), and potassium hydroxide (KOH) have been combined in different proportions to simulate the alkalinity of pore solutions in the rage of 9-14 pH. Chemical composition is more elusive than alkalinity given variation in cement composition, sand, and aggregate sources, and the use of other cementing materials (fly ash, blast furnace slag, silica fume etc).
Karbhari, et al. analyzed solutions obtained from new concrete, older concrete and cementitious extract using Inductively Coupled Plasma analysis (ICP). The solutions were derived by submerging concrete blocks or cement extract in deionized water [6]. The pH varied between 9.5 new concrete and 12.7 for old concrete in a sealed dessicator to avoid interaction with the atmosphere. Twenty three elements were traced. Significant differences were observed for calcium (3-256 ppm), potassium (45-4121 ppm), sodium (83-4331 ppm) and sulfur (1-208 ppm). This analysis clearly indicates the range of possibilities in simulating cement pore solution.

To avoid synthesizing pore solution, Bhise [3], Almusallam and Al-Salloum [5] Dekje [4] and Benkokrane, et al. [49] tested FRP samples encased in mortar or cast in beams. Samples were conditioned in solutions at room and at elevated temperatures.

Rasheeduzzafar, et al. extracted pore solution from plain concrete and concrete contain microsilica [50]. The pH varied from 12.8 to 13.5 while the amount of hydroxide ions (OH) is also reported. Similarly, Shehata, et al. analyzed pore solution obtained from OPC and cement/fly ash mixtures [51]. The study included 12 different types of fly ash based on chemical composition. Hydroxide ion concentrations decreased with time while the quantities varied widely between the different types of fly ash. Lower alkali and hydroxide ion concentrations were measured by Diamond in pore solution extracted from paste containing 30% micro silica with the concentrations obtained from ordinary cement pastes. Additionally pH increased from 13.1 to 13.8 in the case of ordinary cement but decreased in the case of micro silica/cement pastes (13.1 to 12.6) [52].

1.4 Moisture transport

Moisture can be transported through many different mechanisms including diffusion, adsorption and absorption. The rate of moisture propagation is highly dependent on concrete microstructure, temperature and difference in moisture between the boundary and the interior. Microcracks commonly found in concrete accelerate the moisture flow in and out of concrete. In addition, moisture diffuses through the concrete pore structure. Pressure differences will also aid the flow of moisture. A very good example of the latter is a foundation exposed to saturated soil with varying height of water level. Concrete will gain moisture at higher rate than losing moisture [10, 53]. This is very important given that short periods of dry boundary conditions will not affect the moisture content to the same degree as wetter boundary condition of the same length of time. The presence of liquid water on the concrete surface will also have a greater effect on moisture transport than vapor.

The size of the pore affects water infiltration greatly. Capillary action is used to evaluate sorption in cement and concrete pastes (permeability evaluation). Maekawa, et al. propose that adsorption contributes to water transport [39]. In other words, water vapors diffusing in the pores adhere to the pore surface to

form a single layer of water molecules. Vapor fills the pore until condensation occurs at pore openings followed by condensation in the pore. Once the pore is saturated, water will move to the next opening. This explanation assumes no chemical interaction between the water and cement paste.

Transport between concrete constituents can also occur. Pores or area with high porosity (for example ITZ) act as reservoir to supply moisture to the more difficult to permeate areas. In the drying phase, water will most likely escape first through the larger pores.

1.5 Transport of other elements

Moisture gradients are a mechanism for transporting dissolved elements in water to be transported into concrete. This transport mechanism is important when concrete is not saturated or when the exterior surface moisture changes with time. Higher moisture at the boundary will cause an influx of moisture. As the moisture diffuses into the interior, dissolved elements are transported. Concentration gradients will also cause fluctuations of particular compound/element in either water saturated or unsaturated concrete. An additional force that may cause ions to be transported is voltage potential. Voltage potential is used to accelerate chloride ion diffusion in chloride penetration tests [54]. Besides the deliberate application of a potential, voltage differences may be caused by corrosion or galvanic action.

Understanding ion transport mechanisms and their interaction is the topic of numerous studies [55-58]. Chloride permeation into concrete is one of the main causes of corrosion of steel reinforcement. Ponding and analysis for chloride content is a slow and destructive test. The rapid chloride permeability test-ASTM C1202, (also called the Coulomb or electrical resistance test) evaluates concrete by applying 60 volts across two opposing faces. One side is enclosed to 3% sodium chloride solution and the other side to 0.5 M sodium hydroxide solution [54]. Charge and conductance are monitored for 6 hours. Based on the results,

concrete is rated on a scale from high to low permeability for chlorides. The table below was re-created from ASTM 1202 [54]

Table 1. **Measured change in relation to permeation**

Chloride permeation	Charge (Coulombs)
High	>4000
Moderate	2000 to 4000
Low	1000 to 2000
Very Low	100 to 1000
Negligible	<100

Feldman, et al. used ASTM 1202 to explore the effects of w/c ratio and various binders with results indicating good correlation between charge and initial current and change and conductivity [59]. The samples were not analyzed for chloride content.

Using 1 Volt AC at 1 kHz, Zhao, et al. correlated conductivity measurements to those obtained using testing conforming to ASTM 1202 [22]. Samples included concrete made with cement in combination with one of four admixtures: fly ash, slag, silica fume and zeolite. The water to binder (w/b) ratio varied between 0.3 and 0.39.

McGrath and Hooton compared chloride diffusivity values using different DC potentials across the specimen [60]. In addition, they evaluated the possibility of calculating diffusivity values using the transient response to reduce the time required to run the tests. Transient condition values were influenced less by the amplitude of the applied voltage than steady state values. Diffusivity values increased with increasing voltage in the case of steady state diffusion.

Another proposed method to calculate chloride diffusivity was proposed by Streicher and Alexander [61]. A similar setup to the one used in ASTM 1202 is incorporated; however, a lower voltage (2 to 10 V DC) is used. In addition, the

same solution is used on both sides of the sample which has been dried and infused with the solution under vacuum. Streicher and Alexander state that the solution and the sample are in equilibrium with respect to chloride ion concentration. The ratio of the sample conductivity to that of the solution conductivity is equal to the ratio of ion diffusivity through the sample to ion diffusivity through the solution.
Ababneh, et al. developed a model to predict chloride ion diffusion in non saturated concrete [55]. Numerical results compared favorably with limited experimental data for concrete with 0.4 and 0.6 w/c ratios. The conclusion is that moisture diffusion will accelerate chloride intrusion.

Carbonation rate is diffusion and moisture dependent. Al-Khaiat and Fattuhi exposed specimens in a hot and dry climate [62]. Samples were manufactured using different cement types, w/c ratios, admixtures, and curing compounds. Samples were tested for carbonation at different time intervals with no significant change. After the 250th day, carbonation depth varied and values up to 14 mm were measured. As mentioned in the study, the carbonation rate is higher in concrete with relative humidity between 50% - 70 % and negligible below 30%. Perhaps the most important finding is that carbonation depth is higher for higher w/c ratio. This conclusion is corroborated with the general understanding that the higher the w/c ratio is, the higher the resulting porosity and permeability. In a study for samples having a 0.59 w/c ratio and conditioned indoors at 60% RH Parrott measured a carbonation depth of up to 18 mm [63]. The measurements were taken four years after curing.

Prediction of carbonation depth perpendicular to the exposed surface can be estimated by

$$h = k\sqrt{t} \qquad \text{Equation 4}$$

where h is the depth of the affected zone, k is the diffusion coefficient, and t is time.

This equation does not include any information on the chemical reactions that take place during the carbonation process.

1.6 Modeling of concrete behavior and microstructure

Numerous models exist that capture various aspects of the complex behavior of concrete. In assessing any model the reader has to keep in mind the numerous stages of cured concrete in addition to many variations of ingredients, age, microcracks and curing conditions. Models developed for fresh concrete must be able to capture the behavior of excess water, large continuous pores and relatively fast evolving microstructure. Once concrete sets, the mobility of water is limited while the microstructure keeps evolving over several weeks. In addition, different chemical reactions take place at different times during the early life of concrete. Once the structure is exposed to the environment it will be affected by moisture and temperature variations, freeze-thaw cycles, deicing agents, other chemicals, and carbonation etc. The effects on concrete can be localized on the exposed surfaces, varying with depth or initiated within the bulk of the concrete.

Packed regular shape particles are one common way to represent concrete microstructure. Another model is parallel tubes sometimes interconnected. Computers have helped in developing more realistic models that can be incorporated into simulations. For instance, Garboczi, et al. used a random growth model to study w/c ratio, porosity, and diffusivity, among other processes. [64]. Olson, et al. used a computer model that relates impedance spectroscopy behavior to microstructure features of cement paste [65]. Chloride penetration has been modeled using the diffusion equation as mentioned in the section on Transport of other elements. Holly, et al. used finite elements to solve the diffusion equation [66]. Some experimental data is required to obtain parameters used in the simulation. Solutions obtained from concrete that is 28 days old or less fit the experimental data well. Manwart and Hilfer used Monte Carlo methods to create the microstructure of random media [67]. Manwant, et al. reconstructed the microstructure of two sandstones (Berea and Fontainebleau) using stochastic

techniques [68]. The microstructure created was displayed side by side with actual pictures taken of the stones. Models of this nature could be adapted for concrete.

Navi and Pignat simulated hydration for cement and obtained porosity and pore radius distribution at different hydration periods [69]. This modeling did not depend on experimental data. As in many other case of modeling concrete microstructure and behavior, no comparison with experimental data was provided. Models always try to capture known features. Obtaining realistic models that mimic the microstructural behavior of concrete is challenging given its complexity and variability.

1.7 Measurements of moisture in concrete

Measuring moisture in concrete can be difficult given that the interior is not easily accessible and is harsh for sensors. Concrete moisture will change quickly on the surface, but it takes hours to days to get any appreciable change in the interior depending on thickness. In addition, microcracks and other defects can cause the moisture to differ locally from the bulk material for short periods of time. For example, a capillary may fill quickly with water during rain. The slow movement of moisture in concrete should be taken into account in selecting a method to measure moisture. Any method should be able to respond faster than the change in moisture and preferably not too fast as to allow moisture equilibrium at the point of interest.

Moisture measurements at any point will reflect the average value of the surrounding volume. A steep gradient may give the same moisture measurements with a negative gradient or a constant moisture level. To determine the actual moisture profile, either measurements at different locations/depths should be made or the profile should be theoretically calculated based on known boundary conditions and concrete properties. Relative humidity or moisture sensors are an attractive way to measure moisture, however, no

sensor has been found that can survive the harsh environment inside concrete. Use of sensors developed for other applications is possible but the life span of such sensors is short. The sensor will have to survive the high alkaline environment, deicing salts, freeze-thaw cycling and possibly mechanical loading. Nonetheless, RH sensors have been adapted and used in concrete. For example, Grasle, et al. encapsulated commercially available relative humidity sensors in Gore-Tex fabric and embedded the assembly in concrete [70]. A similar approach is been proposed in ASTM 2170-02 [11]. As discussed later, the creation of a cavity may lead to errors in estimating the moisture due to condensation when the temperature changes. An additional constraint is that some sensors need to be conditioned or become inoperable if exposed to liquid water. Conditioning is impossible for sensors embedded in concrete. The presence of liquid water is useful given that water will either be available for transport or to facilitate/participate in chemical reactions. Thus, it is preferable if the moisture sensing system can indicate the presence of liquid water. Additionally, the presence of liquid water may be an indication that the sensor is located on an easy path for water, e.g. a microcrack, and readings may not be indicative of the actual moisture within the concrete.

A very important element in measuring moisture in concrete is what is defined as ‘bound’ and ‘free water.’ Chemically bound water is an integral part of the cured cement paste and its removal can cause permanent changes in the microstructure. Additionally, bound water will not be part of any further chemical reactions. Free water is available for transport within the concrete microstructure or to participate in reactions like the creation of carbonic acid. Some authors define another form of water called “loosely bound water.” Water in this form is not chemically bound but it is attracted to the pore surface by Van der Waals' forces. The thickness of this water layer is assumed to be up to about 6 atoms thick or about 20 angstroms. The pore surface properties will affect the thickness of this layer and consequently the properties exhibited by the water in this layer. As mentioned above, the dielectric properties vary between free and chemically bound water with this layer. This variability is perhaps the most difficult to define

since the properties will vary with distance from the pore surface. Any moisture measurement in concrete should be able to distinguish free and bound water for the information to be useful in assessing the effect on fiber reinforced polymer rebars. As long as water is bound it is not expected to participate in chemical reactions, and it cannot be transported. The state of water is affected by temperature. For instance, the chemically bound water can be released given the input of appropriate energy to overcome the chemical bond. Similarly, water may shift from bound to free and vice versa as a result of temperature fluctuations.

An additional constraint with measuring moisture in concrete is that the dissolved ions in the water that could affect the sensing element and cause some of the properties of water to change. For example, it is well established that ions will lower the electrical resistance of water significantly. Temperature will also affect the amount or free and loosely bound water. Changes in temperature may temporarily shift water from the loosely bound state to the free state and vice versa. It should be noted that in concrete, temperature changes in a much shorter period of time than any significant moisture movement can take place. Also, moisture content will affect concrete's thermal properties and any change in temperature will affect the state of water and possibly cause moisture movement. Techniques to measure moisture in concrete have been introduced by many researches with various levels of success. Recently, ASTM 2170-02 was introduced as a way to measure moisture using relative humidity probes. A description of some of the methods proposed in the literature and used with some success is given briefly below.

1.7.1 Gravimetric: Direct way to measure moisture change

In the gravimetric method, samples are weighed and then dried and weighed again. The difference in weight is a measure of the moisture content. Clearly samples must be physically removed from a structure to perform this test. To improve accuracy, the samples have to be large since aggregates absorb very little moisture. An additional challenge is that the samples must be protected from losing or gaining moisture during removal transport and storing. There are

different methods of drying the samples including heating in an oven at 105°C and sometimes in a vacuum. The process is time consuming as samples may take days to reach a stable dry weight. The potential of changing the microstructure exists and must be taken into account if the sample will be used for further testing or analysis [37-39]. Bound water may be removed in the process, and it is difficult to assess the degree to which this has occurred. Also, repeated measurements at a site are not possible since samples are physically removed from the structure. This method is used in most cases to establish moisture content in a laboratory setting and has limited use in the field. It should be noted that the gravimetric method is the only method that measures the change in water content directly. It is the method of choice by many researches in correlating indirect moisture measurements to moisture content.

1.7.2 Resistance

Moisture presence in concrete affects the DC or AC resistance of the concrete/water system. The resistance can be measured with embedded probes or probes added to an existing structure. The system must be calibrated, and this may not be easy to do since the composition and cure state of concrete change over time. Rajabipour, et al. used resistance measurements to monitor the penetration depth of water successfully, although it was not possible to obtain quantitative results [71]. The DC resistance is more difficult to measure due to the polarization of the concrete/water system. A square pulse is commonly used to obtain the DC resistance. Polarization is avoided because of the alternating nature of the pulse while the current is monitored over the interval of constant voltage. AC resistance is measured in a similar way using a sinusoidal excitation source. In this case the current amplitude and phase difference with respect to the voltage is recorded. For purely resistive systems, the current and voltage will be in phase. Any capacitive or inductive effects will cause a phase shift other than zero unless the capacitive impedance is exactly equal to the inductive impedance. A RCL circuit model is used to calculate the resistive, capacitive, and inductive impedances. The complexity of the model varies depending on the behavior of the physical system. Additionally, the effect of ions found in the pore

water as their concentration changes depending on the age and environmental exposure of concrete must be considered. It is well known and can be easily demonstrated that dissolved ions reduce the resistance of water significantly. This process can be very pronounced when de-icing salts are used over the winter months in areas with cold climates. If the resistance measurements are to be used over a long period of time, there must be a way to measure how the system changes over time.

1.7.3 Capacitive

The same basic ideas applied to resistance measurements are used to infer moisture in concrete by measuring capacitance or the dielectric constant of the concrete water system [72]. Probes embedded in the cement paste are used as capacitor plates and the cement paste itself is the dielectric medium. Capacitance has similar drawbacks as the resistance method although it may be is less affected by chlorides and other element ions in the gel pores. The effect of salt solutions should be considered when using any sensors based on capacitive measurements. Concrete microstructure may change over time and any effect this might have on the measurements needs to be addressed before capacitance measurements are applied in concrete structure monitoring. The analysis to obtain the capacitance or dielectric constant follows the same procedure as in the case of AC resistance. It should be mentioned that capacitance measurements are the basis for many of the commercial relative humidity sensors found in instrumentation. Small hand-held, capacitive-based instruments are widely used to measure RH%. Thus the field of creating and measuring capacitive probes is well established and matured if one considers the large number of relative humidity instruments in the market. Capacitive moisture probes for soil also exist.

1.7.4 Hygrometer

Hygrometers have been used in Finland to measure moisture in concrete [73, 74]. Andrade, et al. also used a hygrometer to measure moisture close to reinforcement in samples. The ports for the hygrometer were drilled after curing.

The samples were cured for one year under controlled conditions before being exposed to moisture and heat variation for one year. Both temperature and humidity of the environment and within the samples were recorded [10].

As mentioned above, the basis for most of the hygrometer is a capacitive sensor. Vissala sells the HH44 systems to measure moisture in concrete slabs. ASTM 2170-02 covers the method of using probes placed in formed cavities in concrete slaps [11]. To measure moisture, a cavity is created by drilling a hole or forming the cavity during casting. A sleeve is secured to allow moisture exchange only at the open end of the sleeve facing the bottom of the hole. A RH probe is placed and sealed in the cavity to measure the relative humidity of the trapped air in equilibrium with the concrete. It is assumed that the cavity's relative humidity is at the same level as the moisture in concrete at the depth the sleeve was inserted. One requirement for the application of RH probes in cavities as proposed in ASTM 2170-02 is that the test article has to be at "service temperature and service relative humidity for at least 48 hours." This may be the single most important factor in limiting the extensive use of this method to measure moisture in the more vital parts of structures like foundations, exteriors of buildings, and bridge decks and columns. Another important limitation of RH probes is that usually they do not operate in 100% RH or liquid water.

1.7.5 Other Non destructive methods

Other non-destructive methods include X-ray, Magnetic Resonance Imaging [75], Gamma rays [76, 77] and microwaves [78]. Drawbacks in the field application of these methods include equipment expense, need for highly skilled personnel, and important safety issues. Additionally, it may be impractical to apply any of these methods to structures while occupied given the danger associated with some of the energy forms used. These methods could be employed in limited cases where cost is not a limiting factor, or to corroborate results obtained by other methods. Clearly it is not possible to dedicate this kind of equipment for testing large number of structures.

1.7.6 Surface moisture

There are methods that are used either to measure or register an indication of moisture mostly on the surface of concrete slabs. These include the anhydrous calcium chloride (ASTM F-1869-04) [79], polyethylene sheet and surface meters that rely on resistance or capacitance to infer moisture. Neither of these methods is exact and as mentioned, they are limited to surface measurements which may lead to false conclusions of the moisture in concrete. Commercial surface meters are used to assess moisture in concrete before the application of additional flooring. Moisture levels in concrete surfaces change very quickly and thus any of these methods to indicate moisture may only capture surface conditions.
A study by Roels, et al. comparing six methods to determine the moisture uptake and profile in building materials, has been conducted on two different materials: calcium silicate and ceramic brick [80]. The methods evaluated were Nuclei Magnetic Resonance (NMR), Magnetic Resonance Imaging (MRI), gamma-ray attenuation, capacitance, X-ray and Time Domain Reflectometry (TDR). On one hand, the results for calcium silicate sample were consistent. On the other hand, brick samples behavior varied between sample and results varied considerably between samples and methods.

It is clear from the discussion that concrete moisture measurement is deficient in accuracy and implementation. In summary, the main deficiencies are:

- Lack of reliable sensors that can operate under the harsh conditions found in concrete structures
- Limited measurements primarily of the surface, which can be grossly inaccurate in predicting the moisture at any depth beneath the surface
- Interference of the measurement technique (e.g. sleeves)
- Impracticality for field applications
- Destructive to the structure
- Costly, difficult to use, or unsafe

Based on the review of available methods to measure moisture, some criteria have been established to rate the usefulness of any method/system that may be considered. These requirements are very general and could apply to many different types of sensors or techniques. In this particular case, these requirements are the minimum for any method that would be employed to measure moisture in concrete. The criteria used in this study to assess the methods used to measure moisture in concrete are as follows:

- Robustness
- Field applicability
- Ease of use
- Inexpensive to acquire and implement
- Useful on both the surface and in depth
- Useful for testing both new and existing structures
- Universally applicable for any type of concrete

1.8 Sensor development

Capacitance and resistance have been used independently as a way to estimate moisture. In all cases, the resistive and dielectric medium is the concrete itself [71, 72, 81]. This approach, as explained above, poses at least two challenges that have not been addressed in studies reviewed:

1) the calibration which is needed to translated the measurements into moisture values
2) a way to observe changes in the concrete microstructure and composition that may affect the relation between measurements and calculated moisture.

In addition, the effect of deicing salts and ions on resistance and capacitance measurements has not been addressed to any significant effect. Hudec examined the possibility of detecting deicing salts using capacitance [72];

however, the results of the experiments conducted for this study did not show that possibility.

The use of capacitance and resistance measurements is simple and for this reason is very appealing. Either method can be incorporated using simple instrumentation at a relatively low cost. In most cases, these two methods have been used by planting metal probes in concrete, taking measurements of either resistance or capacitance and relating that to moisture. The difficulty with this technique is the unknown composition of the cement volume measured and the actual volume between the electrodes contributing to the measurements. Additionally, as cement cures the microstructure will change and possibly affect the relation between moisture and capacitance or resistance values.

To overcome the shortcoming of using capacitance and/or resistance measurements it was decided to prefabricate cement dielectric material that would be cured and characterized before it is utilized in measurements. This provides control over the size, composition and proper cure of the cement paste between the electrodes. To improve the quality and response the electrodes were combined within the cement paste which will henceforth be referred to as sensor. Details of the sensor geometry and material are given in chapter 2. Some preliminary results were obtained using small concrete blocks cut from concrete cylinders [82]. These results are included as the trends are very similar to those obtained from the sensors.

Thesis Statement

Dielectric and resistive properties of cement paste can be used as an indicator of moisture in concrete. Estimating moisture using the combination of resistance and capacitance values is a better alternative to resistance or capacitance as stand alone methods. In addition, if Impedance Spectroscopy is utilized to obtain resistance and capacitance values with respect to moisture changes, more information can be extracted that add to the understanding of concrete microstructure and moisture behavior.

Chapter 2

Capacitive Moisture Sensor development for concrete systems

Capacitive Moisture Sensor development for concrete systems

T. Theophanous, J.J. Lesko
MC 219, Virginia Polytechnic Institute and State University, Blacksburg, VA 24061, USA

Abstract

Moisture in concrete structures is important to concrete and reinforcement durability. Having a reasonable understanding of moisture levels and behavior will provide information as to how moisture is affecting concrete microstructure changes which control the behavior of concrete with respect to strength and durability. Reinforcement embedded in concrete is both protected and degraded by the concrete environment with moisture being potentially the most influential factor. Products of chemical reactions aid in the corrosion of steel reinforcement and degradation of fiber reinforced polymer rebars. Experimental data from moisture sensors developed is presented in this paper. The sensors are based on dielectric and resistive properties of cement paste.

This paper will be submitted to Cement and Concrete Research journal

2.1 Introduction

Degradation of concrete is often attributed to corrosion of the steel reinforcement. Corrosion products occupy a larger volume than the metal itself resulting in cracking of the concrete from the induced tension stresses [21]. The use of fiber reinforced polymer (FRP) rebars addresses the corrosion problem. Additionally, FRP weighs less than steel and is non-magnetic. FRP reinforcement offers superior corrosion resistance; however, it is still affected by moisture, the high alkalinity of concrete, and possibly by other elements present in concrete [1, 3, 49].

Knowledge of the immediate environment surrounding FRP reinforcements will aid the in understanding of the long term behavior of composite rebar. Both mechanical loading and environmental loading (temperature, moisture, etc.) are important in predicting expected life for structures. The concrete surrounding the reinforcement is responsible for transferring loads to and from the reinforcement, and it is also the medium through which moisture and ions reach the reinforcement.

Water is a vital component of concrete. Moisture exchange with the environment occurs continuously through the life of a concrete structure. The rate of moisture exchange is dependent on the difference in moisture between the concrete and the environment and the concrete microstructure which evolves over time [21, 27]. Water is present in concrete as part of the chemical compounds and also as water that can be transported. The presence of water aids the transport of other elements that could affect the concrete and FRP durability. Additionally, water facilitates hydration and chemical reactions that affect the boundary layer around the rebar. Understanding the behavior of water in concrete, and particularly in the vicinity close to the rebar, is vital in predicting the effects on the durability of the FRP.

From a review in chapter 1 of the current available methods to measure moisture in concrete, it is clear that none of the existing methods is suitable for long term moisture monitoring. Gravimetric is perhaps the most widely accepted method to obtain moisture in concrete. Clearly it is destructive and it cannot be used for continuous monitoring. The rest of the moisture monitoring methods reviewed can be divided into four categories. The first category includes X-ray, Magnetic Resonance Imaging [75], Gamma rays [76, 77] and microwaves [78] moisture measurements techniques. Safety to due to radiation exposure, applicability for long term monitoring, cost and accessibility to parts of the structures are some of the drawbacks of the first category. The second category covers methods used primarily to infer moisture in the interior by measurements made on the surface of a concrete member. The requirement for constant temperature for 48 hrs makes such methods inapplicable for field applications. In addition, moisture estimated from such methods reflects an average value of the volume influencing the test. The next category is on the use of relative humidity probes. A good description of the method can be found in ASTM 2170-02 [11]. Relative humidity sensors have been used on an experimental basis in a few cases [10, 73, 74, 83]. ASTM 2170-02 requires constant temperature for 48 hrs, sleeves must be installed to host the probe and liquid water makes most relative humidity probes inoperable. The last category is based on either resistance or capacitance variations of cement paste due to moisture change. As outlined in chapter 1 resistance and capacitance measurements have drawbacks with respect to ions, calibration and microstructure changes of concrete. However, such methods have a lot of potential as indicated by preliminary results published in an earlier paper [82]. Using cement paste as the sensing element has the advantage of being located anywhere within a concrete structure, is permeable to moisture, and is not affected by the presence of liquid water. In addition, properly mixed and cured concrete is durable and expected to last for years.

Using the principles of resistance and capacitance properties of concrete, a method to quantify moisture in concrete has been developed [82]. A parallel plate capacitor setup with concrete as the dielectric medium was used to relate

moisture content to capacitance measurements. The first generation sensors were developed based on the information obtained from the parallel plate setup. Results for both the parallel plate and 1st generation sensors are included in this paper for completeness. In the case of one dimensional diffusion, additional data is available presented here. The focus of this paper is the 2nd generation sensors which have the same geometry as the 1st generation but utilize different cement paste.

2.2 Stand alone, permeable and embeddable moisture sensor

The parallel plate capacitor set up was the base for the sensor development. The sensor can be shaped to different geometries all based on a central conductor surrounded by the second conductor. The dielectric medium can be cement paste or cement /sand mixture, and it is cast to the desired shape. The outer conductor plate was chosen to be non -solid allowing the moisture to enter the sensor faster. The design of this sensor allows for controlling the dimensions, shape, dielectric constant to a certain degree, response time. Most importantly, the sensor can be calibrated before being installed in either new or existing structures. Different sizes and shapes were manufactured using a variety of different electrodes and cement pastes. Pictures of sensors and electrodes are shown in Figure 2.

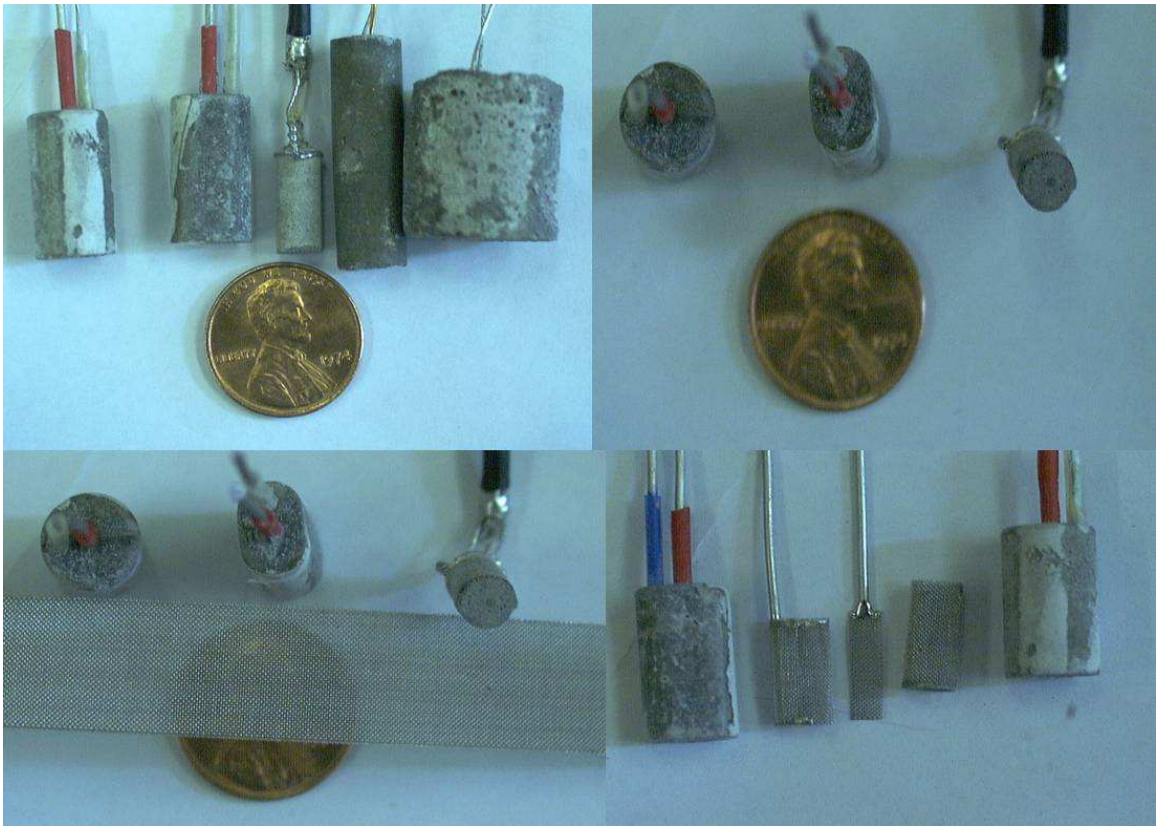

Figure 2. Sensors geometries and components

The sensors used in this study are concentric capacitors with cement paste as the dielectric medium. The outside electrode is made out of 304 stainless steel wire mesh while the central conductor is solid stainless steel wire. The conductors were held in place in a Teflon mold and cement paste was cast encapsulating the conductors as shown in Figure 3. The conductors outside the capacitive active area were insulated using shrink tubing. Each batch of materials was mixed by hand and the mold was fitted with hand held engraver acting as the vibrating source for consolidation. The nominal dimensions of the sensors are shown in Figure 4.

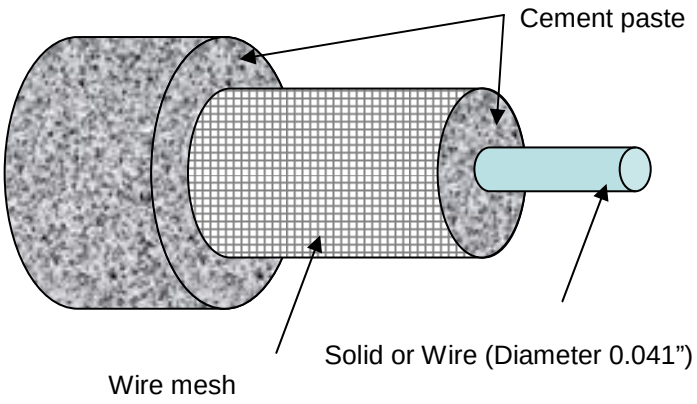

Figure 3. Sensor structure

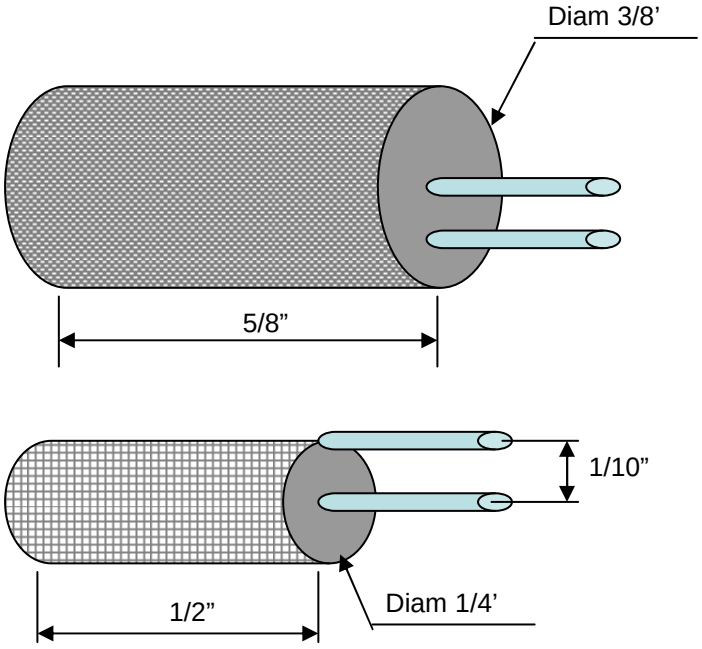

Figure 4. Sensor nominal dimensions

The first generation of sensors was produced and tested for a short period of time to obtain information on the vitality of such a device. The cement/sand mixture was obtained by sieving Quikrete Concrete Mix (No. 1101) dry mixture purchased in a retail store. The dimensions of these sensors conform to those given in Figure 3 and Figure 4. The actual water to cement ratio and the sand to cement ratio is unknown since the composition of the sieved mixture is unknown.

Using information from the first generation of sensors, a second generation was developed and produced. In this case, two grades of sand were used to produce sensors. Both sands contain a distributed size of grains up to the maximum allowed by the sieve used. Details including w/c ratios for each sensor family are given in Table 2. The abbreviation *ppv* refers to *parts per total volume.* Due to limited number of forms, six (6) sensors can be cast at a time. Seven different production days yielded 42 sensors. Fine and coarse sand are grading designations specific to this project.

The cement used was type II made by Roanoke Cement LLC (Troutville, VA). No other admixtures, plasticizers or water reducing agents were used. Both the sand and the cement were obtained from a retail store. A limited number of sensors have also been made with cement paste only. With the exception of values of capacitance at low moisture no other results will be presented regarding cement only sensors. In addition, results will be presented for families P1, P3 and P5 since there is not enough data to this point for all families.

Table 2. **Cement, sand and water rations**

Family name	Cement	Coarse Sand	Fine sand	Cement +sand volume	Water Volume	water/cement	water/cement
	(ppv)	(ppv)	(ppv)	(mL)	(mL)	volume ratio	Mass ratio
P1	1	2	-	n/a	n/a	1.00	0.32
P2	1	2	-	30	9	0.90	0.29
P3	1	2	-	30	10	1.00	0.32
P4	1	-	2	15	4.2	0.84	0.27
P5	1	-	2	16.5	5.6	1.02	0.33
P6	1	-	2	15	5	1.00	0.32
P7	1	-	2	15	5	1.00	0.32

2.2.1 The first generation sensors cure cycle

The first generation sensors were cured in the mold for approximately 24 hours and then transferred to a 100% RH condensing water environment. Testing started about a month after casting.

2.2.2 The second generation sensors cure cycle

After casting, the sensors were kept in the mold for approximately 24 hours enclosed in a polyethylene bag. In the bag, water saturated paper towels were included to keep the moisture environment to 100% RH. The sensors were removed from the mold and stored in polyethylene bags with saturated paper towels for a few weeks before they were transferred to a sealed container on a polyethylene mesh above the water line. Visual inspection of the container showed that the sensors were always wet with moisture condensation forming on them. The temperature was not monitored but the container was kept in the lab environment with temperature varying between 20° and 27° C. The sensors stayed in that environment until the testing phase was initiated. The first sensors were transferred 13 months after manufacturing to conditioning/test chambers.

2.3 Test setup

Figure 5 demonstrates the wire diagram of the experimental set up. The LCR meter used was an HP4275A computer controlled via GPIB and LabVIEW. The mass of the sensors was measured just after running the frequency sweep on a Mettler AE200 balance with 0.0001g resolution. A four (4) wire configuration between the sensors and the LCR was used. To facilitate the ease of transferring sensors to and from containers each sensor was fitted with a polyethylene plug. In addition, the use of plugs kept the disturbance to the environmental condition in the test chambers to a minimum (Figure 6). Saturated salt solutions were used to create different relative humidity environments as detailed in Table 3 [84, 85]. A double container was used to minimize crystal formation on the upper portion of the conditioning chamber housing the sensors. Each chamber could host between 12 and 20 sensors at a time and each sensor could be moved independently. The moisture was monitored using a Rotronic HT260R RH/Temperature meter and at a later stage an OMEGA CNiHT RH/Temperature meter was added to the monitoring system. The temperature was measured with

the above mentioned meters and also with a type K thermocouple. A test fixture was used with the concrete blocks.

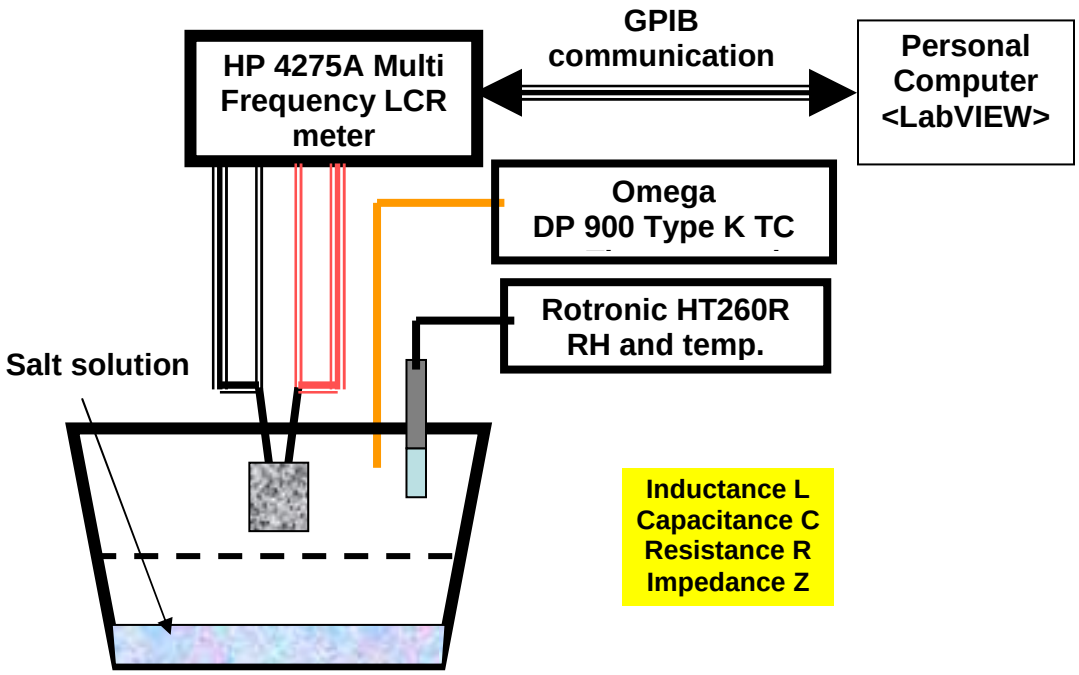

Figure 5. Test setup

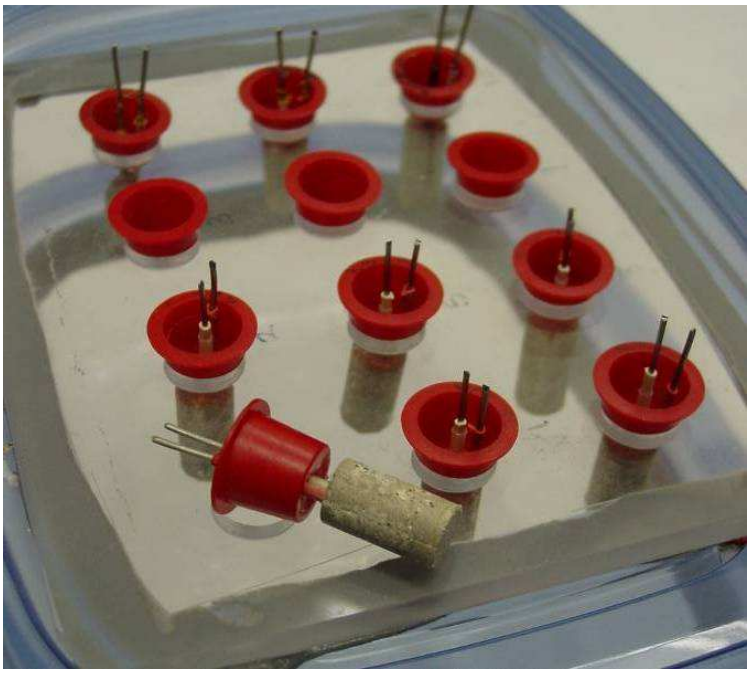

Figure 6. Sensors in controlled environment with polyethylene plugs

Table 3. **Salt solution and other humidity environments**

Salt or other environment		%RH at 15°C	%RH at 20°C	%RH at 25°C	%RH at 30°C
Water	H_2O	100	100	100	100
Sodium carbonate	Na_2CO_3	--	--	89.0	--
Potassium Chloride	KCl	85.9	85.1	84.3	83.6
Sodium Chloride	NaCl	75.6	75.5	75.3	75.1
Calcium nitrate	$Ca(NO_3)_2$	56	55.5	51.0	47.0
Zinc nitrate	$Zn(NO_3)_2$	--	42.0	48.0	--
Potassium carbonate	K_2CO_3	43.2	43.2	43.2	43.2
Calcium chloride	$CaCl_2$	35.0	32.5	31	--
Calcium sulfate	$CaSO_4$*	~2	~2	~2	~2

* Cobalt Chloride ($CoCl_2$) is used as an indicator for saturation of Calcium sulfate.

A LabVIEW program controlled the LCR meter to run through the following sequence of frequency and modes.

Start	→							
10 MHz	L(Q)	→	C(Q)	→	R(C)	→	Z(θ)	→
4 MHz	L(Q)	→	C(Q)	→	R(C)	→	Z(θ)	→
2 MHz	L(Q)	→	C(Q)	→	R(C)	→	Z(θ)	→
1 MHz	L(Q)	→	C(Q)	→	R(C)	→	Z(θ)	→
400 kHz	L(Q)	→	C(Q)	→	R(C)	→	Z(θ)	→
200 kHz	L(Q)	→	C(Q)	→	R(C)	→	Z(θ)	→
100 kHz	L(Q)	→	C(Q)	→	R(C)	→	Z(θ)	→
40 kHz	L(Q)	→	C(Q)	→	R(C)	→	Z(θ)	→
20 kHz	L(Q)	→	C(Q)	→	R(C)	→	Z(θ)	→
10 kHz	L(Q)	→	C(Q)	→	R(C)	→	Z(θ)	→
Stop								

The soak time at each mode (i.e. L, C, R and Z) was 15 seconds which means 60 seconds for each frequency. The parameters in parenthesis (*) indicate a secondary mode running simultaneously with the primary mode.
The data collected contained data for inductance (L), capacitance (C), resistance (R) and impedance (Z). In addition, quality factor (Q), and phase angle (θ)

information was recorded. Capacitance and resistance were the focus as hand held meters exist and could serve as monitors for the sensors in the future. Additionally, the LCR meter was set up to run in parallel mode meaning that a parallel capacitor/resistor model is used by the LCR meter for calculations.

The first generation sensors focused primarily on capacitance and resistance measurements. A shorter version of the sequence shown above was used for the parallel plate setup. Other adjustments to the test setup are explained in the experimental results section.

Before each set of tests, a base measurement was obtained using two solid wires identical to those used to form the connecting wires of the sensors. The two wires were fitted with a polyethylene plug and placed in the same environment as the sensors to be tested. This base line measurement was then subtracted from the test data as it reflects the effects from the wiring and test fixture. The connection between the instrument setup and the calibration wire or the sensors was made via a custom socket/pin arrangement.

As noted, the test environment temperature varied between 20° and 27° C during the period the sensors cured before testing began. The same temperature variations also existed for the period of the experiment.

2.4 Experimental results - parallel plate configuration[3]

Parallel plate capacitors were set up using cured concrete as the dielectric medium. The concrete blocks used (B1- B8) were wet cut on a diamond tile saw from cylinders cast to be tested for strength. No record of the actual composition existed other than the cylinders were stored in the laboratory for at least year. Nominal dimensions of the concrete block samples were 1 x 3/4 x1/2 inches.

[3] The work on the parallel plate capacitor was initiated with Stephen Ross in the summer of 2003. Stephen Ross (ESM undergraduate student) was participating in the Summer Undergraduate Research Program (SURP) at Virginia Tech.

Stainless steel ½ inch square plates were used as electrodes. The same electrodes were used for all concrete blocks.

The test set up regarding the fixture and configuration for the parallel plate capacitive measurements is shown in Figure 7. The data collected was only for capacitance and change in mass. Besides conditioning at room temperature, the blocks were also conditioned in ~ 5% RH at 50°C. C alibration of the test fixture was performed before each set of tests using air gap equal to the concrete block thickness. The relation between moisture and capacitance, fit to a bilinear curve, is shown in Figure 8 [82]. Moisture build-up under the plates was a point of concern as the measurements were affected at high relative humidity environments. In addition, there was no way to evaluate contact resistance and consequently the effect on capacitance at very low relative humidity. Although the data set is not extensive, it does illustrate the change in the trend between moisture and capacitance (bilinear) observed also with the sensors.

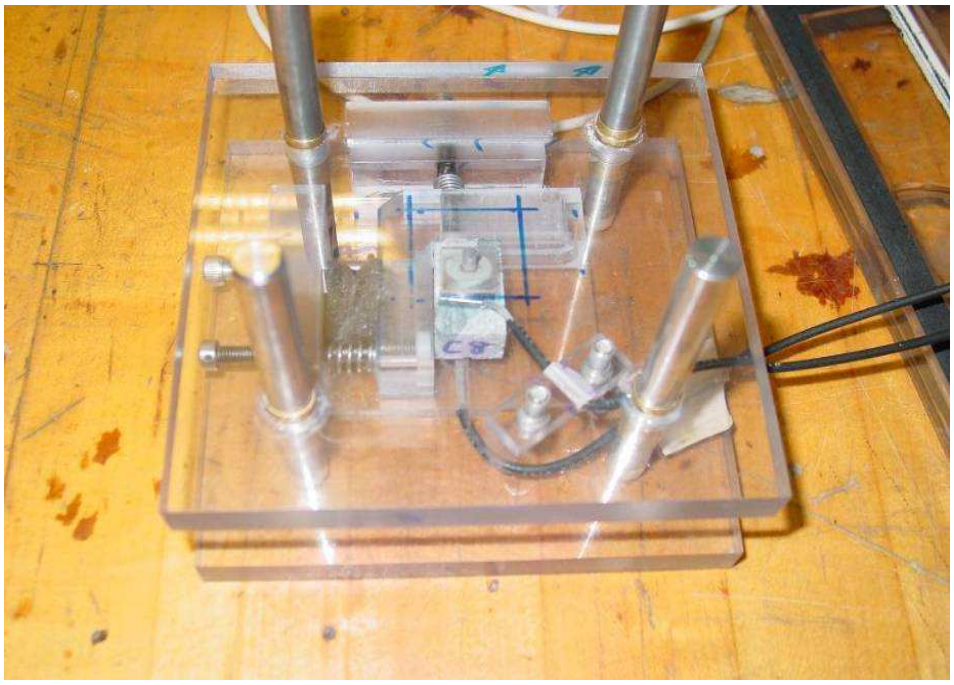

Figure 7. Test fixture with sample. The actual testing was performed in an enclosed controlled environment similar to the conditioning of the samples.

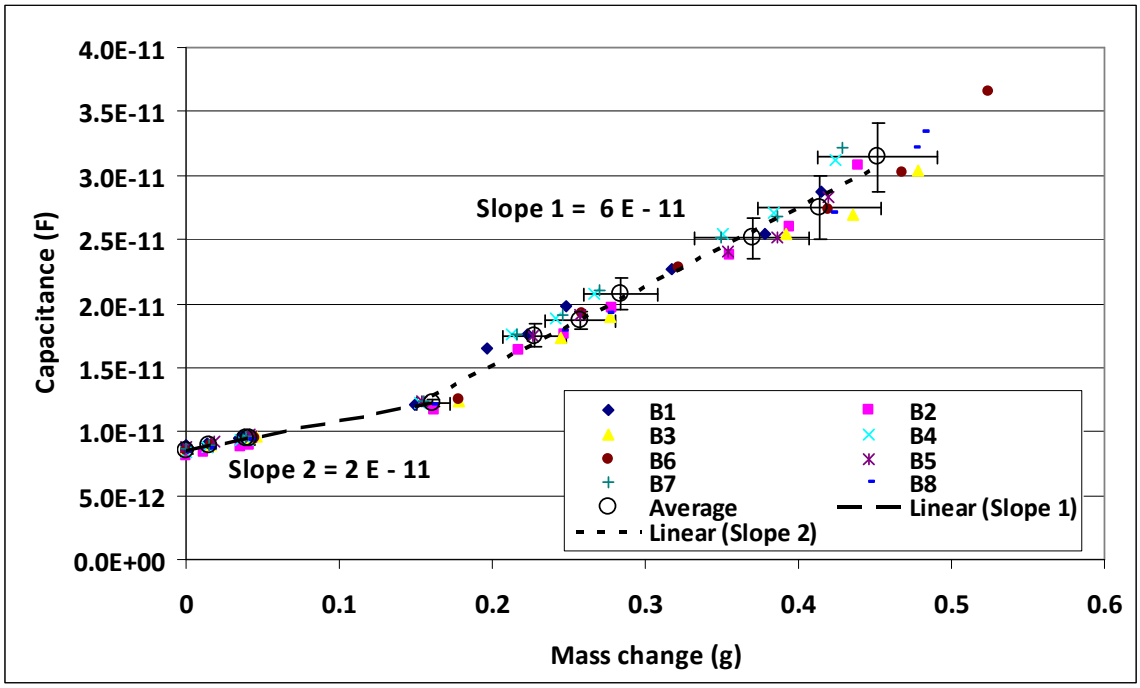

Figure 8. Change in Mass in relation to measured capacitance at 10 MHz for parallel plate capacitor (Error bars are based on one standard deviation)

2.5 Sensors Experiment Results[4]

2.5.1 First Generation Sensors Capacitance measurements

The first generation of sensors was monitored for capacitance, resistance and moisture using the configuration illustrated in Figure 5. The important observation from testing these sensors (S1-S5) was again the bilinear behavior between capacitance and moisture (Figure 9). Moreover, it should be noted that the slopes and the % mass change at which the change in behavior occurs are different than those of the parallel plate setup.

[4] The first and second generation of sensors was manufactured and tested with help form Ian Doran (BSE undergraduate student) and Susie Frasca (ESM undergraduate student) at Virginia Tech.

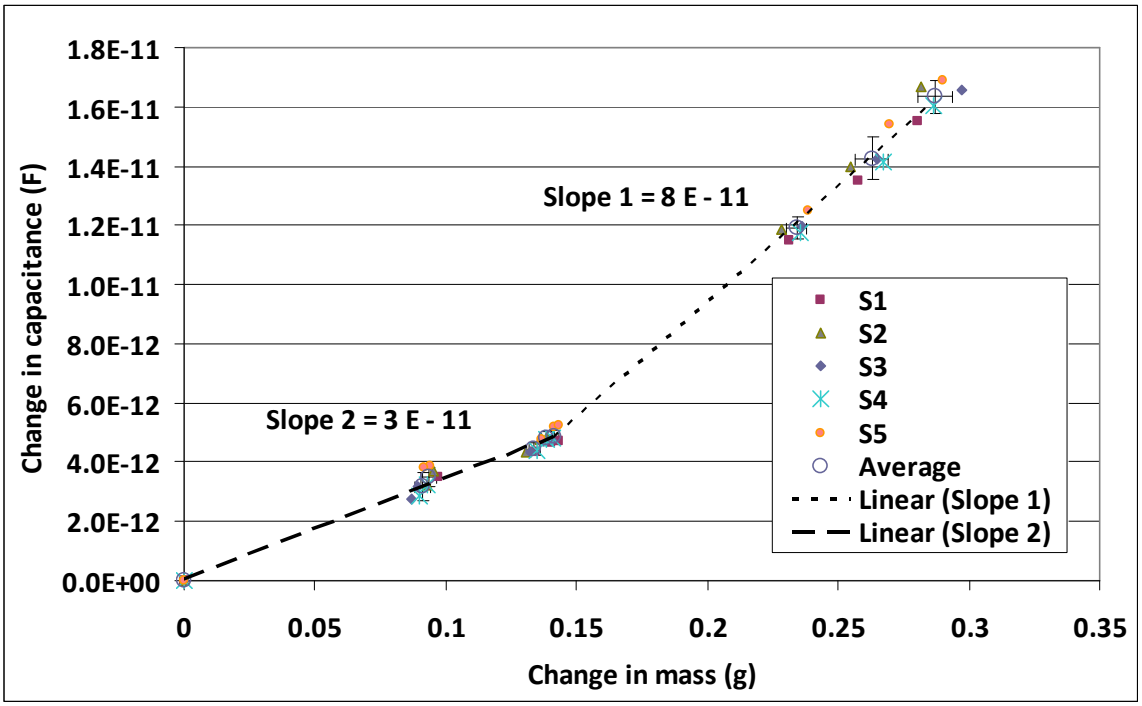

Figure 9. Relation between moisture change and capacitance for 1st generation sensors (Error bars are based on one standard deviation)

2.5.2 First Generation Sensors Wet dry cycling

One criterion for the sensors developed for this study is their applicability for placement within concrete members cast for new construction. To evaluate the effect of liquid water, sensors have been cycled between liquid water and lower humidity as show in Figure 10. The sensors return to the same stable value upon saturation. Worth noticing is also the time it takes for the sensor to saturate versus the drying rate. Clearly, saturation is a much faster process.

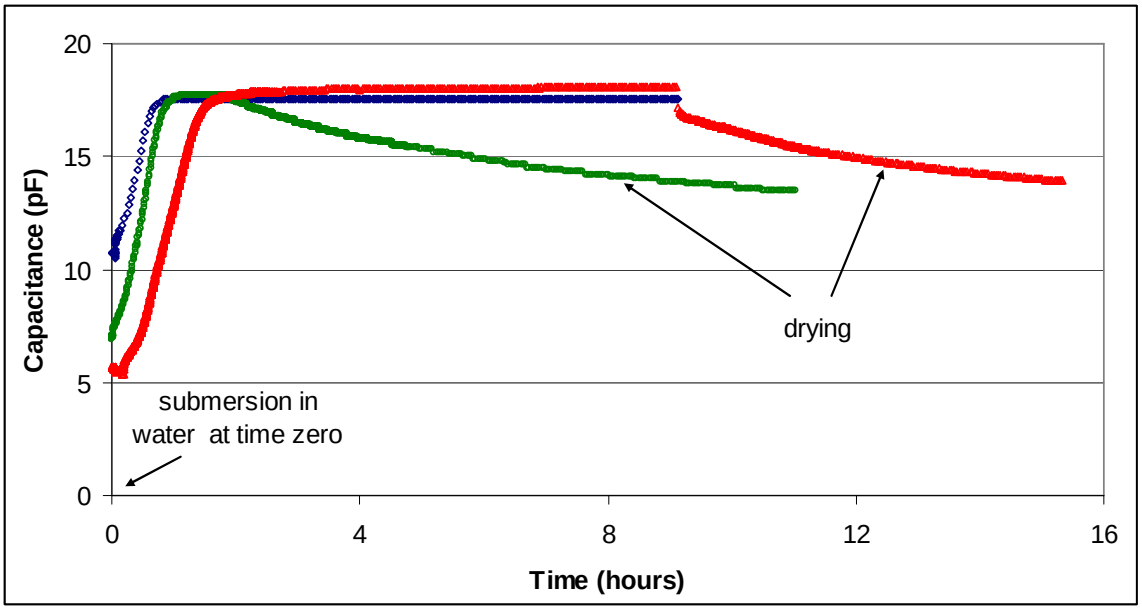

Figure 10. **Wet dry cycling of sensor**

2.5.3 Embedded, first generation sensors in one dimensional moisture gradient measurements

The first generation sensors have been also used in a one dimensional moisture diffusion monitoring experiment through a concrete block. The experimental configuration is shown in Figure 11. The sensors were embedded in old concrete from the same batch of cylinders the blocks for the parallel plate set up were obtained. Holes (3/8)" were drilled at the desired location and depth. Cement paste was used to fill in the gap between the sensor and the concrete and also to secure the sensors in place. Each sensor was fitted with a coaxial cable terminated to a BNC connector. The same length of coaxial cable/BNC connector was used to obtain a base measurement before each set of testing. The sides of the concrete block were sealed with a bituminous based moisture barrier which was covered with polyethylene membrane. The bottom side of the block was kept in contact with water while the top side was sealed in a chamber conditioned with desiccant. The desiccant environment was monitored periodically and moisture levels up to ~15% were measured as desiccant saturation occurred. In addition, the water level diminished at least four times due to malfunction of the water level

device and for reasons beyond the researcher's control[5]. The change in capacitance with respect to time is shown in Figure 12. The change in resistance with respect to time is shown in Figure 13. As expected, the capacitance increased and resistance dropped for the sensor closest to the water as a result of moisture uptake. The behavior of the sensors near the surface exposed to the desiccant was exactly the opposite. In this case, the capacitance dropped and resistance increased. Figure 14 reveals the relation between resistance capacitance for the sensors used in this experiment. The measurements span over 3 1/2 years and the sensors give stable readings in relation to the moisture gradient that exists within the concrete block.

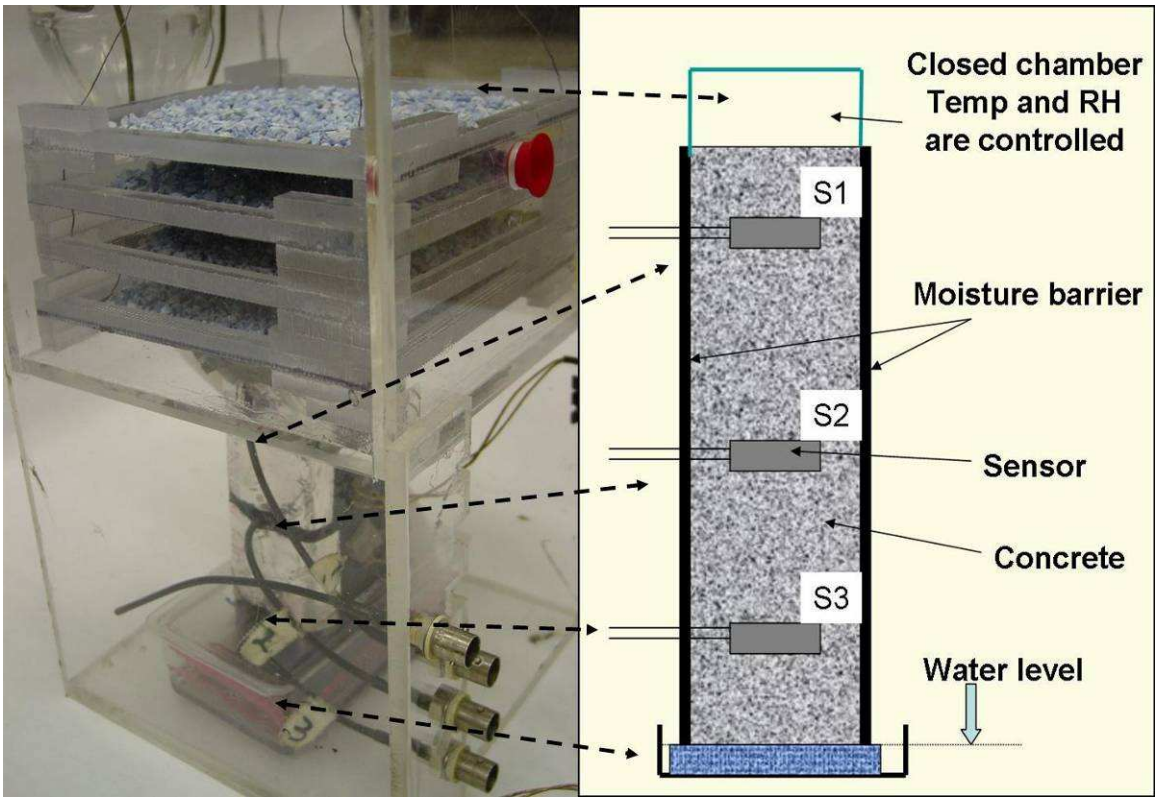

Figure 11. **One dimensional moisture diffusion measurements with sensors**

[5] The events at Virginia Tech on April 16, 2007 shut down Norris Hall, where the test setup was located, for approximately four months. No testing or monitoring of any of the tests was performed during this time. Moisture transport is time dependent and there is a gap in the data collected. P1 and P5 sensors were transferred to a 100 % RH environment some time between April 16th and August 2007 but the time and date was not recorded.

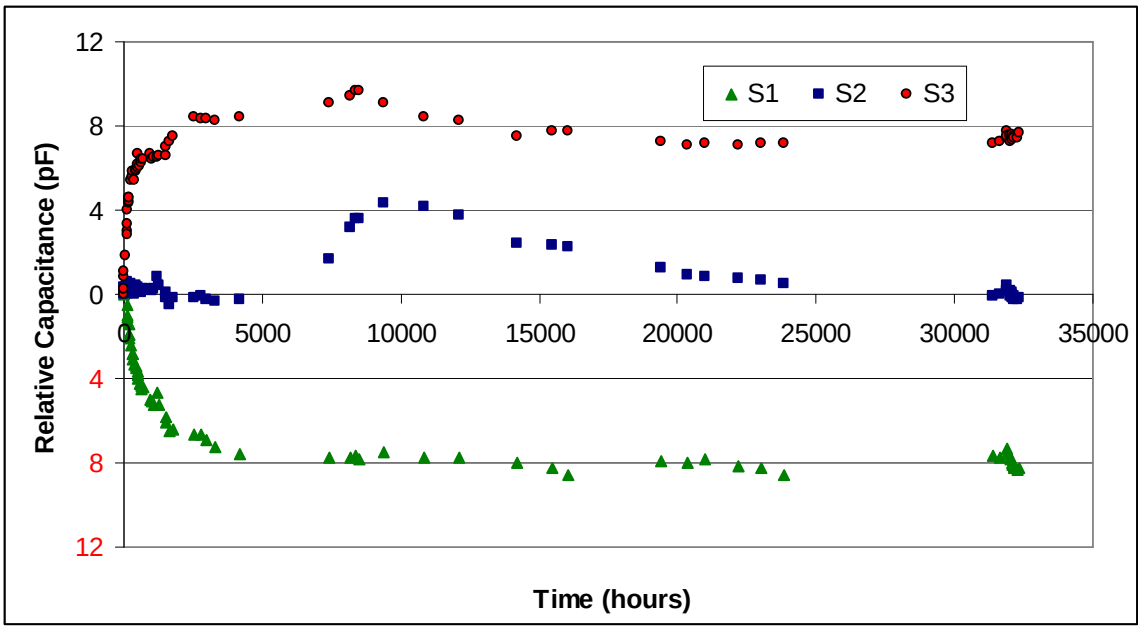

Figure 12. Capacitance change with respect to time for sensors embedded in concrete block

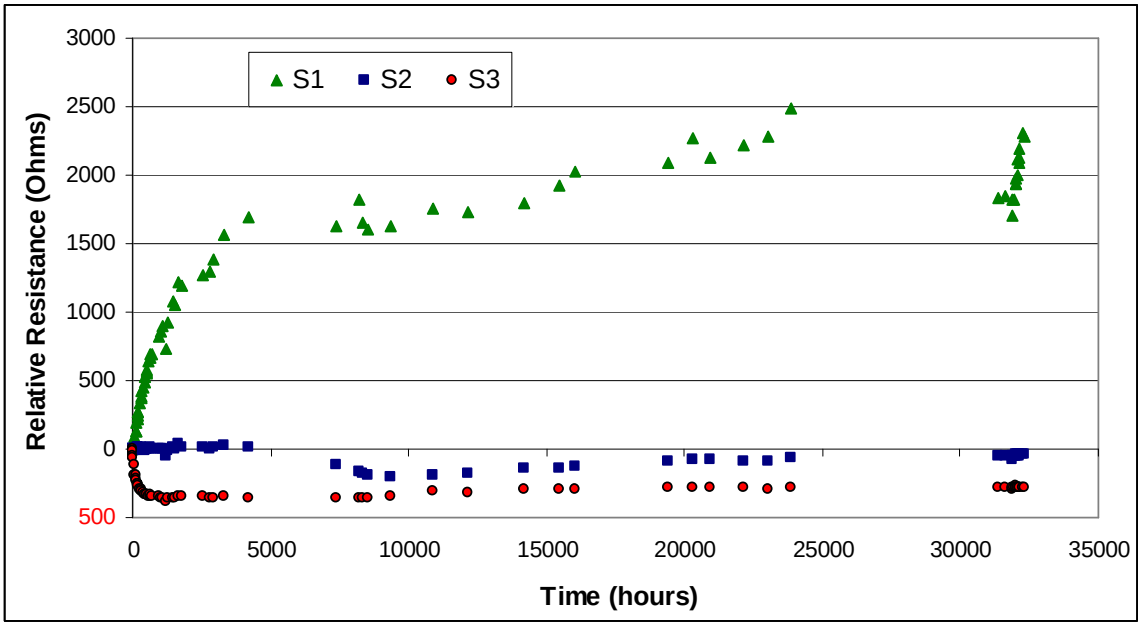

Figure 13. Resistance change with respect to time for sensors embedded in concrete block

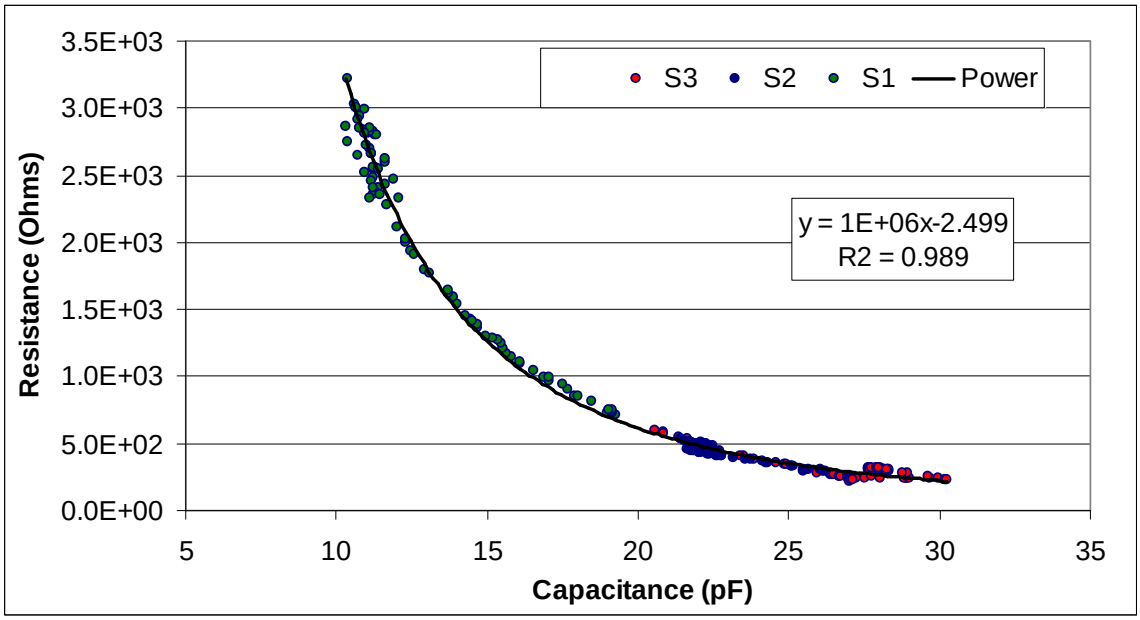

Figure 14. **Relation between resistance and capacitance for sensors embedded in concrete block**

2.6 Experimental results for second generation sensors

Since each of the seven families followed a different path through the moisture levels, results will be presented separately for each family. Sensors in the P1 family will be used to illustrate the trends and behaviors. Cumulative results from all sensors will be presented as needed.

Figure 15 through Figure 17 illustrates the moisture environment exposure history of each of the following sensor families: P1, P3 and P5 respectively (Solid blue line). Additionally, the mass behavior for each sensor in that family is included on the same plot. The %relative humidity indicated is the nominal value the saturated salt solutions used will produce at 25°C. As indicated, some of the data is not available[6]. The data after this period shows abnormalities which could not be investigated fully as the experimental setup was recreated. For instance,

[6] The events at Virginia Tech on April 16, 2007 shut down Norris Hall, where the test setup was located, for approximately four months. No testing or monitoring of any of the tests was performed during this time. Moisture transport is time dependent and there is a gap in the data collected. P1 and P5 sensors were transferred to a 100 % RH environment some time between April 16th and August 2007 but the time and date was not recorded.

there is a sharp drop in mass in two consecutive measurements six (6) days apart in series P5 for some of the sensors (Figure 17). This occurred around the 6800 hours mark. Calibration and temperature data available for that period did not indicate any abnormal behavior in the instruments. Yet, sensor P5-6, showed sudden changes in mass both positive and negative before the 6800 hour mark without any visible loss or gain of mass. The lag of history data throughout the life of the sensors makes it impossible to trace definitively the cause of some of the changes observed. The values of resistance and capacitance recorded appear to be appropriate for the mass recorded, i.e., the data points follow the trend and cannot be singled out from the resistance or capacitance data. Further investigation is warranted to understand this behavior.

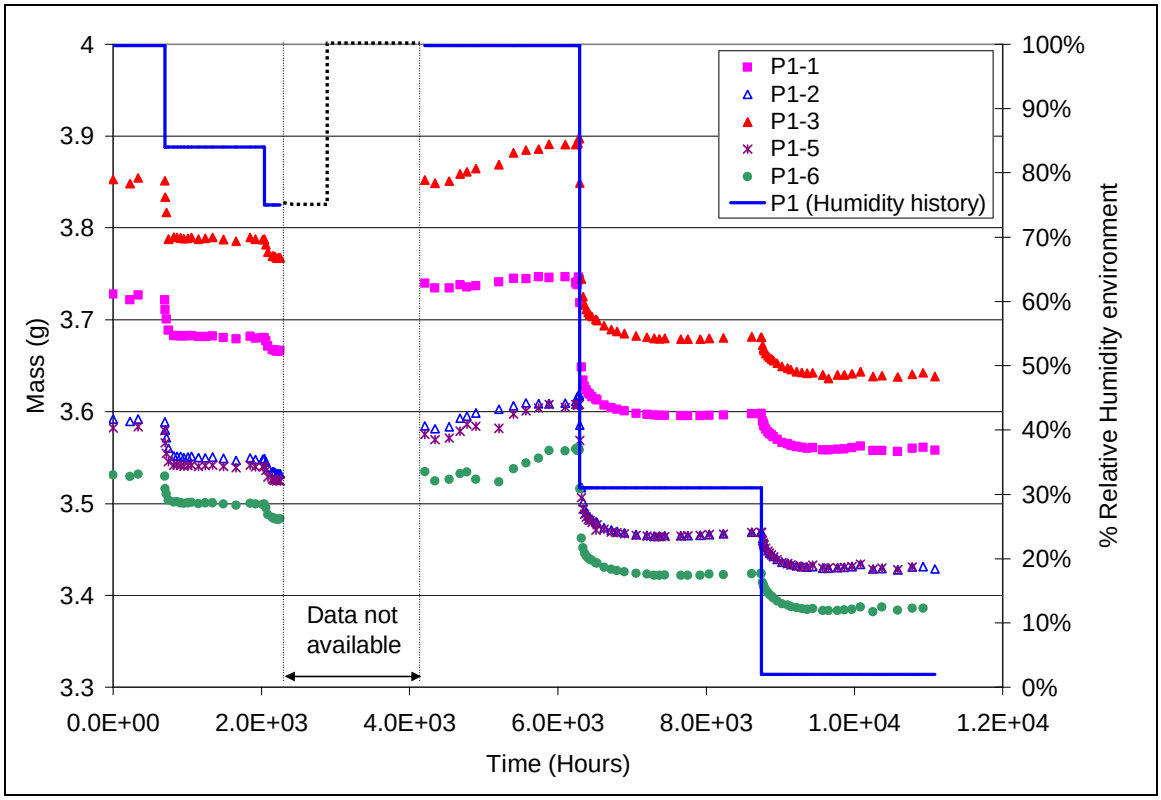

Figure 15. Humidity and mass history for P1 family.

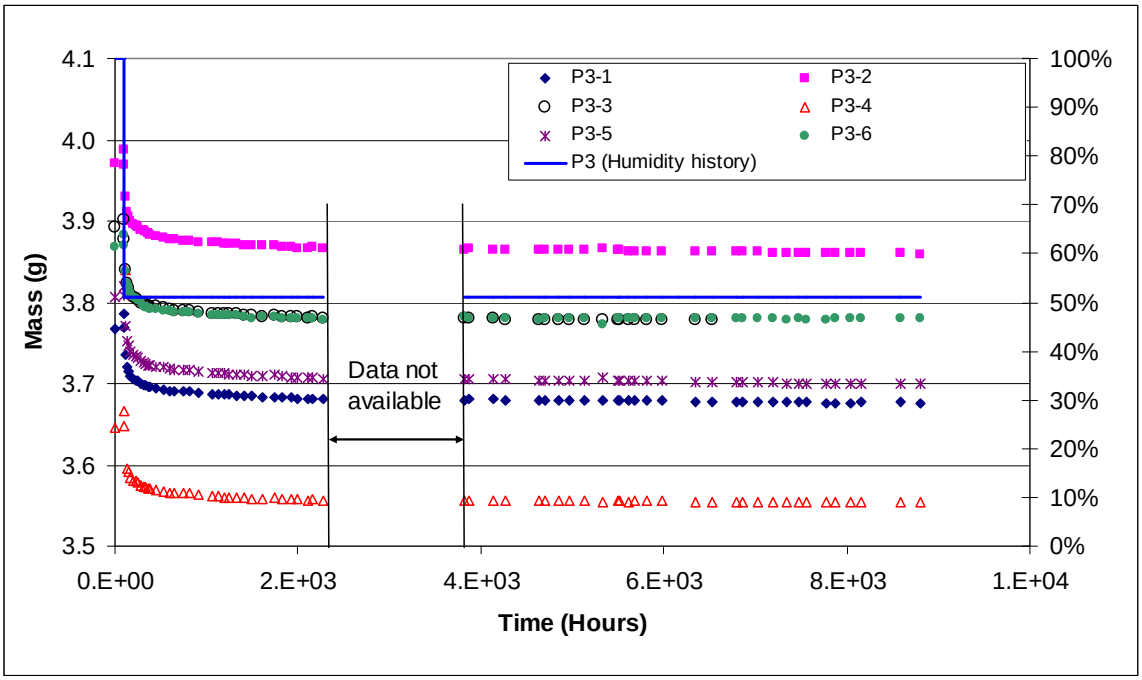

Figure 16. Humidity and mass history for P3 family.

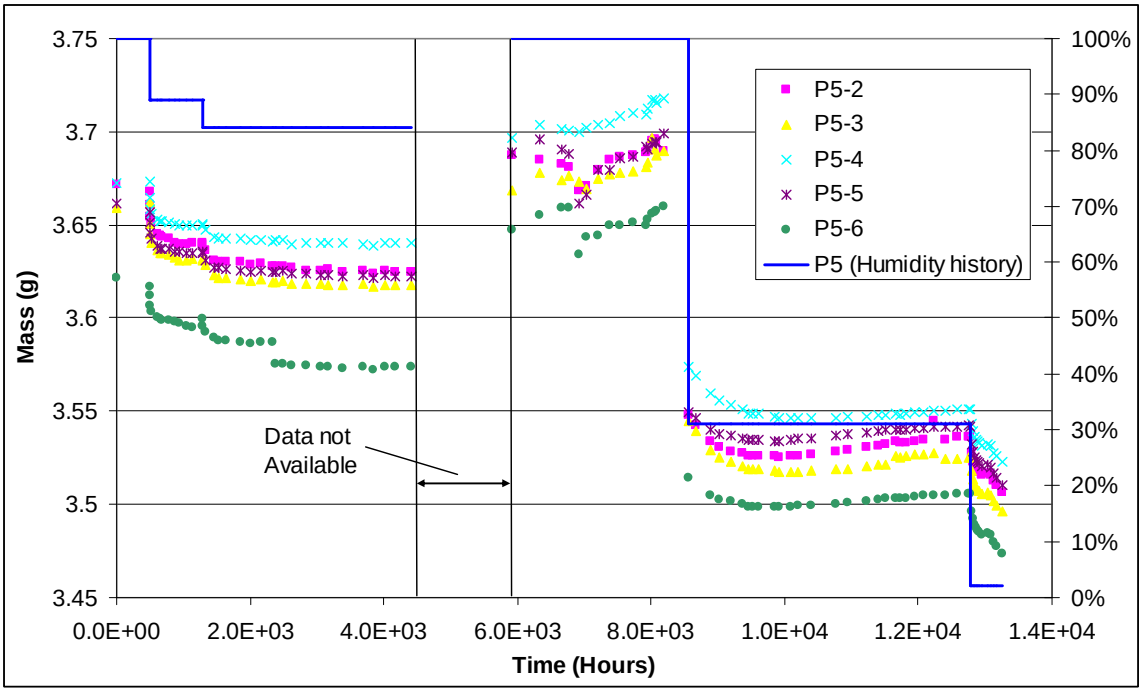

Figure 17. Humidity and mass history for P5 family

The sensors were conditioned at each moisture level indicated until nearly steady state conditions were achieved. Steady state conditions were assessed by the change in mass. Measurements were taken both at steady state and transient state. The mass at steady state follows the moisture levels closely in a linear

fashion as illustrated in Figure 18 and Table 4. The mass of the sensors is between 3 and 4 grams. The mass changes less than 10% between submersion and ~0% RH. Mass measurements at a 100% condensing moisture levels show significant scatter due to the difficulty of removing excess moisture. The relation between mass change and moisture uptake is similar for all sensors (Table 4). The mass and %RH values used to obtain the moisture-%RH relation reflect the last measurement before the sensors were transferred to a different moisture environment.

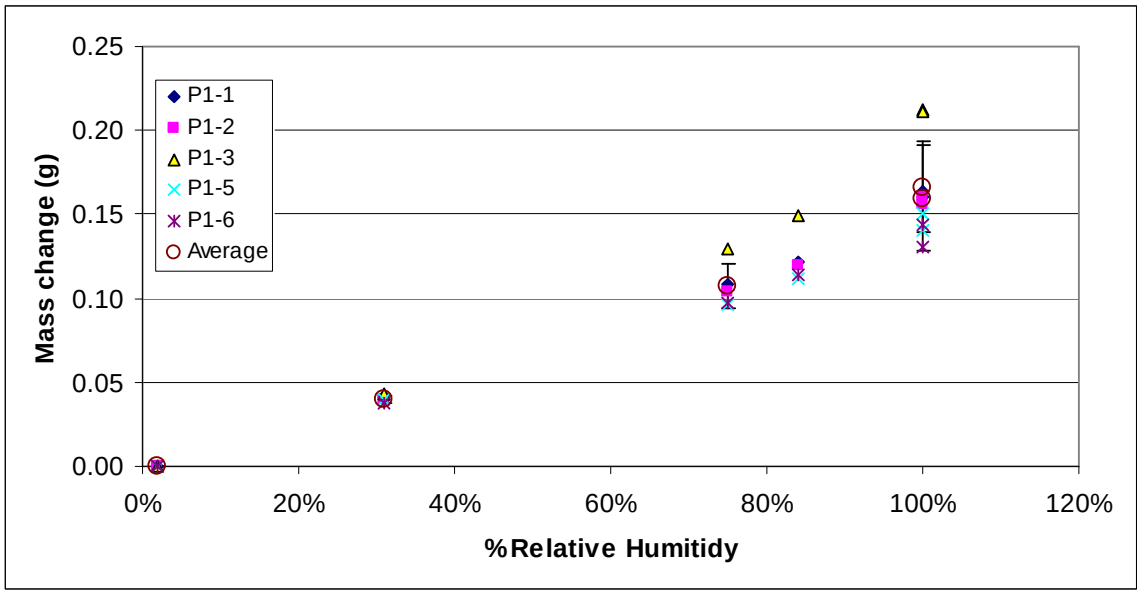

Figure 18. Mass change in relation to moisture environment for P1 family. Error bars are one standard deviation based on average value

Table 4. Slope (s_m) for mass in relation to %RH environment

Coarse	Slope	R^2	Coarse	Slope	R^2	Fine	Slope	R^2
P1-1	0.143	0.990	**P3-1**	0.158	0.960	n/a	n/a	n/a
P1-2	0.139	0.989	**P3-2**	0.185	0.959	**P5-2**	0.159	0.989
P1-3	0.187	0.973	**P3-3**	0.173	0.961	**P5-3**	0.161	0.990
n/a	n/a	n/a	**P3-4**	0.159	0.960	**P5-4**	0.151	0.992
P1-5	0.127	0.988	**P3-5**	0.183	0.962	**P5-5**	0.146	0.995
P1-6	0.122	0.993	**P3-6**	0.150	0.958	**P5-6**	0.140	0.986
Average	**0.144**		**Average**	**0.168**		**Average**	**0.151**	
STDEV	**0.026**		**STDEV**	**0.015**		**STDEV**	**0.009**	

The capacitance change has a bilinear trend observed both in the blocks and in the first generation of sensors (Figure 8 and Figure 9). The resistance change is

nonlinear and increases significantly as moisture in the sensor diminishes. As shown in Figure 19 the resistance slope becomes very large, and the resistance values go beyond the capabilities of the instrumentation used. The trends for both resistance and capacitance are similar for frequencies between 10 MHz and 1 MHz. At 200-400 kHz range it is possible to see the behavior changing especially for the capacitance where three distinct regions can be observed (Figure 20). The change in resistance becomes sharper. The capacitance behavior changes once more below 200 kHz where the capacitance shows an increasing trend with moisture decrease (Figure 21). The discrete test frequencies used in these tests were dictated by the instrumentation. Thus the exact frequencies where behavior changes occur can not be indicated. Due to variability in the sensors the frequencies indicated here are typical. Specific details for each sensor can be found in Table 5 and Table 7. Another change in behavior is also visible around 0.04 g mass change which is attributed to the moisture conditioning procedure followed (moisture step change from 100% down to 31% RH). Concrete adsorption desorption hysteresis loop is well documented [10, 53]. In addition, the diffusion coefficient is moisture dependent; causing variations to the moisture distribution as moisture escapes at different rates from the microstructure.

Recall that values mentioned here are specific to sample P1-1 used as a demonstration case. The resistance behaves similarly through the whole range of frequencies considered with the exception of the rate of change with moisture. It should be noted that the second generation sensors were only conditioned at room temperature while the blocks and 1st generation sensors were conditioned at 50°C and below 4% RH which caused an additional reduction in moisture.

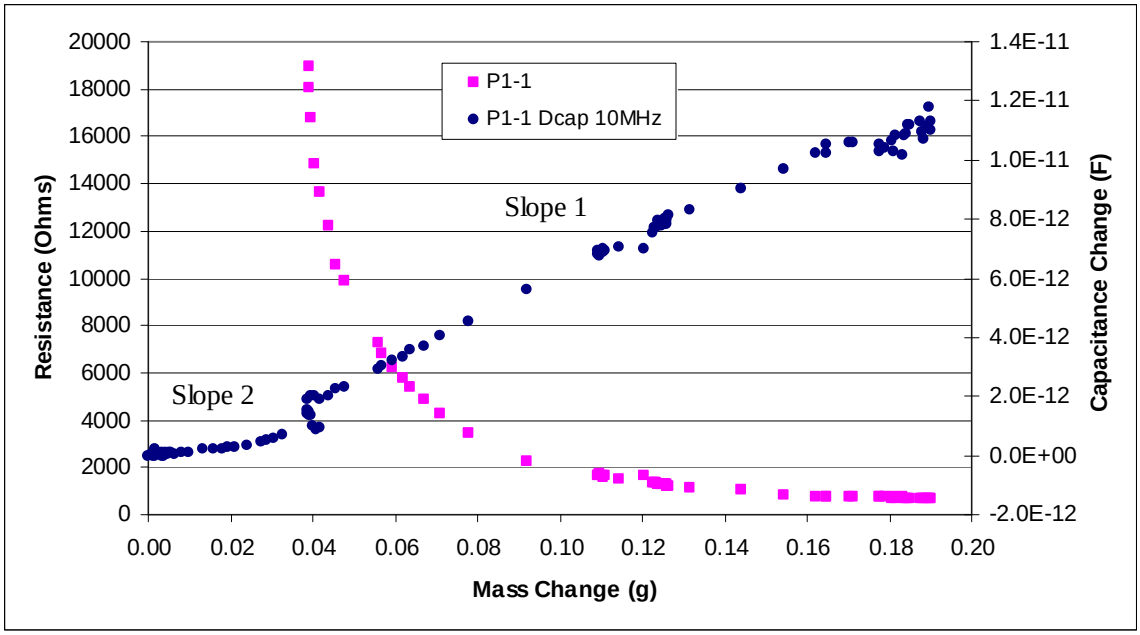

Figure 19. Capacitance and resistance behaviors with moisture change at 10 MHz

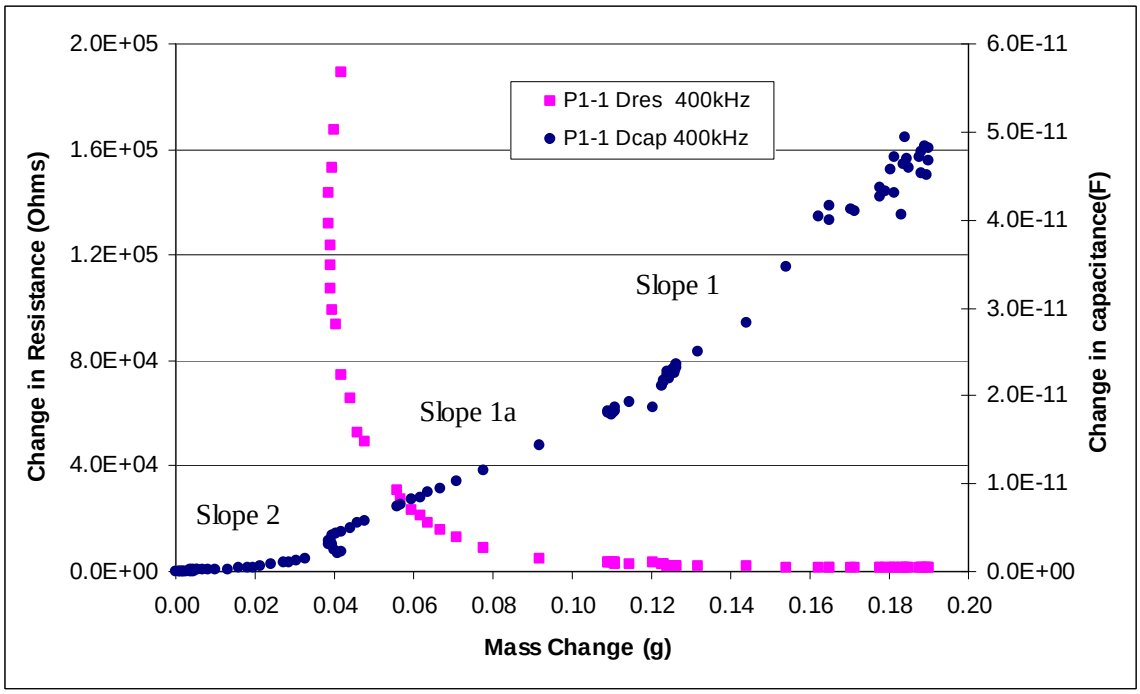

Figure 20. Capacitance and resistance behaviors with moisture change at 400 kHz

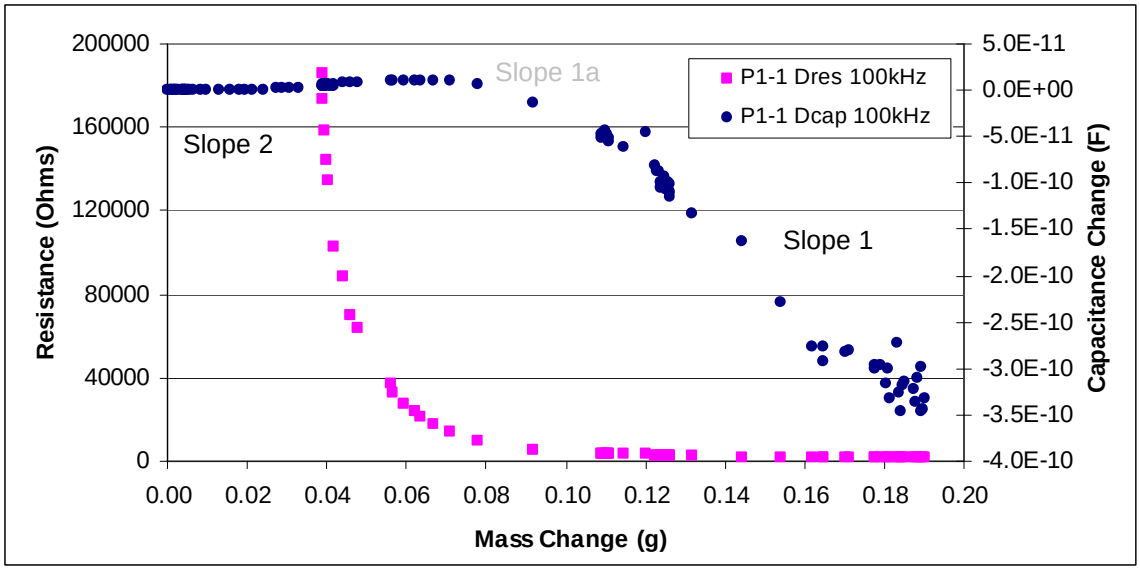

Figure 21. **Capacitance and resistance behaviors with moisture change at 10 kHz**

The capacitance decreases in a bilinear fashion as moisture decreases for frequencies above 400 kHz. Slope 1 is the slope at the high moisture levels and slope 2 is the slope at low levels which denote moisture behavior. The intermediate moisture slope (Slope 1a) appears in the 200-400 kHz range. These results are shown in Table 5, Table 6 and Table 7. The following three tables list the y axis intercept for slope 1, slope 1a and slope 2 respectively (Table 8, Table 9 and Table 10).The R2 value for slope 1 was above 0.96 with exception of results at 200 kHz where the lowest R2 was 0.89. Slope 2 results show a greater scatter due to a small mass change given the conditioning of sensors at room temperature only. Figure 22 through Figure 24 demonstrate the normalized slope values for P1, P3 and P5 sensors. The error bars are calculated based on one standard deviation of average values. Normalization was carried out in the following manner:

$$Normalized - slope = \frac{Slope(f = xHz)}{Slope(f = 10MHz)} \qquad \text{Equation 5}$$

Table 5. **Slope 1 values of capacitance in relation to mass change**

	10 MHz	4 MHz	2 MHz	1 MHz	400 kHz	200 KHz
P1-1	6.14E-11	7.27E-11	8.82E-11	1.24E-10	3.94E-10	1.58E-09
P1-2	6.28E-11	7.39E-11	9.08E-11	1.21E-10	3.07E-10	1.12E-09

P1-3	6.23E-11	7.78E-11	9.43E-11	1.43E-10	6.03E-10	2.39E-09
P1-5	6.36E-11	7.57E-11	9.32E-11	1.27E-10	2.96E-10	1.11E-09
P1-6	5.30E-11	6.32E-11	8.03E-11	1.06E-10	2.15E-10	5.13E-10
Average	**6.06E-11**	**7.27E-11**	**8.94E-11**	**1.24E-10**	**3.63E-10**	**1.34E-09**
St-Dev	**4.34E-12**	**5.62E-12**	**5.60E-12**	**1.36E-11**	**1.49E-10**	**6.97E-10**
P3-1	5.61E-11	6.61E-11	8.01E-11	1.06E-10	2.24E-10	7.25E-10
P3-2	3.96E-11	4.66E-11	5.59E-11	7.22E-11	1.37E-10	4.20E-10
P3-3	5.82E-11	6.84E-11	8.36E-11	1.12E-10	2.37E-10	7.82E-10
P3-4	5.65E-11	6.57E-11	7.75E-11	1.01E-10	2.44E-10	9.58E-10
P3-5	7.00E-11	8.27E-11	9.87E-11	1.38E-10	3.93E-10	1.54E-09
P3-6	5.69E-11	6.74E-11	8.22E-11	1.08E-10	2.16E-10	6.75E-10
Average	**5.62E-11**	**6.61E-11**	**7.97E-11**	**1.06E-10**	**2.42E-10**	**8.50E-10**
St-Dev	**9.68E-12**	**1.15E-11**	**1.38E-11**	**2.10E-11**	**8.35E-11**	**3.79E-10**
P5-2	8.15E-11	9.51E-11	1.17E-10	1.52E-10	2.58E-10	6.31E-10
P5-3	7.83E-11	9.24E-11	1.14E-10	1.47E-10	2.42E-10	5.74E-10
P5-4	7.17E-11	8.47E-11	1.06E-10	1.36E-10	2.10E-10	4.23E-10
P5-5	8.26E-11	9.77E-11	1.21E-10	1.55E-10	2.47E-10	5.46E-10
P5-6	8.28E-11	9.74E-11	1.21E-10	1.55E-10	2.47E-10	5.45E-10
Average	**7.94E-11**	**9.35E-11**	**1.16E-10**	**1.49E-10**	**2.41E-10**	**5.44E-10**
St-Dev	**4.65E-12**	**5.35E-12**	**6.35E-12**	**8.09E-12**	**1.84E-11**	**7.57E-11**

Table 6. **Slope 1a values of capacitance in relation to mass change.**

	10 MHz	**4 MHz**	**2 MHz**	**1 MHz**	**400 kHz**	**200 KHz**
P1-1	n/a	n/a	n/a	n/a	2.1E-10	4.44E-10
P1-2	n/a	n/a	n/a	n/a	2.11E-10	3.93E-10
P1-3	n/a	n/a	n/a	n/a	2.19E-10	4.78E-10
P1-5	n/a	n/a	n/a	n/a	2.43E-10	4.64E-10
P1-6	n/a	n/a	n/a	n/a	1.64E-10	2.37E-10
Average	n/a	n/a	n/a	n/a	**2.09E-10**	**4.03E-10**
St-Dev	n/a	n/a	n/a	n/a	**2.86E-11**	**9.83E-11**
P3-1	n/a	n/a	n/a	n/a	1.75E-10	2.79E-10
P3-2	n/a	n/a	n/a	n/a	1.17E-10	1.89E-10
P3-3	n/a	n/a	n/a	n/a	2.03E-10	3.25E-10
P3-4	n/a	n/a	n/a	n/a	2.21E-10	4.19E-10
P3-5	n/a	n/a	n/a	n/a	1.86E-10	3.E-10
P3-6	n/a	n/a	n/a	n/a	1.86E-10	3E-10
Average	n/a	n/a	n/a	n/a	**1.81E-10**	**3.02E-10**
St-Dev	n/a	n/a	n/a	n/a	**3.56E-11**	**7.42E-11**
P5-2	n/a	n/a	n/a	n/a	1.94E-10	3.86E-10
P5-3	n/a	n/a	n/a	n/a	3.1E-10	3.96E-10
P5-4	n/a	n/a	n/a	n/a	2.7E-10	3.47E-10
P5-5	n/a	n/a	n/a	n/a	4.06E-10	5.15E-10
P5-6	n/a	n/a	n/a	n/a	4.03E-10	5.12E-10
Average	n/a	n/a	n/a	n/a	**3.17E-10**	**4.31E-10**
St-Dev	n/a	n/a	n/a	n/a	**9.02E-11**	**7.75E-11**

Table 7. **Slope 2* values of capacitance in relation to mass change**

	10 MHz	4 MHz	2 MHz	1 MHz	400 kHz	200 KHz
P1-1	1.20E-11	1.28E-11	1.51E-11	1.79E-11	2.55E-11	3.17E-11
P1-2	8.77E-12	8.85E-12	1.02E-11	1.12E-11	1.45E-11	1.71E-11
P1-3	9.84E-12	1.14E-11	1.32E-11	1.54E-11	2.11E-11	2.58E-11
P1-5	7.44E-12	7.63E-12	8.50E-12	9.63E-12	1.15E-11	1.31E-11
P1-6	6.48E-12	6.55E-12	7.55E-12	8.33E-12	1.13E-11	1.33E-11
Average	**8.91E-12**	**9.45E-12**	**1.09E-11**	**1.25E-11**	**1.68E-11**	**2.02E-11**
St-Dev	**2.16E-12**	**2.60E-12**	**3.19E-12**	**4.02E-12**	**6.28E-12**	**8.21E-12**
P5-2	5.66E-13	1.89E-13	2.03E-12	2.44E-12	3.01E-12	4.62E-12
P5-3	5.71E-12	4.00E-12	8.84E-12	1.07E-11	1.47E-11	1.92E-11
P5-4	4.68E-12	5.11E-12	8.39E-12	1.12E-11	1.65E-11	2.14E-11
P5-5	-2.99E-13	-7.62E-13	4.14E-13	6.61E-13	5.01E-13	1.26E-12
P5-6	8.95E-12	8.23E-12	9.03E-12	1.07E-11	1.28E-11	1.58E-11
Average	**3.92E-12**	**3.35E-12**	**5.74E-12**	**7.12E-12**	**9.51E-12**	**1.25E-11**
St-Dev	**3.81E-12**	**3.68E-12**	**4.17E-12**	**5.13E-12**	**7.25E-12**	**9.00E-12**

*Note: Slope 2 data for P3 family is not available as the lower moisture environment used for P3 was 51% RH environment

Table 8. **y axis Intercept for slope 1**

	10 MHz	4 MHz	2 MHz	1 MHz	400 kHz	200 KHz
P1-1	-1.55E-13	-3.02E-13	-2.63E-13	-1.46E-12	-2.68E-11	-1.46E-10
P1-2	-3.71E-13	-4.53E-13	-4.93E-13	-1.22E-12	-1.67E-11	-9.54E-11
P1-3	-1.92E-13	-5.83E-13	-5.74E-13	-3.33E-12	-6.26E-11	-2.89E-10
P1-5	5.29E-14	-7.42E-15	4.46E-14	-6.64E-13	-1.09E-11	-7.73E-11
P1-6	-5.39E-13	-7.50E-13	-1.07E-12	-1.76E-12	-1.10E-11	-3.98E-11
P3-1	8.67E-13	1.06E-12	1.43E-12	1.71E-12	-2.20E-13	-1.31E-11
P3-2	5.77E-13	7.00E-13	9.81E-13	1.23E-12	7.12E-13	-7.38E-12
P3-3	1.15E-12	1.38E-12	1.83E-12	2.19E-12	6.55E-13	-1.28E-11
P3-4	1.42E-12	1.88E-12	2.66E-12	3.63E-12	3.38E-12	-9.02E-12
P3-5	1.12E-12	1.37E-12	1.91E-12	2.08E-12	-4.86E-12	-4.18E-11
P3-6	1.19E-12	1.44E-12	1.90E-12	2.36E-12	1.36E-12	-8.44E-12
P5-2	1.90E-12	1.30E-12	9.87E-13	2.15E-13	-1.33E-11	-9.08E-11
P5-3	2.13E-12	1.48E-12	1.18E-12	7.23E-13	-1.93E-11	-1.07E-10
P5-4	2.23E-12	1.61E-12	1.31E-12	9.02E-13	-1.77E-11	-7.74E-11
P5-5	1.75E-12	8.77E-13	4.09E-13	-2.59E-13	-6.77E-12	-5.75E-11
P5-6	-1.38E-12	-1.68E-12	-2.16E-12	-2.84E-12	-9.42E-12	-6.02E-11

Table 9. **y axis intercept for slope 1a**

	10 MHz	4 MHz	2 MHz	1 MHz	400 kHz	200 KHz
P1-1	n/a	n/a	n/a	n/a	-4.84E-12	-1.52E-11
P1-2	n/a	n/a	n/a	n/a	-4.74E-12	-1.19E-11
P1-3	n/a	n/a	n/a	n/a	-5.81E-12	-1.89E-11
P1-5	n/a	n/a	n/a	n/a	-5.57E-12	-1.41E-11
P1-6	n/a	n/a	n/a	n/a	-3.81E-12	-6.26E-12
P3-1	n/a	n/a	n/a	n/a	1.68E-12	1.53E-12
P3-2	n/a	n/a	n/a	n/a	1.26E-12	1.21E-12
P3-4	n/a	n/a	n/a	n/a	1.89E-12	1.66E-12
P3-5	n/a	n/a	n/a	n/a	3.69E-12	4.57E-12
P3-5	n/a	n/a	n/a	n/a	2.06E-12	7.77E-13
P3-6	n/a	n/a	n/a	n/a	2.59E-12	2.92E-12
P5-2	n/a	n/a	n/a	n/a	2.97E-13	-3.84E-12
P5-3	n/a	n/a	n/a	n/a	-3.08E-12	-4.63E-12
P5-4	n/a	n/a	n/a	n/a	-2.11E-12	-3.41E-12
P5-5	n/a	n/a	n/a	n/a	-6.91E-12	-9.49E-12
P5-6	n/a	n/a	n/a	n/a	-9.47E-12	-1.21E-11

Table 10. **y axis intercept for slope 2**

	10 MHz	4 MHz	2 MHz	1 MHz	400 kHz	200 KHz
P1-1	-1.57E-14	-2.53E-14	-3.34E-14	-5.08E-14	1.34E-16	-1.79E-14
P1-2	-1.37E-14	-8.39E-15	-1.02E-14	-2.27E-14	9.52E-15	5.15E-15
P1-3	-2.31E-13	-5.66E-14	-8.71E-14	-1.13E-13	-8.33E-14	-1.03E-13
P1-5	-2.84E-15	-1.49E-15	-4.96E-15	-1.09E-14	1.26E-14	1.63E-14
P1-6	-2.13E-14	-2.71E-14	-3.01E-14	-4.10E-14	-5.16E-15	-8.19E-15
P3-1	-2.08E-14	-2.78E-14	-3.52E-14	-5.05E-14	-1.07E-13	-1.36E-13
P3-2	6.68E-14	5.23E-14	4.82E-14	5.02E-14	1.34E-13	1.46E-13
P3-4	4.99E-14	5.24E-14	5.23E-14	6.21E-14	5.88E-14	6.61E-14
P3-5	-1.22E-13	-4.76E-14	-2.93E-15	5.53E-14	1.11E-13	2.43E-13
P3-5	2.98E-14	4.15E-14	4.70E-14	5.96E-14	6.78E-14	7.63E-14
P3-6	7.21E-14	8.26E-14	9.83E-14	1.17E-13	1.45E-13	1.98E-13
P5-2	1.00E-15	-7.60E-15	-1.98E-14	-2.36E-14	4.29E-21	-2.46E-14
P5-3	-3.18E-14	-2.17E-14	-5.70E-14	-6.23E-14	1.14E-20	-8.94E-14
P5-4	-2.73E-14	-2.99E-14	-5.12E-14	-5.78E-14	1.49E-20	-8.55E-14
P5-5	2.91E-15	4.90E-15	-1.04E-14	-1.40E-14	2.56E-22	-7.82E-15
P5-6	-1.84E-14	-1.17E-14	-1.66E-14	-2.06E-14	2.89E-17	-2.81E-14

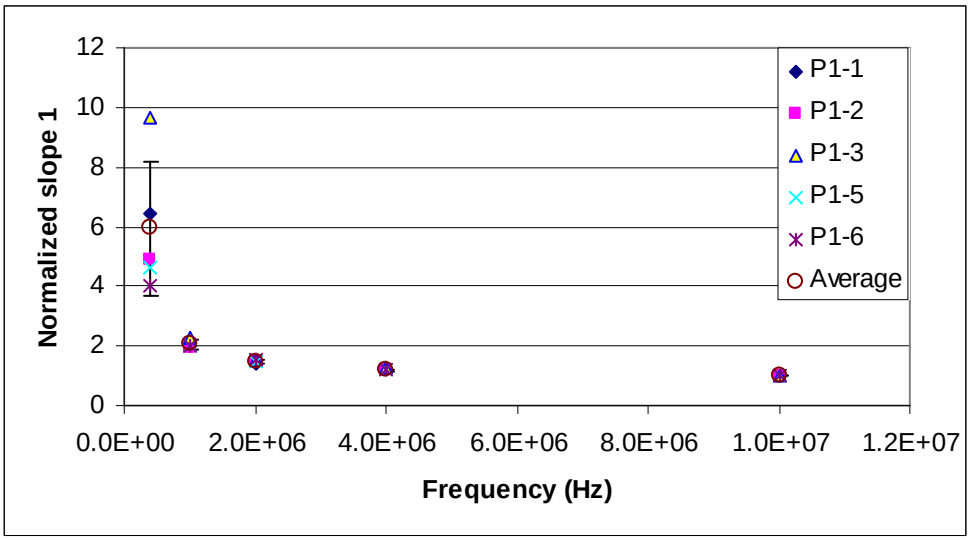

Figure 22. Normalized slopes of capacitance vs. Moisture for P1

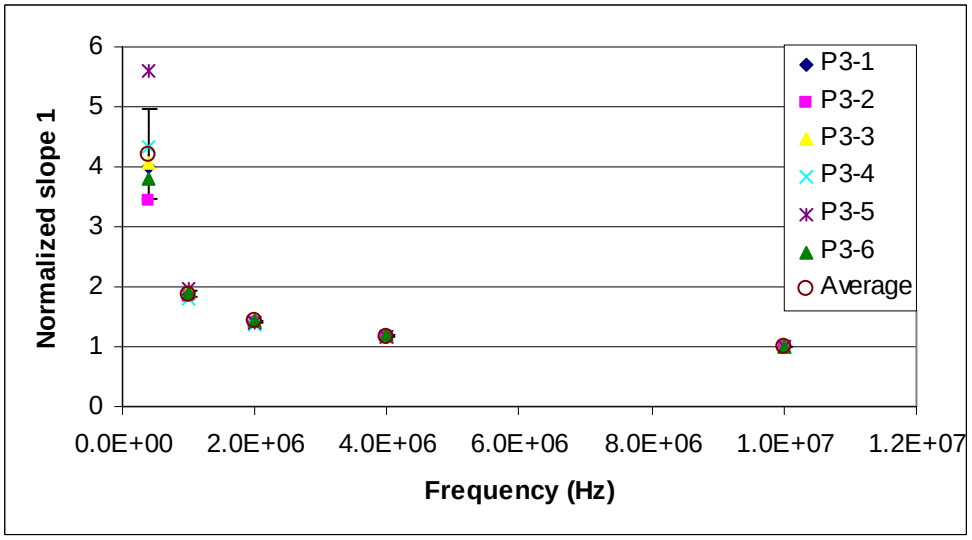

Figure 23. Normalized slopes of capacitance vs. Moisture for P3

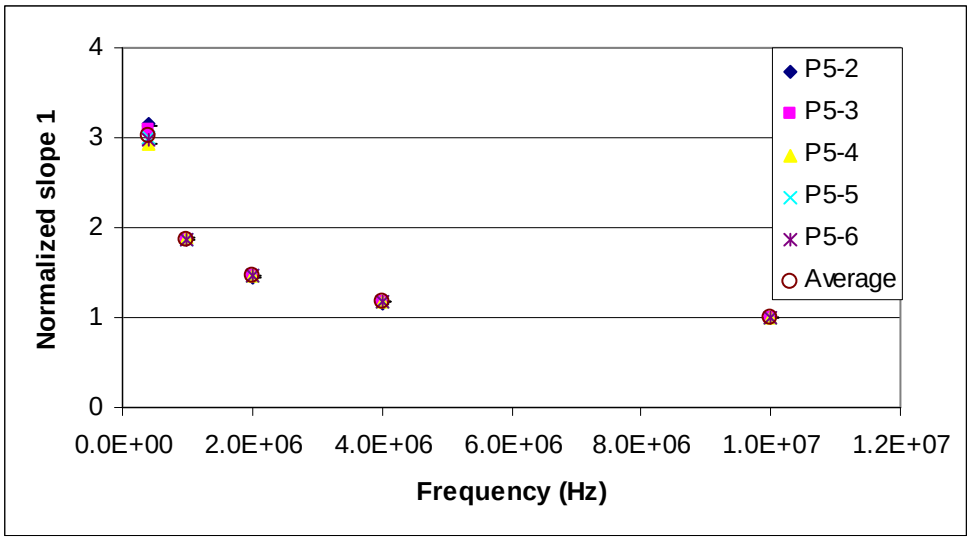

Figure 24. **Normalized slopes of capacitance vs. Moisture for P5**

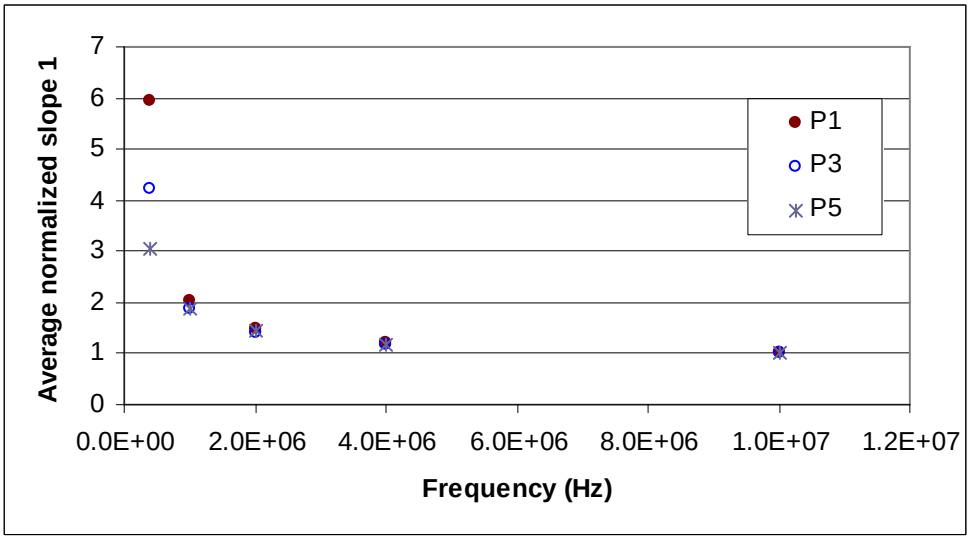

Figure 25. **Average normalized slope 1 values for P1, P3 and P5 families of sensors**

The slope 1 data was normalized using Equation 5 and fit to a third order polynomial with a 0.98 or higher R2 value (Table 11). The function was chosen to provide the data the best fit for a range 200 kHz to 10 MHz. The values of constants a, b, c and d for P1-6 and P5 sensors are quite different than the constants values calculated for the rest of the sensors.

Table 11. **Third order polynomial constants used to fit slope 1 data**

	a	b	c	d
P1-1	-0.0707	3.300	-51.5	268.4
P1-2	-0.0737	3.385	-52.0	266.9
P1-3	-0.0563	2.696	-43.2	231.2
P1-5	-0.0623	2.955	-46.7	245.5
P1-6	-0.0371	1.739	-27.4	144.6
Average	-0.0600	2.815	-44.1	231.3
STDEV	0.0145	0.662	10.1	50.9
Average (Excluding P1-6)	**-0.0658**	**3.084**	**-48.3**	**253.0**
STDEV (Excluding P1-6)	**0.0079**	**0.319**	**4.19**	**17.9**
P3-1	-0.0674	3.110	-47.9	246.5
P3-2	-0.0688	3.155	-48.3	246.5
P3-3	-0.0675	3.111	-47.9	246.5
P3-4	-0.0635	2.989	-47.0	247.0
P3-5	-0.0696	3.173	-48.4	246.8
P3-6	-0.0696	3.173	-48.4	246.8
Average	**-0.0677**	**3.119**	**-48.0**	**246.7**
STDEV	**0.0023**	**0.069**	**0.52**	**0.23**
P5-2	-0.0485	2.219	-34.0	174.9
P5-3	-0.0491	2.240	-34.2	175.0
P5-4	-0.0527	2.343	-34.9	174.9
P5-5	-0.0506	2.285	-34.5	175.1
P5-6	-0.0506	2.285	-34.5	175.1
Average	**-0.0503**	**2.274**	**-34.4**	**175.0**
STDEV	**0.0016**	**0.048**	**0.35**	**0.07**

The constants between families appear to be different. However, if each constant is divided by constant (a) the following ratios listed in Table 12 will be obtained:

Table 12. **Normalized polynomial constant representing slope 1**

	a'	b'	c'	d'
Average P1	1	-46.9	737	-3871
STDEV P1	0	0.75	23.1	180
Average P3	1	-46.1	709	-3646
STDEV P3	0	0.55	16.8	129
Average P5	1	-45.2	685	-3481
STDEV P5	0	0.50	15.12	112

2.7 Conclusions

Moisture sensors for concrete based on dielectric and resistive properties of cement paste has been developed and characterized. The sensor is permeable to moisture thus not interfering with the moisture transport and its operation is not influenced by liquid water. Although the relation between moisture and capacitance is at least bilinear in nature, the sensors can provide qualitative moisture measurements when embedded in concrete. The trend between capacitance and moisture is not influenced by the geometry or composition of concrete used. Capacitance could be used alone as an indication of moisture. However, measuring both values and comparing with the power law calculation can be used to check the sensor operation. Embedded sensors provided data for over three and half years with stable readings of capacitance and resistance. The sensors manufactured and tested were not optimized for durability, sensitivity or response time. Further experimental work is needed to establish response and performance in other than room temperatures, the presence of deicing agents used on roads, and other compounds the sensors might encounter when installed in the field.

Chapter 3

Evaluation of a standalone permeable concrete moisture sensor using Impedance Spectroscopy

Evaluation of a standalone permeable concrete moisture sensor using Impedance Spectroscopy

T. Theophanous, J.J. Lesko
MC 219, Virginia Polytechnic Institute and State University, Blacksburg, VA 24061, USA

Abstract

In Chapter 2, resistance and capacitance values were related to moisture in sensors that were developed to monitor moisture in concrete. In this chapter, the sensor behavior will be observed from the impedance prospective which includes resistance and capacitance information. Impedance values were obtained using Impedance Spectroscopy (IS) techniques and the values provide additional information to map the moisture sensor behavior. Some of the findings include multiple time constants and frequency dependent responses. In addition, existing mixing rules for predicting the effective dielectric response cannot capture the behavior of moist concrete. The resistance is related to capacitance through a power law relationship. However, neither resistance nor capacitance follows the Universal Dielectric Response theory (UDR) with respect to frequency.

This paper will be submitted to Cement and Concrete Research journal

3.1 Introduction

Observing physical systems is always challenging, given that probing a system should not affect the system and provide information only about the quantity of interest. In many cases the response obtained is that of lumped system and it is up to the researcher to interpret the results using physics basic principles and suitable models. In chapter 2, moisture sensors developed based on resistive and capacitive properties of cement were characterized. Impedance spectroscopy (IS) techniques were used to obtain resistance and capacitance values in relation to moisture content. In this chapter, the impedance measurements will be considered as there is more information that can be extracted beyond resistance and capacitance values. As mentioned above, the response in the case of IS is that of a lumped system. The instrumentation employed in the experimental setup uses a model to perform some calculations in order to return values of resistance capacitance, inductance and impedance over the frequency range of 10 kHz to 10 MHz. Taking into account the limitations of a lumped system response and the model used by the instrumentation, the data contains information about the microstructure and possible reasons of the impedance response of cement paste.
Taking a step further than impedance measurements, the dielectric constants of cement and water in conjunction with mixing rules are considered as means to predict the effective dielectric constant of moist hydrated cement paste.

3.2 Impedance Spectroscopy (IS), dielectric constants and LRC circuits

Impedance Spectroscopy (IS) uses the behavior of an LRC circuit (combination of inductors resistors and capacitors in a circuit) to capture and explain the behavior of a physical systems. The relation between the applied voltage and current is evaluated though an appropriate LRC model. LRC circuits are well understood and they are used widely to model various physical phenomena (circuits, dynamics, viscoelasticity, etc). The behavior of an LRC circuit is

frequency dependent and can be mathematically expressed in the complex plane. The model i.e., LRC circuit can be phenomenological, which means that it can capture the behavior without any specific knowledge of the system. Ideally each element of the model will represent an element or a group of elements of the system and have some physical meaning.

Concrete has been studied using IS to evaluate permeability shrinkage, hydration and water behavior among other topics [86-93]. The resistivity and dielectric constant of many of the concrete constituents have been measured. Given the many variations in composition, density, and cure states values for dielectric contact for cementing materials vary. In general the values listed are in the range between 3 and 10 for a range of frequencies spanning the low MHz to GHz range. For example, Hu, et al. report a value of approximately 7 for concrete conditioned at 0 %RH in the range of 1MHz to 1 GHz [94]. Similarly, Al-Qadi, et al. measure values between 6 (w/c ratio 0.55) and 12 (w/c ratio 0.35) at 40 MHz [95]. Values obtained at 10 MHz were 2.5 to 3 times higher. Pokkuluri studied the effect of admixtures, chlorides and moisture on dielectric constant of concrete [96]. The values reported start in the mean teens and drop below 10 at higher frequencies for most of the cement mixtures used.

The dielectric constant of liquid water is well established over a wide range of temperatures. For example, the *Handbook of Chemistry and Physics* lists the dielectric constant for water as function of temperature [97]. Free water has a dielectric constant of about 80 at 20°C.

The dielectric constant of bound water was calculated to be about 3 [98, 99]. Marino, et al. calculated the bound water in bone to have a value between 3 and 6 [100]. By simulation, Senapati and Chandra showed that the dielectric constant of water will be well below 80 just by confinement in a small space excluding the effect from electrostatic forces [101].

The behavior of ice is very different since the water molecules do not have the freedom to align with respect to the applied field. The dielectric constant reported for ice is between 3 and 6. Fen-Chong and Fabbri measure both the dielectric constant of water and ice. Ice at 0°C gave a value of 3.2 at frequencies of 1 MHz and higher [102]. Water dielectric constant dropped to values below 10 at frequencies in the THz region. The dielectric constant of ice is above 80 for frequencies below 1000 Hz as reported by Fen-Chong and Fabbri.

To measure dielectric properties electrodes are employed. Usually a contact resistance exists between the electrodes and the sample and can be identified in the measurements. Perhaps more difficult to interpret is what is called a double layer capacitor. It is usually attributed to a difference in ion concentration in the very thin layer close to the electrodes or other surfaces that could act as electrodes. It is controlled by mass transport properties within the effective zone of the double layer capacitor [103, 104]. An additional factor that may affect the measurements of dielectric constants is effective area. Porous or rough electrodes will affect the results obtained for electrochemical impedance spectroscopy [103].

Electrical resistivity (specific electrical resistance) may be easier to measure. However the effect of polarization when measuring DC resistance must be accounted for. Electrical resistivity and dielectric constant are temperature dependent and the effects of temperature should be evaluated. The properties of water vary considerably depending on the state of the water.

Concrete behavior with respect to impedance spectroscopy will involve aggregate, hydrated cement paste (including bound water), free or loosely bound water and voids.

3.2.1 LRC circuits AC impedance

Using the idea of transfer functions typically a LRC circuit can be analyzed using impedance.

Transfer function *G(jω)*

$$G(j\omega) = Z_T(j\omega) = \frac{output}{input} = \frac{V(j\omega)}{I(j\omega)} \qquad \text{Equation 6}$$

Where Z_T is the impedance, *V* is the applied voltage and *I* is the resulting current.

Each of the three components in the LRC circuit has an impedance Z

$$Z_R = R \qquad \text{Equation 7}$$

$$Z_c = -\frac{1}{j\omega C} \qquad \text{Equation 8}$$

$$Z_L = j\omega L \qquad \text{Equation 9}$$

$$\omega = 2\pi f \qquad \text{Equation 10}$$

Z_R, Z_C and Z_L are the impedance of resistor (R), capacitor (C) and inductor (L) respectively.
f is the frequency and ω is the angular velocity
$j^2 = -1$

The three components (L, R and C) can be combined in any configuration that represents the behavior of the system. The total impedance of the system can be obtained by adding impedances following the series and parallel addition of resistances. Usually inductance is present only if the physical system is changing

during the test. For instance, if a chemical reaction is taking place inductance may be present [103].

As with all modeling LRC circuits representation of a system has limitations. The response obtained may be influenced by multiple components of the system and it may be impossible to separate each component [103].

3.3 Test setup

Figure 5 demonstrates the wire diagram of the experimental set up. The LCR meter used was an HP4275A computer controlled via GPIB and LabVIEW. The mass of the sensors was measured just after running the frequency sweep on a Mettler AE200 balance with 0.0001g resolution. A four (4) wire configuration between the sensors and the LCR was used. To facilitate the ease of transferring sensors to and from containers each sensor was fitted with a polyethylene plug. In addition, the use of plugs kept the disturbance to the environmental condition in the test chambers to a minimum (Figure 6). Saturated salt solutions were used to create different relative humidity environments as detailed in Table 3 [84, 85]. A double container was used to minimize crystal formation on the upper portion of the conditioning chamber housing the sensors. Each chamber could host between 12 and 20 sensors at a time and each sensor could be moved independently. The moisture was monitored using a Rotronic HT260R RH/Temperature meter and at a later stage an OMEGA CNiHT Temperature/ %RH probe was added to the monitoring system. The temperature was measured with the above mentioned meters and also with a type K thermocouple.

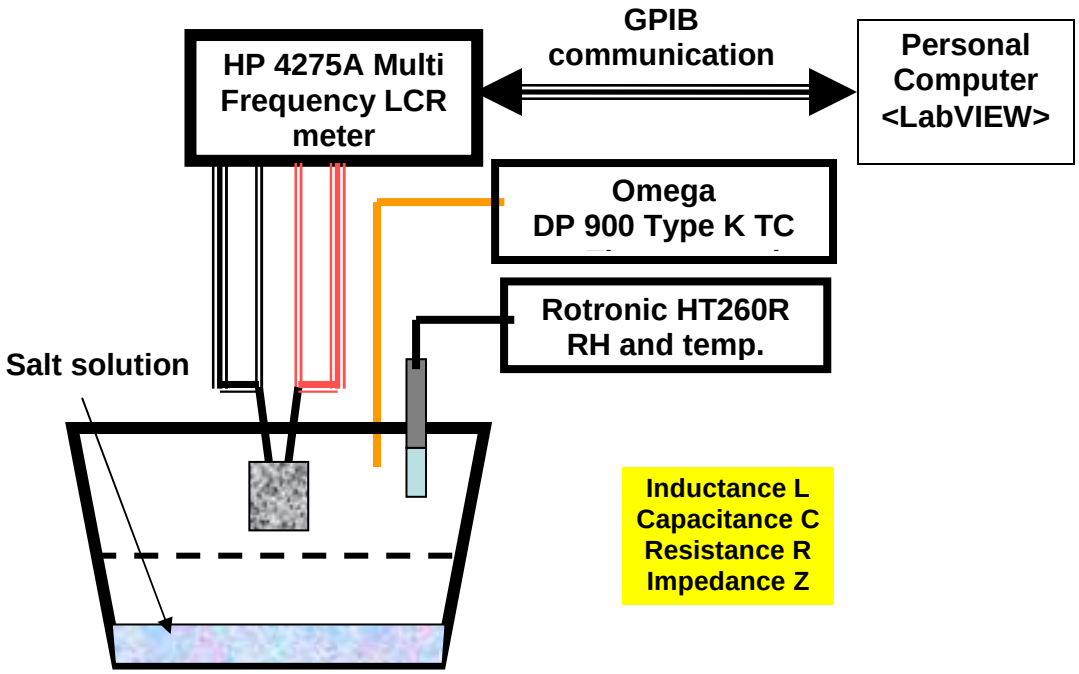

Figure 26. Test setup

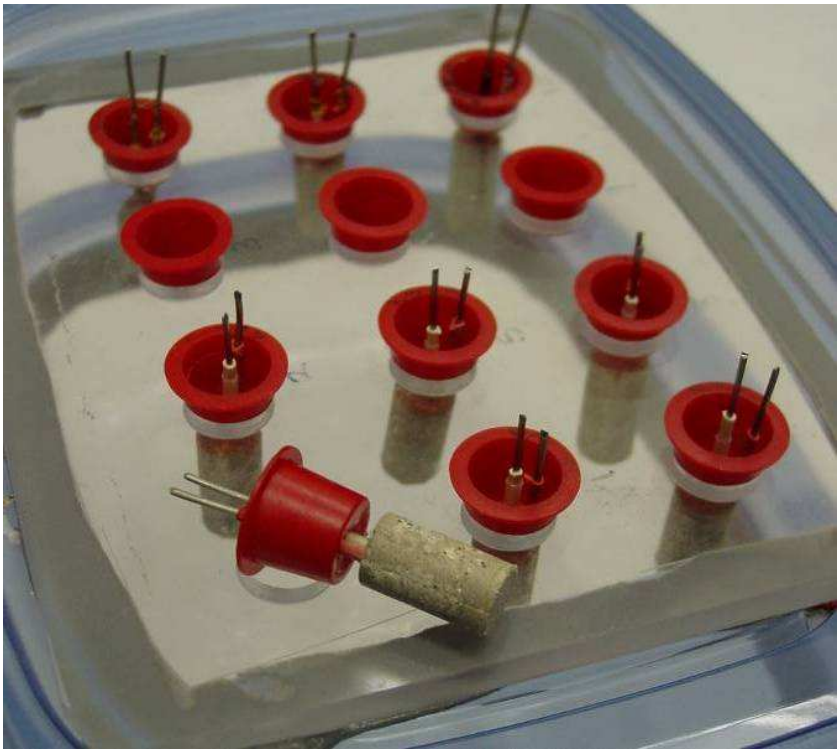

Figure 27. Sensors in controlled environment with polyethylene plugs

Figure 28 illustrates the moisture environment exposure history for sensor families P1, P3 and P5 respectively. The % relative humidity indicated is the nominal value the saturated salt solutions will produce at 25°C. Ideally, the sensors would be exposed to a particular moisture level until constant mass condition is achieved. However, in the interest of time, sensors were transferred to the next relative humidity environment when the mass change between consecutive measurements was below one thousand of a gram.

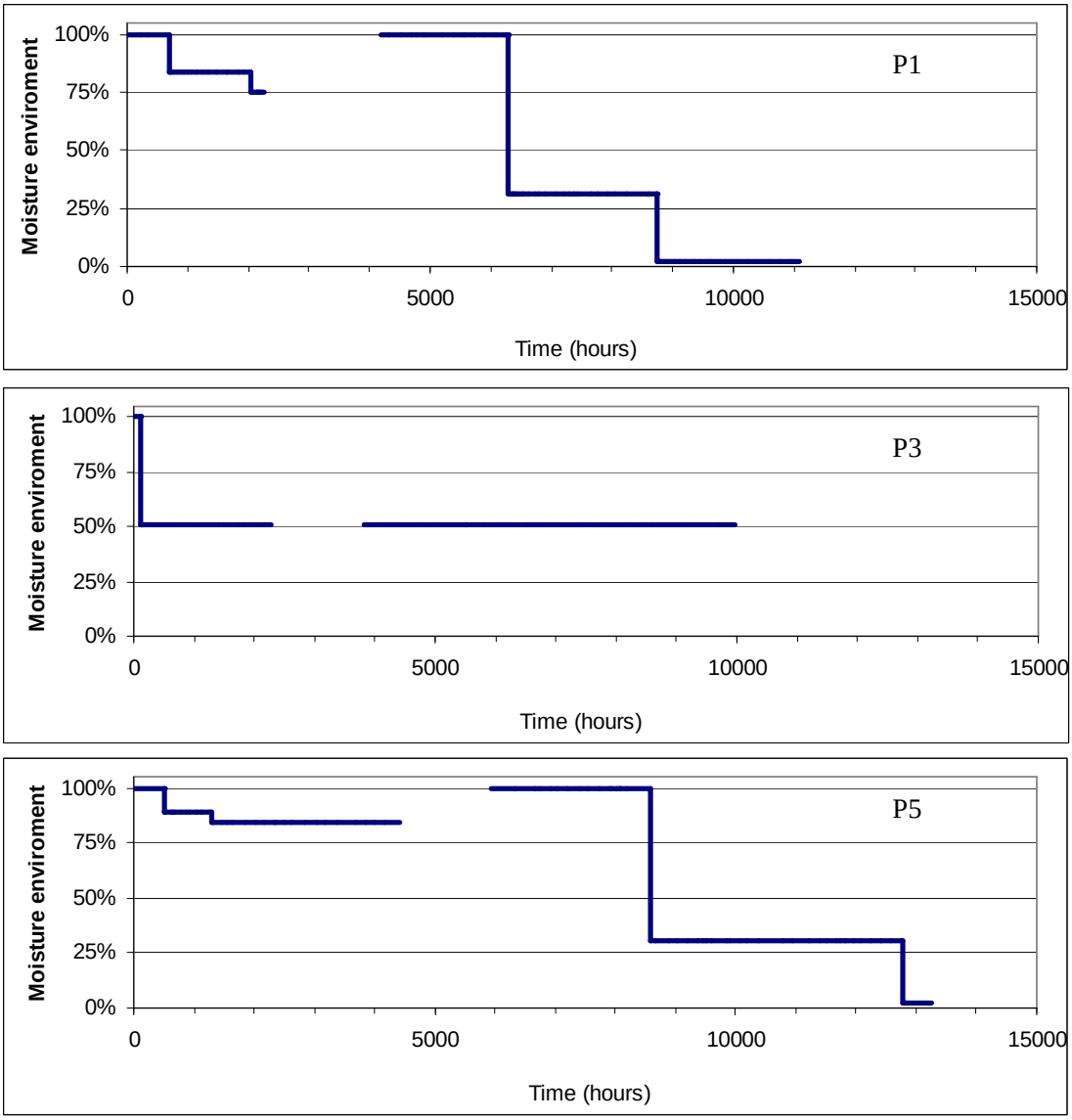

Figure 28. Moisture exposure history for P1, P3 and P5 families[7]

[7] The events at Virginia Tech on April 16, 2007 shut down Norris Hall, where the test setup was located, for approximately four months. No testing or monitoring of any of the tests was performed during this time. Moisture transport is time dependent and there is a gap in the data collected. P1 and P5 sensors were

3.4 Experimental results - Impedance spectroscopy

From observation of capacitance behavior, it is clear that at least two distinct trends are present between capacitance and resistance. For frequencies above 400 kHz and up to 10 MHz this relation closely follows a power law (Figure 29). Below 200 kHz, the power law does not capture the data unless most of the high moisture data is eliminated from the power law fit. Moreover, the behavior changes completely as shown in Figure 30. Capacitance changes rapidly from increasing positive values to increasing negative values in the inductive region.

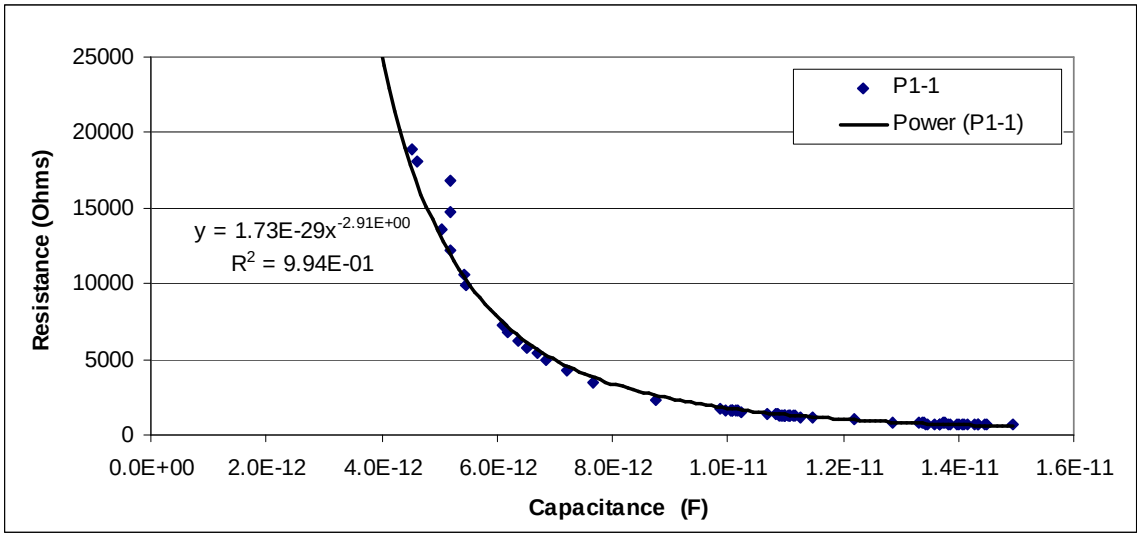

Figure 29. **Resistance relation to capacitance at 10 MHz**

transferred to a 100 % RH environment some time between April 16th and August 2007 but the time and date was not recorded.

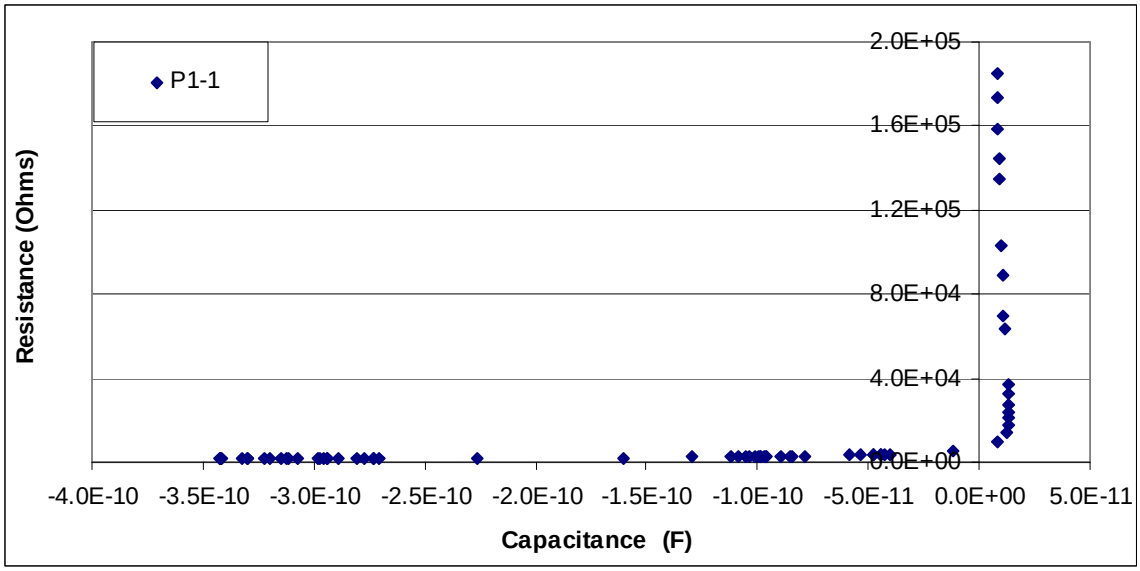

Figure 30. **Resistance relation to capacitance at 100 kHz**

In this chapter, experimental data included are for families P1, P3 and P5. However, seven (7) families of sensors have been manufactured and tested. Below is a plot of Resistance vs. Capacitance for all seven (7) families at 10 MHz (Figure 31). The data is not normalized and is given as a qualitative comparison that sensors' behavior for all families is very similar. However, a systematic analysis must be used to verify the similarities and/or differences between sensors and sensor families.

The relationship between capacitance and frequency is vitally important given resistance is related to capacitance through the power law relation. Capacitance exhibits at least two distinct behaviors with respect to mass change. Also, the relation of capacitance and frequency is a continuous function of moisture in the sensor. Figure 32 illustrates selected values of capacitance at different moisture levels. A log scale was used for the purpose of clarity. Specific values of minimum and maximum capacitance recorded for each sensor are listed in Table 13 through Table 15 for families P1, P3 and P3 respectively. It should be noted that steady state conditions have not been achieved at low relative humidity indicated for each table.

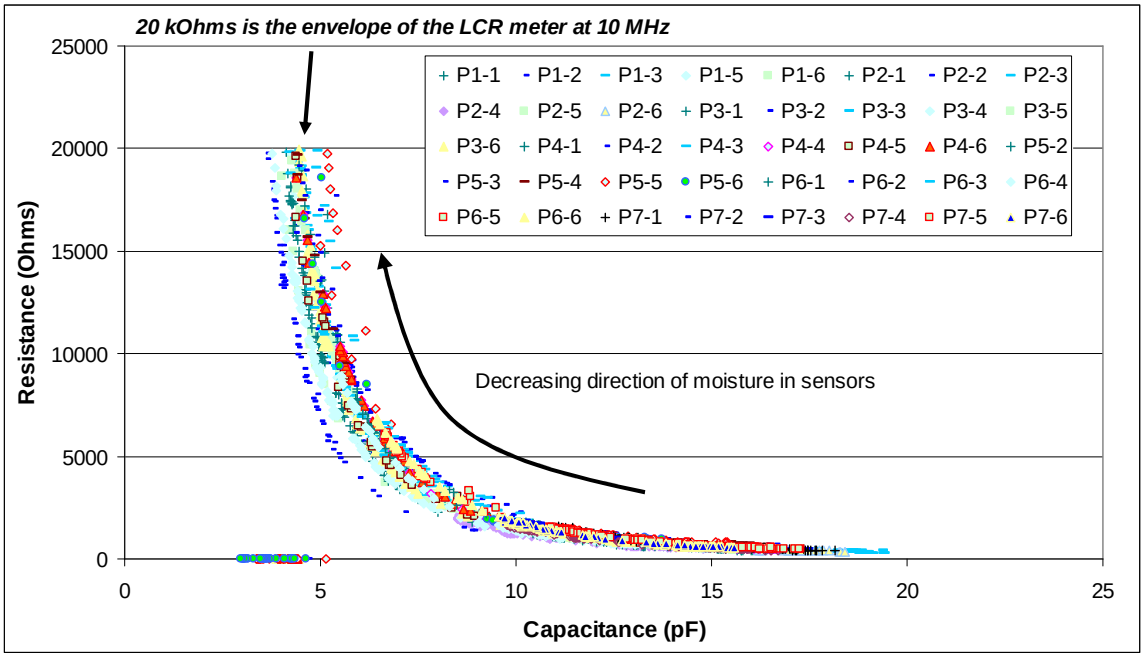

Figure 31. Resistance vs. Capacitance for all sensors in P1 through P7 families.

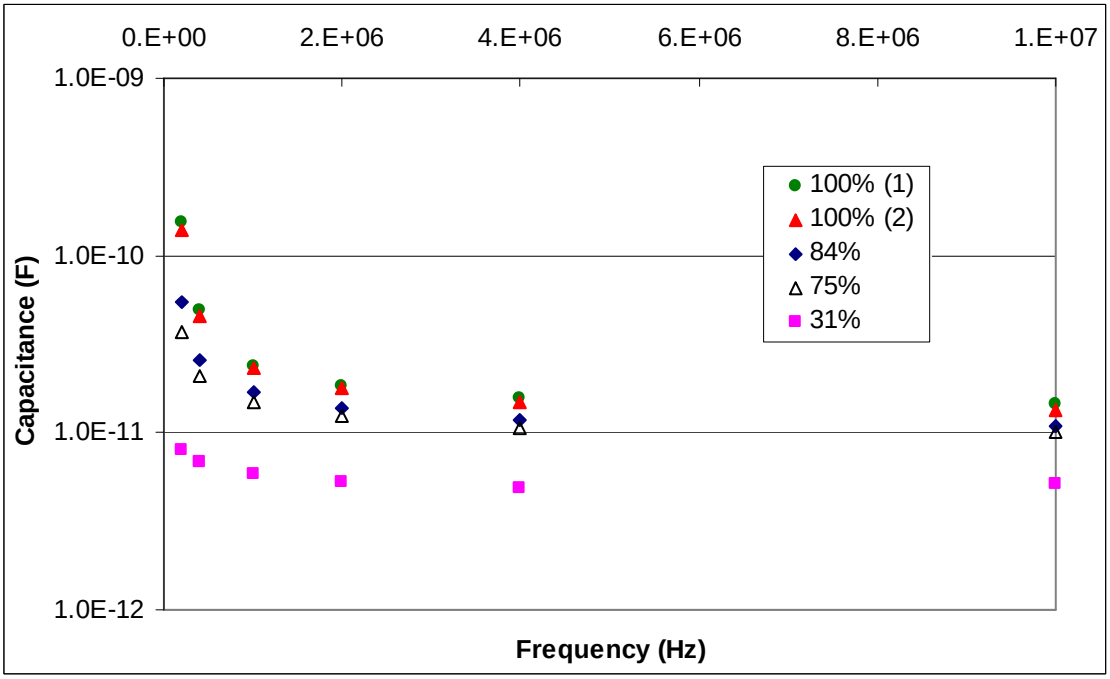

Figure 32. Capacitance-frequency response for P1-1

Table 13. **Family P1 range of capacitance values recorded (100% RH to ~2% RH)**

Frequency (Hz)	10E6	4E6	2E6	1E6	4E5	2E5
P1-1						
Maximum C (F)	1.49E-11	1.64E-11	1.93E-11	2.50E-11	5.23E-11	1.61E-10
Minimum C (F)	3.14E-12	2.76E-12	2.76E-12	2.79E-12	2.84E-12	2.88E-12
P1-2						
Maximum C (F)	1.42E-11	1.56E-11	1.89E-11	2.41E-11	4.34E-11	1.14E-10
Minimum C (F)	2.73E-12	2.39E-12	2.38E-12	2.40E-12	2.43E-12	2.46E-12
P1-3						
Maximum C (F)	1.94E-11	2.23E-11	2.65E-11	3.69E-11	9.89E-11	3.42E-10
Minimum C (F)	3.08E-12	2.71E-12	2.70E-12	2.74E-12	2.78E-12	2.81E-12
P1-5						
Maximum C (F)	1.41E-11	1.58E-11	1.88E-11	2.43E-11	4.63E-11	1.33E-10
Minimum C (F)	2.95E-12	2.57E-12	2.56E-12	2.57E-12	2.60E-12	2.63E-12
P1-6						
Maximum C (F)	1.17E-11	1.30E-11	1.59E-11	2.03E-11	3.11E-11	5.78E-11
Minimum C (F)	2.56E-12	2.23E-12	2.22E-12	2.22E-12	2.25E-12	2.28E-12

Table 14. **Family P3 range of capacitance values recorded (100% RH to 51% RH)**

P3-1	10E6	4E6	2E6	1E6	4E5	2E5
Maximum C (F)	1.10E-11	1.20E-11	1.43E-11	1.78E-11	2.94E-11	7.01E-11
Minimum C (F)	4.52E-12	4.42E-12	4.86E-12	5.49E-12	6.66E-12	7.85E-12
P3-2						
Maximum C (F)	8.76E-12	9.58E-12	1.12E-11	1.38E-11	2.17E-11	4.85E-11
Minimum C (F)	3.62E-12	3.51E-12	3.83E-12	4.28E-12	5.13E-12	5.99E-12
P3-3						
Maximum C (F)	1.25E-11	1.37E-11	1.63E-11	2.05E-11	3.52E-11	8.91E-11
Minimum C (F)	4.75E-12	4.58E-12	4.99E-12	5.56E-12	6.62E-12	7.68E-12
P3-4						
Maximum C (F)	1.21E-11	1.34E-11	1.60E-11	2.04E-11	3.70E-11	1.01E-10
Minimum C (F)	4.66E-12	4.74E-12	5.36E-12	6.23E-12	7.88E-12	9.67E-12
P3-5						
Maximum C (F)	1.42E-11	1.59E-11	1.88E-11	2.45E-11	4.93E-11	1.49E-10
Minimum C (F)	5.04E-12	5.03E-12	5.64E-12	6.49E-12	7.97E-12	9.46E-12
P3-6						
Maximum C (F)	1.13E-11	1.24E-11	1.47E-11	1.83E-11	2.91E-11	6.55E-11
Minimum C (F)	4.66E-12	4.49E-12	4.87E-12	5.42E-12	6.44E-12	7.46E-12

Table 15. **Family P5 range of capacitance values recorded (100% RH to ~2% RH)**

Frequency (Hz)	10E6	4E6	2E6	1E6	4E5	2E5
P5-2						
Maximum C (F)	1.57E-11	1.77E-11	2.13E-11	2.76E-11	5.20E-11	1.41E-10
Minimum C (F)	2.60E-13	2.30E-13	2.30E-13	2.10E-13	2.30E-13	2.50E-13
P5-3						
Maximum C (F)	1.66E-11	1.88E-11	2.27E-11	2.97E-11	5.59E-11	1.47E-10
Minimum C (F)	4.20E-13	3.80E-13	3.50E-13	3.80E-13	4.30E-13	4.70E-13
P5-4						
Maximum C (F)	1.60E-11	1.81E-11	2.26E-11	3.00E-11	5.46E-11	1.25E-10
Minimum C (F)	1.74E-13	1.80E-13	2.10E-13	2.10E-13	2.80E-13	3.40E-13

P5-5						
Maximum C (F)	1.54E-11	1.70E-11	2.10E-11	2.77E-11	4.92E-11	1.14E-10
Minimum C (F)	3.46E-13	3.20E-13	3.14E-13	2.70E-13	2.80E-13	2.90E-13
P5-6						
Maximum C (F)	1.54E-11	1.70E-11	2.10E-11	2.77E-11	4.92E-11	1.14E-10
Minimum C (F)	3.36E-12	2.93E-12	2.92E-12	2.95E-12	3.00E-12	3.04E-12

A mathematical function to capture the data must first represent the data over the whole range with reasonable accuracy. Simplicity is also desired. The function below can reproduce the experimental data, but it is complex and a large number of constants must be known (Equation 11). Having a mathematical representation of the capacitance change with respect to moisture and frequency can be used to explore the sensors behavior to gain further understanding of the parameters involved in the overall response.

$$C(f,x) = Exp(A(x) * f^2 + B(x) f + D(x)) \qquad \text{Equation 11}$$

Note that there is dependency on moisture (x) through A, B and D. Moisture dependency of A, B and D is presented in Figure 33 and Figure 34. Notice the similarity in the shape of the curves. A stretched exponential, hyperbolic tangent and polynomial are very good candidates. However, this suggests the need for more constants to capture the overall sensor behavior. A sample of calculated capacitance values using the above methods with respect to experimental data can be found in Figure 35. It should be mentioned that each function mentioned above does not represent the experimental data consistently. The double fit required to capture C(f, x) compounds fitting errors in addition to scatter in the experimental data. Since the capacitance-mass behavior has distinct regions, each one could be considered separately. Clearly, each region's boundaries must be defined. In addition, matching conditions between regions must be established for smooth transition. This represents a significant number of constants to be defined beyond A, B and D.

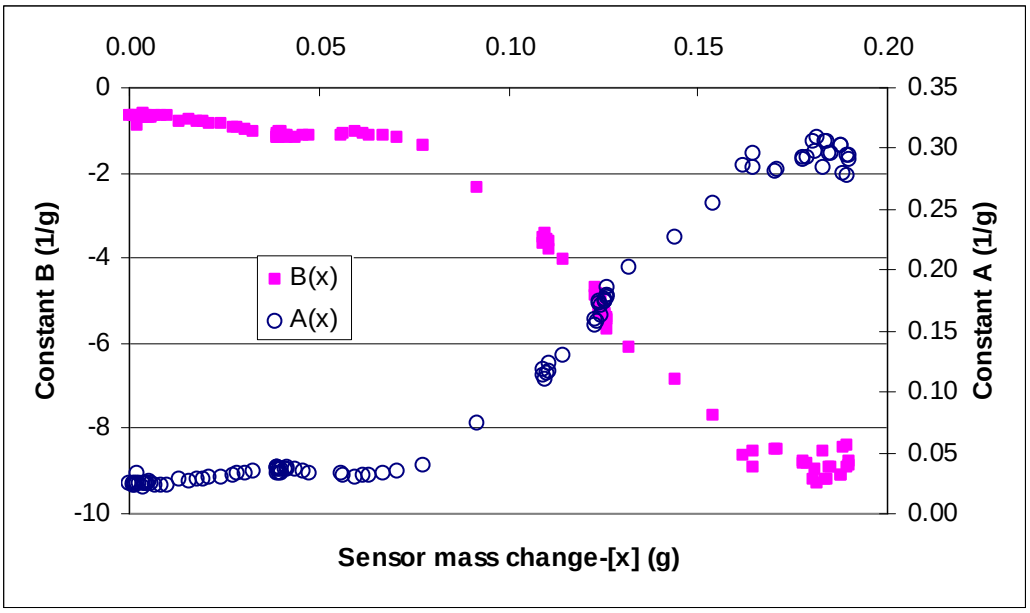

Figure 33. Dependence of A(x) and B(x) on moisture

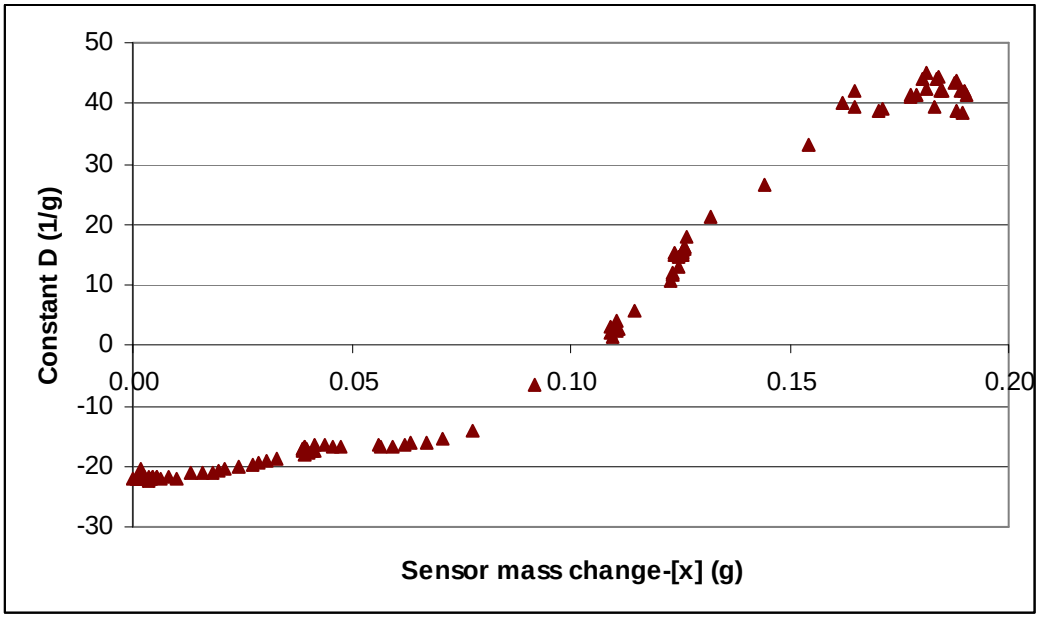

Figure 34. Dependence of D(x) on moisture

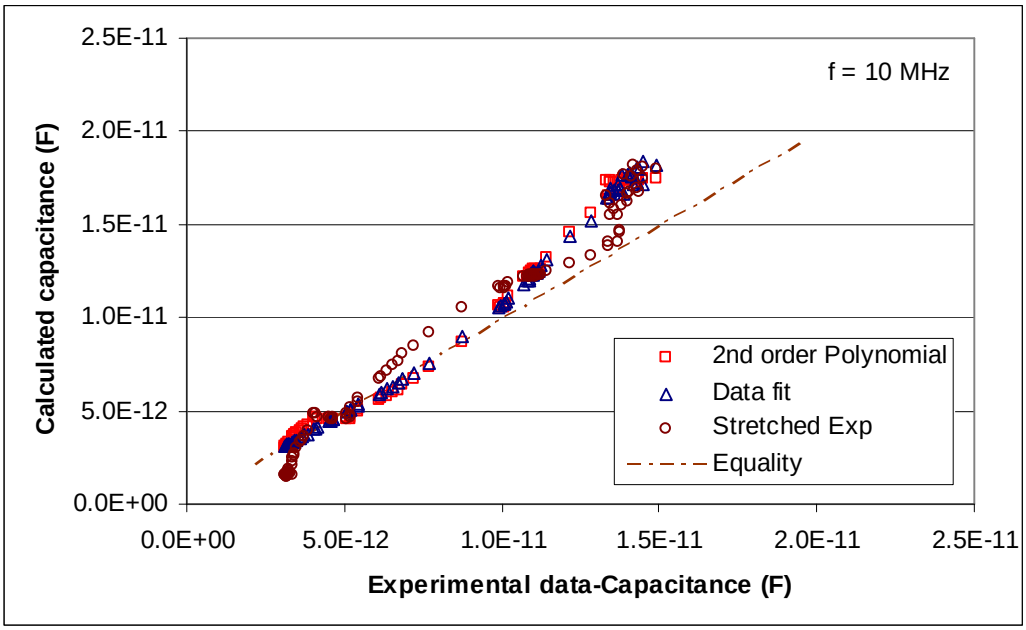

Figure 35. **Calculated capacitance compared to experimental values for sensor P1-1**

As previously noted, the relation between capacitance and resistance follows a power law relationship (Figure 19) and it can be mathematically represented by Equation 12. The values of m (exponent) and A (constant) are listed in Table 16 and Table 17 respectively for the range of 200 kHz to 10 MHz. The average m value for each family is plotted against frequency in Figure 36. The scatter in m values obtained is very small and compares favorably between families. The trend is similar and there is overlap of one standard deviation band for each family. On the other hand, the values for constant A vary by orders of magnitude.

$$R = \frac{A}{c^m} \qquad \text{Equation 12}$$

Table 16. **Exponent (m) from fitting the R-C data to a power relationship**

Frequency	1E+07	4E+06	2E+06	1E+06	4E+05	2E+05
P1-1	-2.910	-3.027	-3.014	-2.903	-2.270	-1.473
P1-2	-2.605	-2.814	-2.780	-6.145	-2.287	-1.545
P1-3	-2.772	-2.771	-2.762	-2.595	-1.941	-1.304
P1-5	-2.713	-2.868	-4.851	-6.413	-7.490	-1.543
P1-6	-2.481	-2.757	-2.659	-2.526	-2.376	-1.853
Average	**-2.696**	**-2.848**	**-3.213**	**-4.116**	**-3.273**	**-1.544**
St-Dev	**0.163**	**0.109**	**0.925**	**1.981**	**2.363**	**0.199**

P3-1	-2.960	-2.941	-2.987	-2.984	-2.704	-1.934
P3-2	-3.093	-3.054	-3.090	-3.077	-2.814	-2.780
P3-3	-2.952	-2.904	-2.913	-2.868	-2.538	-2.615
P3-4	-2.741	-2.721	-2.783	-2.765	-2.436	-2.248
P3-5	-2.817	-2.811	-2.891	-2.872	-2.399	-1.607
P3-6	-3.025	-2.945	-2.947	-2.913	-2.659	-1.958
Average	**-2.931**	**-2.896**	**-2.935**	**-2.913**	**-2.592**	**-2.190**
St-Dev	**0.131**	**0.116**	**0.102**	**0.107**	**0.162**	**0.445**
P5-2	-2.604	-2.797	-2.776	-2.663	-2.309	-1.668
P5-3	-2.682	-2.773	-2.744	-2.681	-2.296	-1.671
P5-4	-2.580	-2.670	-2.624	-2.560	-2.258	-1.708
P5-5	-2.908	-2.900	-2.897	-2.795	-2.429	-1.808
P5-6	-2.813	-3.017	-2.907	-2.799	-2.420	-1.803
Average	**-2.717**	**-2.831**	**-2.789**	**-2.700**	**-2.343**	**-1.732**
St-Dev	**0.140**	**0.132**	**0.117**	**0.100**	**0.077**	**0.069**

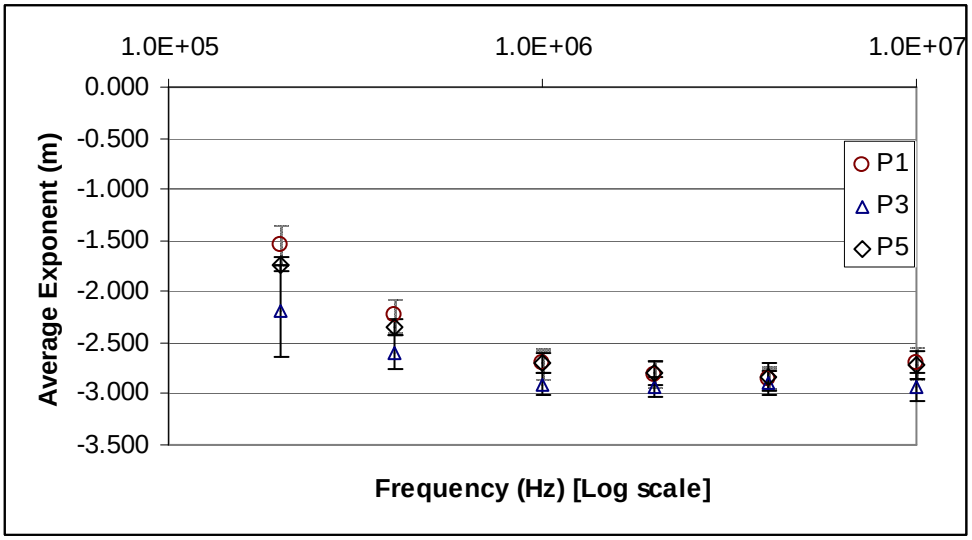

Figure 36. Average power law exponent from fitting R-C data. The error bars are calculated based on one standard deviation.

Table 17. Constant (A) from fitting R-C data to a power law relation

Frequency	**1E+07**	**4E+06**	**2E+06**	**1E+06**	**4E+05**	**2E+05**
P1-1	1.73E-29	1.71E-30	4.25E-30	1.39E-28	3.12E-21	2.81E-12
P1-2	3.69E-26	3.55E-28	1.55E-27	1.48E-26	1.79E-21	4.26E-13
P1-3	6.97E-28	1.41E-27	3.18E-27	4.15E-25	1.40E-17	2.10E-10
P1-5	2.45E-27	9.27E-29	3.62E-28	4.37E-27	1.43E-21	4.71E-13
P1-6	8.43E-25	1.45E-27	3.30E-26	1.75E-24	1.78E-22	1.66E-16
Average	**1.77E-25**	**6.61E-28**	**7.62E-27**	**4.36E-25**	**2.80E-18**	**4.27E-11**
St-Dev	**3.73E-25**	**7.11E-28**	**1.42E-26**	**7.54E-25**	**6.27E-18**	**9.33E-11**

P3-1	3.55E-30	1.08E-29	6.31E-30	1.35E-29	4.15E-26	2.25E-17
P3-2	7.90E-32	3.90E-31	2.98E-31	8.19E-31	1.79E-27	8.27E-27
P3-3	5.37E-30	3.32E-29	5.04E-29	3.04E-28	3.10E-24	7.86E-25
P3-4	9.46E-28	3.13E-27	1.26E-27	4.09E-27	4.38E-23	1.02E-20
P3-5	1.73E-28	3.90E-28	9.72E-29	3.13E-28	1.21E-22	9.21E-14
P3-6	7.62E-31	1.09E-29	1.96E-29	8.97E-29	1.35E-25	1.25E-17
Average	**1.88E-28**	**5.96E-28**	**2.39E-28**	**8.02E-28**	**2.79E-23**	**1.54E-14**
St-Dev	**3.77E-28**	**1.25E-27**	**5.00E-28**	**1.62E-27**	**4.85E-23**	**3.76E-14**
P5-2	4.66E-26	7.01E-28	2.18E-27	6.86E-26	1.35E-21	2.87E-14
P5-3	7.05E-27	1.40E-27	5.29E-27	4.87E-26	1.97E-21	2.70E-14
P5-4	8.67E-26	1.71E-26	1.01E-25	9.88E-25	4.68E-21	9.39E-15
P5-5	2.29E-29	5.38E-29	1.09E-28	2.69E-27	6.81E-23	9.18E-16
P5-6	2.49E-28	2.84E-30	8.37E-29	2.45E-27	8.37E-23	1.03E-15
Average	**2.81E-26**	**3.85E-27**	**2.18E-26**	**2.22E-25**	**1.63E-21**	**1.34E-14**
St-Dev	**3.80E-26**	**7.43E-27**	**4.46E-26**	**4.29E-25**	**1.89E-21**	**1.36E-14**

As previously noted, earlier values of impedance and phase angle were also collected. Typical results for impedance and phase angle for P1-1 are shown in Figure 37 and Figure 38. Typically, impedance is presented in a *Nyquist* plot which contains information of frequency, phase angle and impedance values. It is customary in EIS to change the sign of the imaginary part from negative to positive. This norm was applied in the results presented below. Notice the negative impedance values (inductive behavior) at high moisture levels and lower frequencies are consistent with the results for capacitance presented earlier. Additionally, the semicircles formed are either stretched or have their center below the real axis. The phase angle behavior is another view of how the behavior changes. For instance, the phase angle at 10 MHz changes gradually from approximately -90 degrees (capacitive behavior) down to mid thirties. On the other hand, at low frequencies the phase angle change is very sharp.

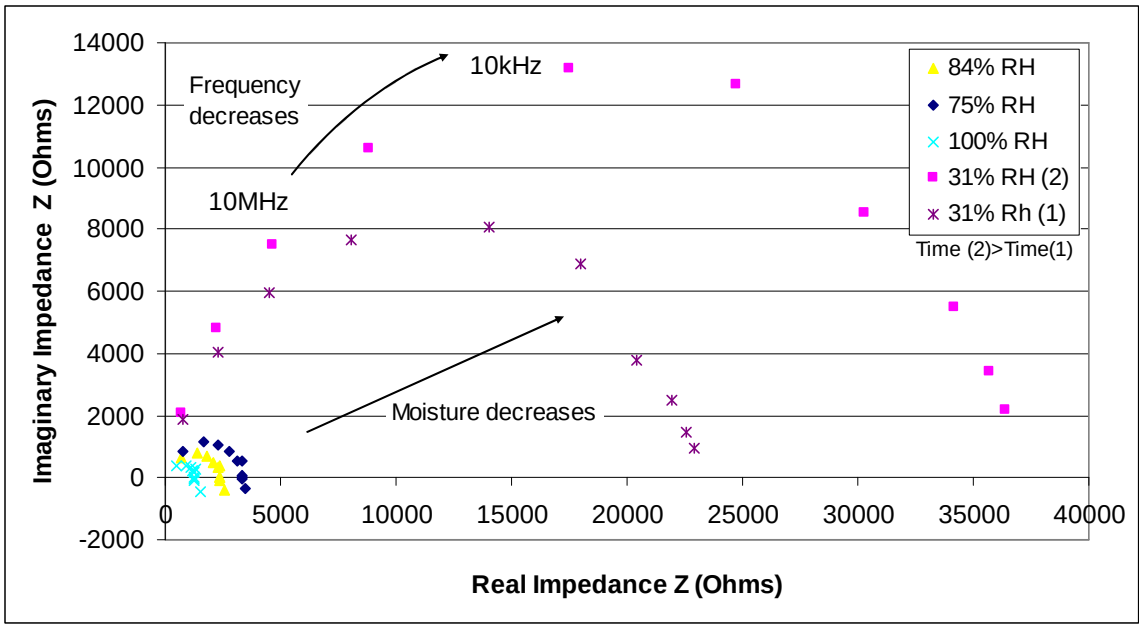

Figure 37. Selected values of impedance for sensor P1-1

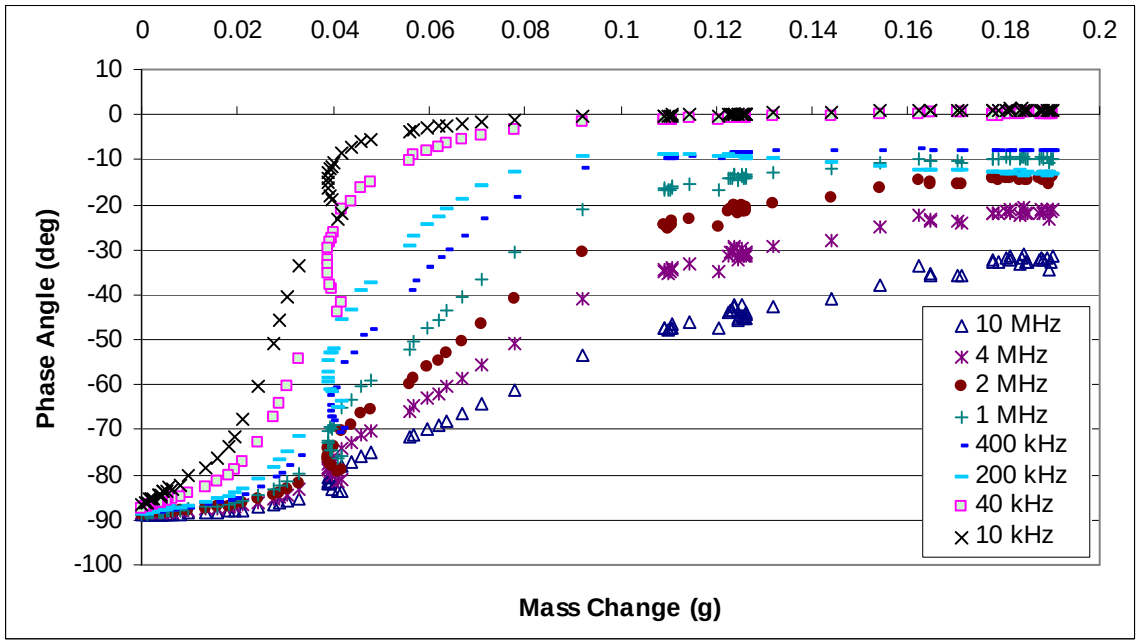

Figure 38. Phase angle for sensor P1-1

Figure 39 and Figure 40 show the real and imaginary parts of the impedance as calculated using the phase angle and impedance magnitude. Two different behaviors with the transition around 400 kHz frequency have been distinguished. Figure 39 is the typical behavior above 400 kHz. The peak in the real part

becomes sharper as frequency decreases towards the 400 kHz. At lower frequencies the real part is monotonically increasing as moisture drops (Figure 40).

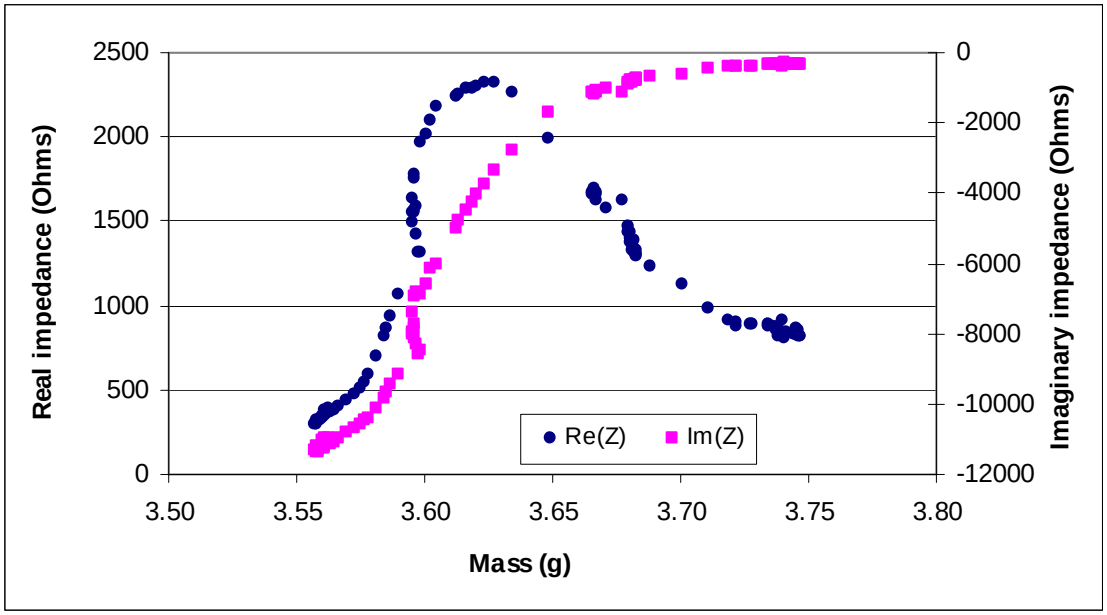

Figure 39. **Real and imaginary impedance for P1-1 at 4 MHz**

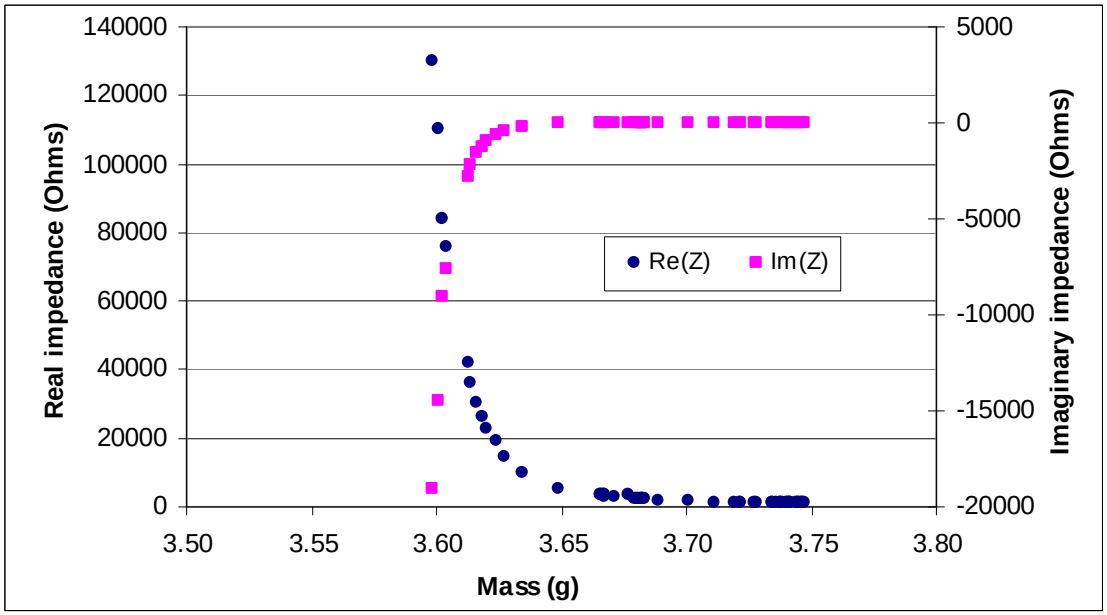

Figure 40. **Real and imaginary impedance for P1-1 at 10 kHz**

As described in Figure 16, the P3 family was transferred from a 100% to 51% RH environment. Slope 1 was calculated using data spanning approximately the first

1250 hours (T1) during which time the sensors spent in the 51% RH. The behavior of the P3 sensors through the rest of the time in that environment (an additional ~T2=7550 hours) a deviation from the single slope 1 behavior was observed. T1 represents 14.2% of the total time. The mass change through time T2 is of the order of 10% as can be seen in the Table 18:

Table 18. **Per cent mass change for P3 sensors conditioned at 51% RH**

	P3-1	P3-2	P3-3	P3-4	P3-5	P3-6
% Mass Change during time T2	9.45	9.25	7.85	2.38	10.07	9.31

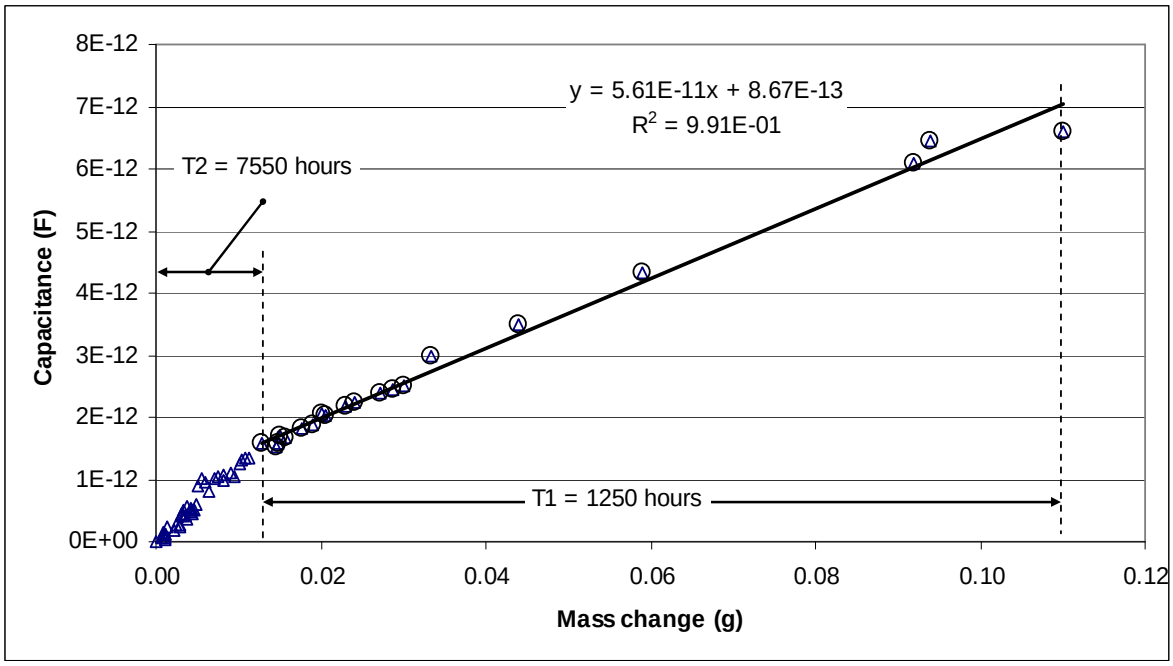

Figure 41. **Deviation from linear behavior for long term constant RH conditioning of P3 family. Representative sample P3-1 is shown.**

The change in the relationship between capacitance and mass may be an indication that secondary diffusion or other processes are taking place with the sensor. A similar phenomenon was also observed in P1 and P5 when samples reside for some time at low RH environment when transferred for a 100% RH (see Figure 20 around the 0.04 g mass change). Experiments using smaller %RH steps and long residence times at each step may provide additional information. Another possible cause of this deviation from the linear relationship

may be due to aging of the sensors, i.e., evolution of concrete microstructure due to hydration and/or carbonation. The observations from the moisture behavior in the sensors raise questions regarding moisture measurements in concrete using gravimetric methods to obtain moisture content. Using more aggressive techniques to dry samples may shorten the time needed to achieve equilibrium. However, changes to the microstructure may occur as indicated by measurements of surface area of samples dried using different techniques [37-39].

3.4.1 Temperature effects on measurements

The sensors were stored and conditioned in salt solutions enclosed environments. The conditioning chambers were kept in the lab environment where the temperature is controlled. The temperature varied between 20° and 27°C as recorded or observed over the course of th e study. The data reflects this range of temperatures. The relative humidity in an enclosed chamber with saturated salts solutions is temperature dependent. The variation of %RH with temperature is different for each salt used. Table 3 summarizes the salts used and the %RH for 15° – 30°C temperature range.

For some salts, the %RH dependency temperature is very mild in the temperature range considered. For example, for sodium chloride (NaCl) the %RH varies about 1% for temperatures between 15° and 35°C. For greater understanding of sensor behavior in relation to temperature variations, consider the definition of relative humidity (Equation 13).

$$\%RH = \frac{Pw}{Pws} * 100 \qquad \text{Equation 13}$$

Where:
%RH is the % relative humidity
Pw is the partial pressure of water vapor
Pws is the partial pressure of water vapor at saturation

Pw depends only on the amount of water vapor present in the air while *Pws* is temperature dependent as shown in Figure 42. Buck's suggested equation was used to calculate the saturation curve in Figure 42 [105]. If temperature increases, the relative humidity will drop given a fixed amount of water vapor. In the case of NaCl salt solution, the relative humidity is constant for the temperature range considered. In order to maintain constant relative humidity, water must evaporate from the solution into the air. When the temperature drops, water vapor in the air condenses and thus relative humidity does not change. In light of the fact that the sensors are in the chamber, some water will either enter or leave the sensors as the temperature changes for equilibrium with the environment to be maintained. Temperature increase suggests that more vapor is needed to maintain constant relative humidity in the chamber which means the water content of the sensors drops resulting in higher resistance and lower capacitance measurements.

This phenomenon is consistent with the overall sensors behavior and test results. The opposite occurs when temperature drops. Thus the relation between capacitance and moisture is related to the amount of water in the sensor and not the %RH. As previously noted, at steady state the capacitance can be linked to %RH. This suggests that measurements at one temperature could be used to predict the sensors' response at a different temperature for a given relative humidity environment. The temperature sensors used to measure temperature have a very small mass and adjust to moderate temperature changes quickly. Thus, there is discrepancy between the actual temperature within the sensor and the environment which is reflected in the data. Ideally, all measurements would have been performed at the same temperature. The above observation of relation between temperature, % RH and the measurements does not eliminate the need to establish sensor behavior both at higher and lower than room temperatures as other phenomena may be involved and activated at other temperatures.

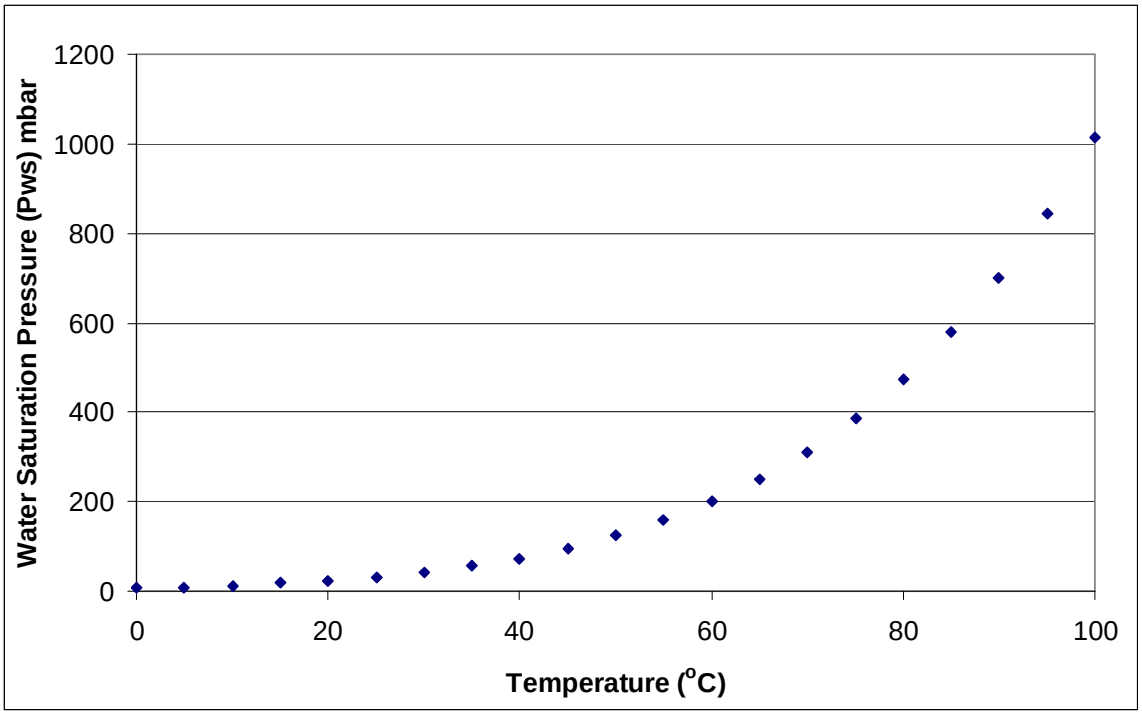

Figure 42. **Water vapor saturation pressure**

3.4.2 Experimental results and theoretical calculations for test setup validation

To establish the effects of geometry and experimental setup, commercially available capacitor and resistors were tested. The values obtained are within the tolerances of the components used. Additionally, sensors with glass fibers as the dielectric medium were manufactured at 3 different lengths. The capacitance followed linearly the increase in length as expected. Solid stainless and wire mesh conductors were tested in de-ionized water and in air to evaluate the effect of the wire mesh conductors. No significant differences were found (Table 19). Theoretical calculations based on the dielectric constant of air and water and sensor geometry will be discussed in the following section on dielectric constants. The LCR meter used has three different settings for the excitation voltage amplitude. Amplitude (no load) of 1 Volt was used in the experiments. Experiments at 0.1 and 0.01 Volts open circuit amplitudes produced identical results to the 1 volt amplitude used for all experiments presented in this work. This is necessary to ensure we are operating in the linear region with respect to

input and out put signals and that the values recorded are not influenced by the amplitude of the excitation signal.

Table 19. **Capacitance values obtained using two types of outer electrode**

	Type of outside contactor/dielectric medium				
	solid	wire mesh	solid	wire mesh	wire mesh
Frequency (Hz)	Air	Air	Water	Water	Water
10E6	7.09E-13	6.71E-13	4.94E-11	4.73E-11	4.65E-11
4E6	6.17E-13	5.84E-13	4.04E-11	3.93E-11	3.78E-11
2E6	6.07E-13	5.74E-13	4.01E-11	3.93E-11	3.76E-11
1E6	6.05E-13	5.73E-13	4.01E-11	4.03E-11	3.82E-11
4E5	6.05E-13	5.72E-13	4.10E-11	4.88E-11	4.34E-11
2E5	6.02E-13	5.70E-13	4.49E-11	8.42E-11	6.83E-11

3.5 Dielectric constants

To implement the power law, the constant and the exponent must be known to calculate resistance values from known capacitance or vice versa. Ideally, the dielectric properties of the constituents (water, sand, cement paste, air) and the geometry of the sensor are used to calculate capacitance and then resistance using the power Law. To this end, the constituents are known, however calculation based on their properties yield results that are not represented in the experimental results. It is reported that the relative dielectric constant of dry cement paste or concrete is about 10 or below [106, 107].Senor measurements in desiccant environment gave values between 2 and 5 for coarse (P1 family), fine (P5 family) and cement only sensors. Using the same electrode geometry as in the sensors and air or de-ionized water as the dielectric medium, the dielectric constants obtained are shown in Figure 43. A mild frequency dependency is visible in addition to the difference in dielectric values. Exploring this difference in reported and experimental values is very important. On the other hand, in comparisons of experimental values with theoretical calculation we can use the measured dielectric constants. Theoretical calculations used do not take into account end effects (fringing) or that water is self polarizing

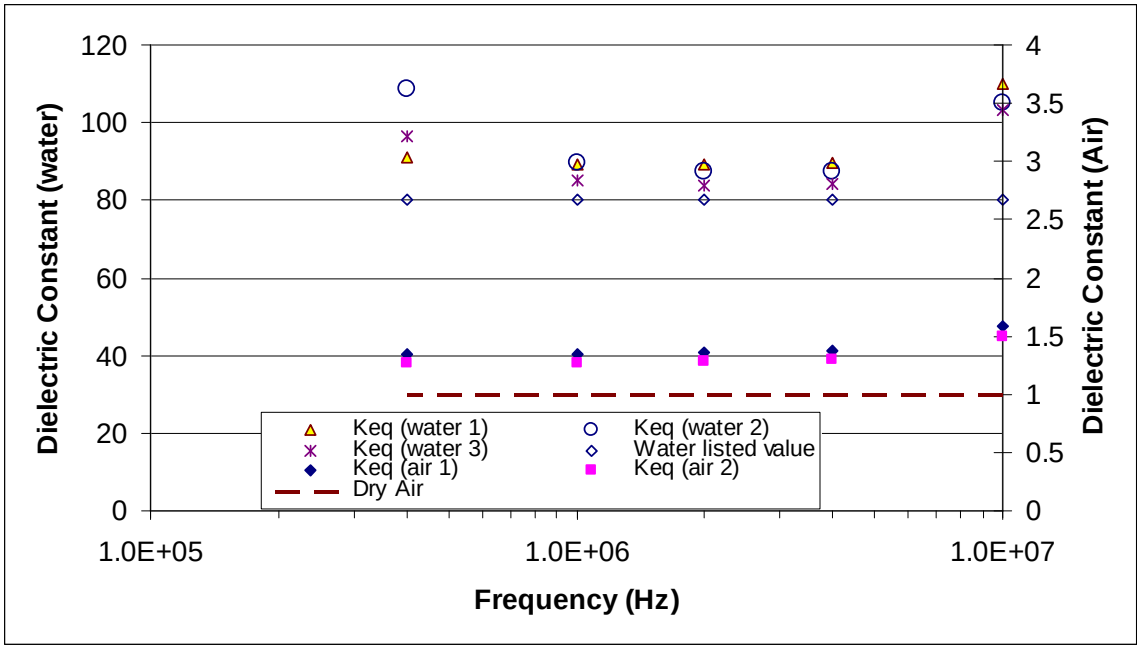

Figure 43. **Dielectric constants as measure using sensor geometry and electrodes**

As noted above, the dielectric constants of water, air and desiccant environment (< 5% RH) conditioned sensors were measured using similar electrodes and the same experimental setup. Specifically, capacitance was recorded and the dialectic constant was calculated using the equation for a concentric cylindrical capacitor (Equation 14) and the sensor geometry (Figure 3 and Figure 4). In calculating the dielectric constant as described it is assumed that the experimental setup behaves as an ideal capacitor. Usually the distance between electrodes is small compared to the surface area to minimize edge effects. For the sensor, the ratio of radius to length is approximately 0.25. To account for the discrepancy in measured and tabulated dielectric constants, a value of 110, 6 and 1.5 for water, cement and air respectively will be used for some basic comparisons. These values are the highest measured over the frequency range of 400 kHz to 10 MHz.

As will be illustrated, the enhanced values used cannot account for the large dielectric constants observed. Since we have at least two constituents, water and cement paste, a mixing rule must be employed to calculate the overall effect. At a minimum, any mixing rule used must be able to capture the measured effective

dielectric constant of the sensors conditioned in a desiccant environment. The specific condition was chosen since desiccant room temperature environment was one of the reference relative humidity environments selected for this study. The implied assumption is that that the dielectric constant will depend on cement paste only in this environment. A more aggressive drying environment was not considered due to the unknown effects on the concrete microstructure as discussed previously in chapter 1. There are numerous mixing rules mentioned in the literature. For example, Maron and Maron evaluated at least six mixing rules [108]. Using the geometry of the sensor, two mixing rules were used to calculate dielectric constants as a function of water volume fraction. Of course, the effective dielectric constant calculated with any of the mixing rules is not frequency dependent. On this basis, two separate figures will be used to illustrate major differences. Figure 44 shows the calculated dielectric constant based on the logarithmic mixing rule (Equation 15) and power law (Equation 16). The following plot (Figure 45) demonstrates the dielectric constants calculated using the sensor geometry and from experimental results for P1-1. The calculated values for dielectric constants fall short of predicting the experimental values except at zero moisture content which was the only criterion in selecting the mixing rules to be used (Figure 44).

$$C = \varepsilon_o * \varepsilon' \frac{2 * \pi * l}{\ln(b/a)} \qquad \text{Equation 14}$$

Where:

ε_o = 8.54×10−13 F/m (permittivity of free space)
ε' is the real dielectric constant of the dielectric medium in the capacitor
l – height of the cylindrical electrode
α – diameter of inner electrode
b – diameter of outer electrode

$$\ln(\varepsilon') = \sum_i vf_i \ln(\varepsilon'_i) \qquad \text{Equation 15}$$

$$(\varepsilon')^b = \sum_i vf_i (\varepsilon'_i)^b \qquad \text{Equation 16}$$

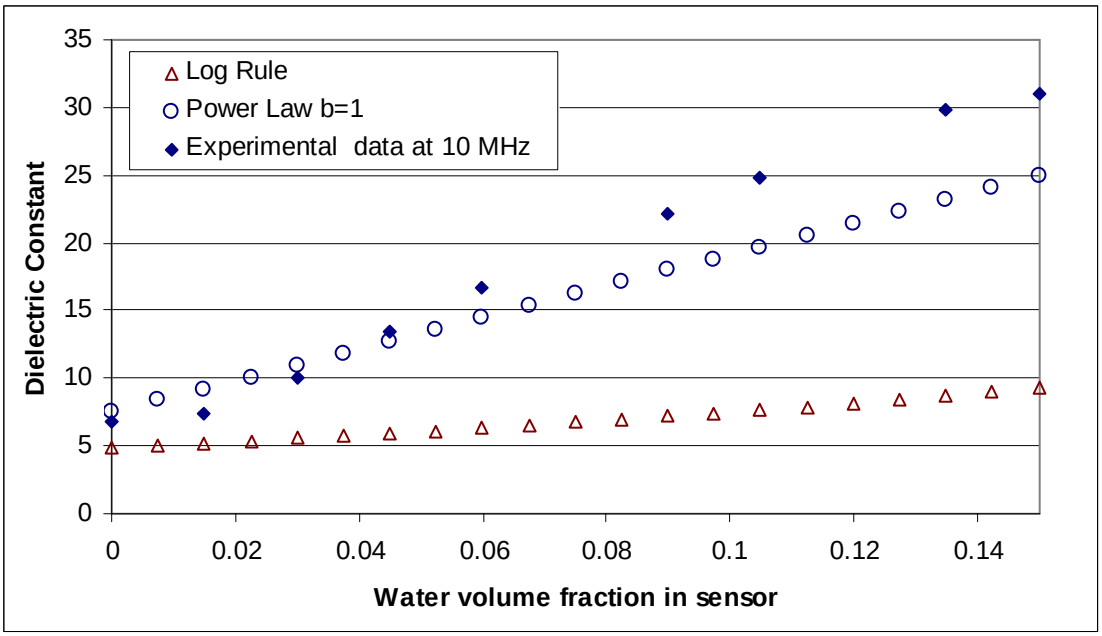

Figure 44. Mixing rules and resulting dielectric constants

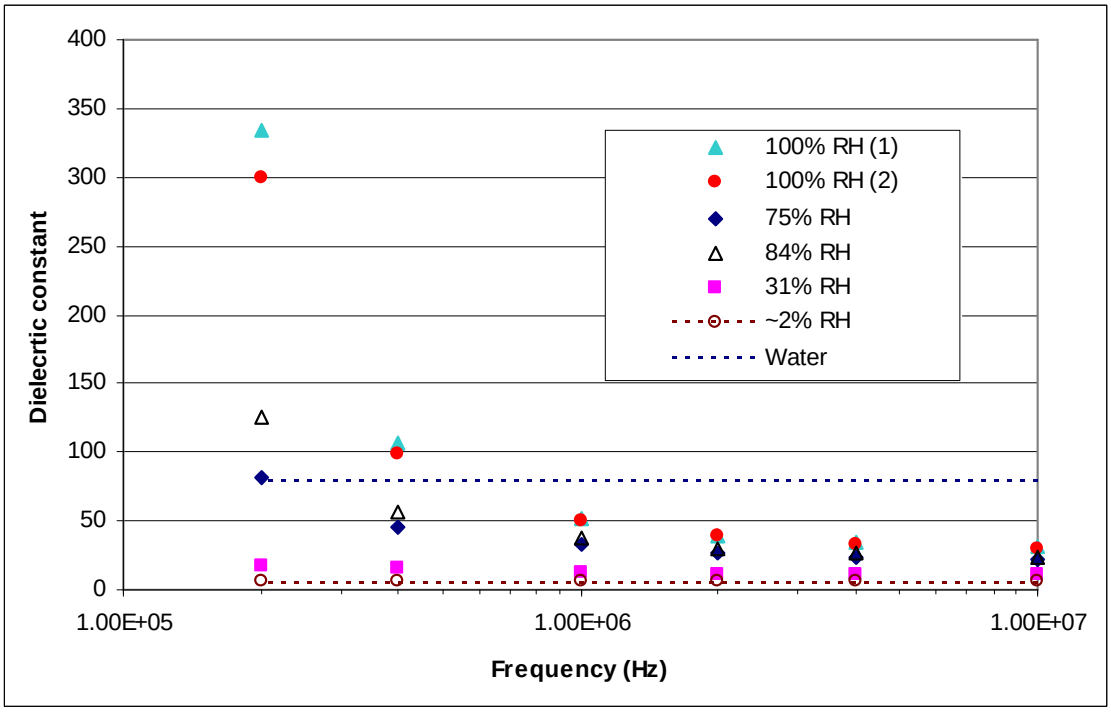

Figure 45. Calculated dielectric constants using experimental values and concentric capacitor geometry

3.6 Power Law and Universal Dielectric Response (UDR)

The power law has been used successfully to capture the behavior of insulating materials with conductive inclusions. This is the case of many composite dielectric materials and holds true for the case of the cement/sand dielectric medium used in the sensors. The experimental data (Resistance Vs Capacitance) in this work also exhibits power law behavior (Figure 29 and Table 16). Previously, we observed effective dielectric constants which are much higher than any of the constituents, especially at higher moisture levels (Figure 45).

The behavior of dielectric materials with respect to frequency follows in many cases the Universal Dielectric Response (UDR) [109]. It is also used to model conductance measurements with respect to frequency. The UDR states that the real part of the dielectric constant is proportional to $1/\omega^{(n-1)}$ and resistance is proportional to ω^n with n taking values between 0.6 and 1 in most cases [110]. In the experiments presented in this work, neither the capacitance (thus the dielectric constant), nor resistance follows the UDR behavior well. The frequency range considered was 400 kHz to 10 MHz given the behavior of capacitance changes dramatically below the 200 kHz. Throughout the range of moisture level in the sensors, the fit of the data to UDR equations is relatively poor with R^2 values below 0.9 in most cases. As moisture drops there is some improvement to the fit. The range of data available to evaluate the possibility of using the power function to represent the data at low moisture content is limited as the values of resistance quickly exceeded the instrumentation operating envelope.

3.7 Discussion

The experimental results indicate a direct relation between moisture in the sensor and the values of capacitance and resistance. Further, at steady state, the relative humidity environment used can also be linked to the experimental values as shown in chapter 2.

At steady state the mass change Δm is given by

$$\Delta m = s_m * \%RH \qquad \text{Equation 17}$$

s_m -- slope listed in Table 4

In addition the temperature effect can be introduced using Equation 18

$$\%RH = \frac{Pw}{Pws} * 100 \qquad \text{Equation 18}$$

Pws is a function of temperature (Figure 42).

The change in capacitance is related to mass changes both at steady and transient conditions via Equation 19. The resistance can be calculated from capacitance using Equation 20

$$\Delta C = S_i * \Delta m + I_i \qquad \text{Equation 19}$$

Where

S_i is slope1, slope1a or slope2 (Table 5, Table 6 and Table 7 respectively)

I_i is the y axis intercept (Table 8, Table 9 and Table 10)

$$R = A / C^m \qquad \text{Equation 20}$$

The above equations are valid for a single frequency as capacitance is frequency dependent. As an alternative to calculating capacitance for each frequency separately, Equation 11 can be used. The difficulty with Equation 11 is the large number of parameters that need to be defined. Reversing the process, i.e., estimating moisture based on capacitance and resistance measurements is possible if all constants in the above equations have been defined.

The behavior of capacitance to moisture changes is trilinear at lower frequencies (200 ~ 400 kHz) and bilinear at higher frequencies (1 ~ 10 MHz). Possibly, using

higher than 10 MHz excitation frequency signal may improve the relation between moisture and capacitance. Also, simple mixing rules may be able to capture the effective dielectric constant from measured values of each constituent. This is based on the observation that at 10 MHz the dielectric constant estimated by the power law mixing rule (Equation 16) was close to the experimental values. The maximum difference is about 30% when using the calculated dielectric constants of 110, 6 and 1.5 for water, cement and air respectively as explained earlier (Figure 44). If the tabulated dielectric constant values for water and air are used, namely 80 for water and 1 for air, the difference increases to approximately 65%. In both cases, the difference between calculated and experimental values increases as moisture increases.

3.8 Conclusions

Impedance spectroscopy techniques were used to explore moisture behavior of cement composite dielectric materials. The results indicate that resistance and capacitance are related through a power law relationship. The impedance behavior is similar for frequencies above 1 MHz and changes as frequency drops below this frequency. Multiple relaxations, i.e., time constants are present and the response changes from that of almost ideal capacitor at low moisture content to that of real capacitor with phase angle close to zero at high moisture content. The relation between moisture and impedance values is complex and cannot be captured by a simple mathematical expression. A frequency/moisture polynomial is proposed as way to represent the capacitance experimental values given measured water and dry hardened cement paste dielectric properties are not frequency dependent. However, moist cement paste properties indicate a strong frequency dependency. Due to the frequency effects, mixing rules cannot predict the effective dialectic response of moist cement paste.

Chapter 4

Random RC networks as a simulation technique for investigating the impedance behavior of moisture transport in concrete

Random RC networks as a simulation technique for investigating the impedance behavior of moisture transport in concrete

T. Theophanous, J.J. Lesko
MC 219, Virginia Polytechnic Institute and State University, Blacksburg, VA 24061, USA

Abstract

In chapters 2 and 3, experimental impedance spectroscopy response of hardened cement/sand paste was reviewed. In this chapter, random R-C circuits are used to capture features of the impedance response observed in the experiments. This type of modeling does not require specific information of microstructure geometry or properties at the individual microstructure feature. It has features of a lumped system with the benefits of a randomly created network. Simple geometric assumptions that modify the random R-C network values and layout are employed to represent moisture changes within the cement paste.

This paper will be submitted to Cement and Concrete Research journal

4.1 Introduction

Modeling the complex concrete microstructure poses many challenges due to the range of dimensional scales involved, the large number of hydration and products and the random nature of concrete. In many cases the actual composition is unknown as hydration reaction products vary depending on localized water/cement/sand composition and availability, temperature, and cure regime [21, 27]. Modeling attempts of concrete microstructure are mostly in the area of predicting strength, porosity and permeability [65-69]. In addition, models reviewed either lag evolution information or capture young concrete behavior. An additional difficulty is the specific properties of each element of the microstructure which cannot be defined unless the microstructure is known both with respect to dimensions and composition. This is even more important especially in the case of extensive properties like resistance and capacitance. In chapters 2 and 3, the impedance response of sensors based on dielectric properties of cement paste was presented. Impedance response of the sensors is a result of the lumped system, i.e., concrete microstructure and composition and separation of each individual element is not possible unless the microstructure is known. Even having specific information on concrete composition, geometry and properties, LRC circuits models (Inductors, resistors and capacitors) are used to capture the experimental results. Although impedance response poses the challenges mentioned above, it is a well established technique that can be easily applied both in the field and in a laboratory environment. In addition, the extensive nature of resistance and capacitance could be exploited in a modeling setting to capture impedance response of cement paste without knowing specific information on concrete microstructure.

4.2 Review of modeling of concrete behavior and microstructure

Numerous models exist that capture various aspects of the complex behavior of concrete. In assessing any model the reader has to keep in mind the numerous stages of cured concrete in addition to many variations of ingredients, age,

microcracks and curing conditions. Models developed for fresh concrete must be able to capture the behavior of excess water, large continuous pores and relatively fast evolving microstructure. Once concrete sets, the mobility of water is limited while the microstructure keeps evolving over several weeks. In addition, different chemical reactions take place at different times during the early life of concrete. Once the structure is exposed to the environment it will be affected by moisture and temperature variations, freeze-thaw cycles, deicing agents, other chemicals, and carbonation etc. The effects on concrete can be localized on the exposed surfaces, varying with depth or initiated within the bulk of the concrete.

Packed regular shape particles are one common way to represent concrete microstructure. Another model is parallel tubes sometimes interconnected. Computers have helped in developing more realistic models that can be incorporated into simulations. For instance, Garboczi, et al. used a random growth model to study w/c ratio, porosity, and diffusivity, among other processes. [64]. Olson, et al. used a computer model that relates impedance spectroscopy behavior to microstructure features of cement paste [65]. Chloride penetration has been modeled using the diffusion equation as mentioned in chapter 1 in the the section on transport of other elements. Holly, et al. used finite elements to solve the diffusion equation [66]. Some experimental data is required to obtain parameters used in the simulation. Solutions obtained from simulating concrete behavior fit the experimental data well. Manwart and Hilfer used Monte Carlo methods to create the microstructure of random media [67]. Manwant, et al. reconstructed the microstructure of two sandstones (Berea and Fontainebleau) using stochastic techniques [68]. The microstructure created was displayed side by side with actual pictures taken of the stones. Models of this nature could be adapted for concrete.

Navi and Pignat simulated hydration for cement and obtained porosity and pore radius distribution at different hydration periods [69]. This modeling did not depend on experimental data. As in many other case of modeling concrete microstructure and behavior, no comparison with experimental data was

provided. Models always try to capture known features. Obtaining realistic models that mimic the micro-structural behavior of concrete is challenging given its complexity and variability. As mentioned earlier the fact that resistance and capacitance are extensive properties could be used to explore concrete impedance response.

4.3 Modeling using random R-C network circuits and simulation

Motivation

The experimental results from the sensors have illustrated that the relation between moisture and capacitance/resistance is very complex (Chapter 1 and 2). The reasons for this behavior are not well understood. For example, the dielectric constants of water and dry sensors exhibited very little frequency dependence. When combined, i.e., moisture increased in the sensor, the dielectric constant increased as frequency decreases. This amplification was larger for higher moisture content (Figure 43, Figure 45). The interaction between water and cement microstructure is as difficult to understand as the cement microstructure it self. Hydration products are of the order of nanometers while fine aggregate used in the sensors have dimensions in millimeter range. Creating a model that will span this range of dimensions and also contain specific information on the variety of compounds found in cement paste is probably unrealistic. Models that have recreated concrete microstructure have been developed based mostly on geometry features of porosity and permeability [111, 112]. Chemical interaction and the behavior of water in the pore structure are still unknown. Recreating the microstructure of sensors could serve as a platform to validate and explore further the experimental results. Another option is to use basic principles and definitions of capacitance and resistance, RC networks and impedance spectroscopy within the range of frequencies used in the experimental portion of this project (200 kHz to 10 MHz). This can serve as a tool to connect the experimental result to basic principles and definitions rather than verifying the experimental results.

4.4 Impedance spectroscopy, cement and random R-C networks

Impedance spectroscopy (IS) measurements can be very difficult to interpret unless there is a good understanding of the physics of the samples being tested. IS data can be represented with numerous models and selecting a specific model should reflect features of the material tested. The sensors were experimentally tested as capacitors and the basic capacitor model will be the starting point. Mathematical models for real capacitor contain ideal capacitors in conjunction with resistors. One of the simplest and commonly used models is shown below in Figure 46.

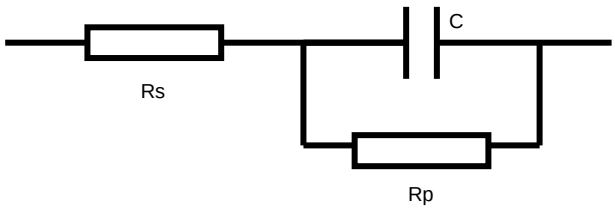

Figure 46. **Model of real capacitor**

A model similar to the above is also used internally by the LCR meter in the experimental portion of this project to calculate values of capacitance and resistance (Rs=0). The simplicity of this model makes it very attractive. This model will produce a perfect semicircle in the complex impedance plane. The center of the semicircle will be on the real axis and its diameter is equal to Rp. The center is located at distance Rs+Rp/2 on the real axis. In many real cases, the rise of a perfect semicircle in impedance measurements may be the exception. Incomplete, skewed, depressed and semicircles with partially straight line portions are commonly observed [103]. Besides the basic elements of resistance, capacitance and inductance other elements have been developed to capture behavior observed in experimental work, such as Warburg, constant phase element (CPE), Williams-Watts fractional element and transmission line [103].

The experimental results indicate that the center of the circle is below the real axis (Figure 47) for data not crossing the real axis. To account for this, the ideal capacitor in the simple model shown in Figure 46 can be substituted with a constant phase element. A CPE will yield a straight line in the complex impedance plane. The combination of a resistor in parallel with a CPE is also known as ZARC [113]. The depressed behavior is attributed to dispersion of activation energies which causes distribution of time constant (RC) [103, 104]. The CPE does not have a physical analog, meaning that this is a mathematical tool to fit the data [103].

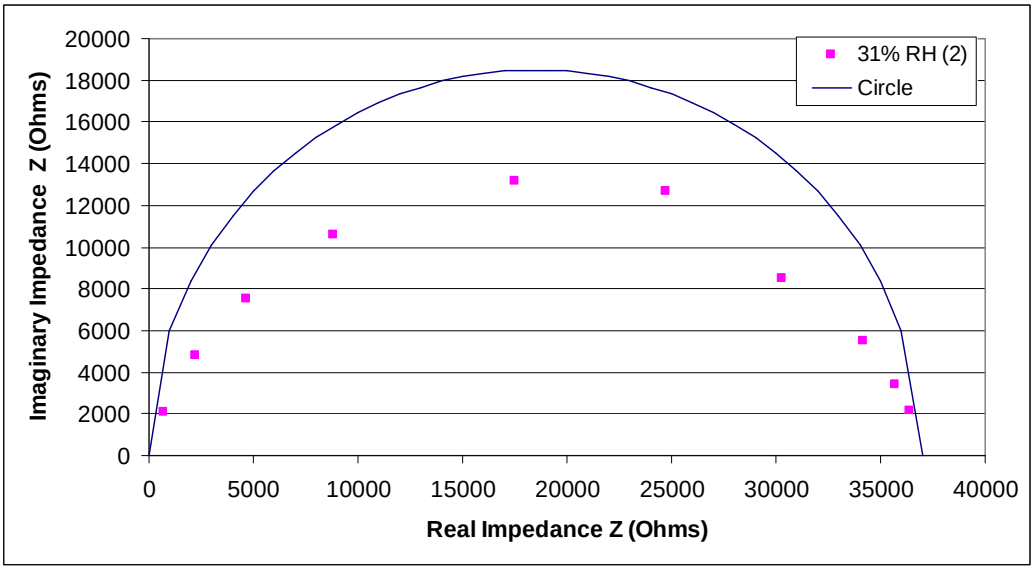

Figure 47. **Depressed semicircle from experimental data**

Considering a distributed time constant, the depressed semi-circle can be achieved by connecting in series a number of circuits shown in Figure 46. Note that Rs was set to zero since it will only move the center of the semicircle on the real axis. Below is the comparison between a single circuit and ten circuits with varying values of resistance Rp (Figure 48):

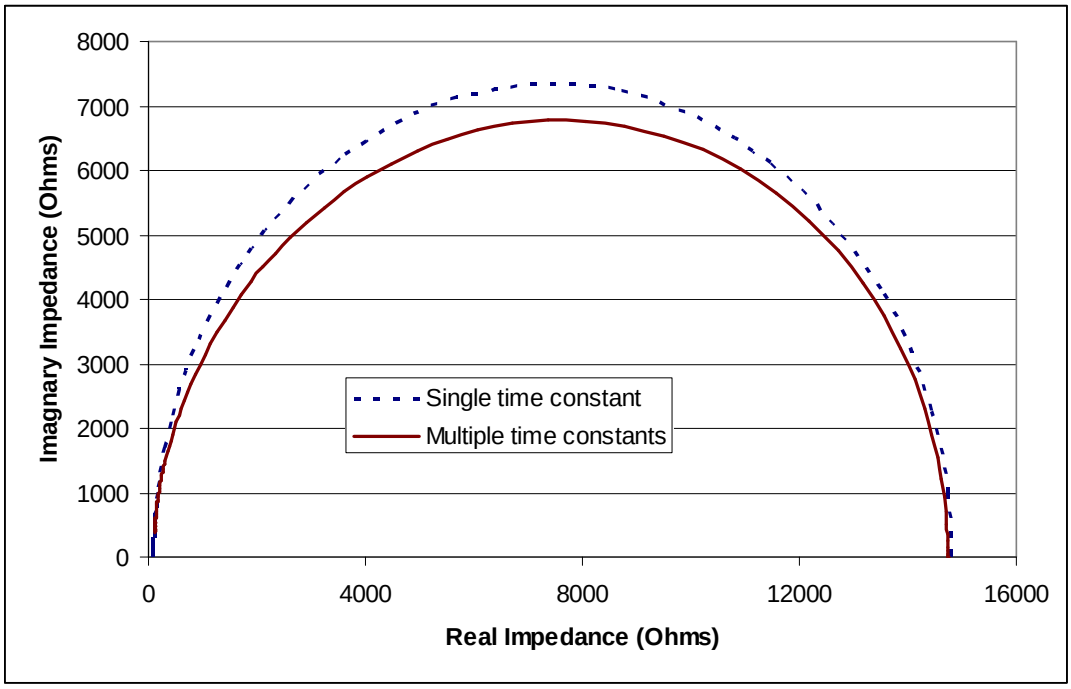

Figure 48. **Distributed time constants behavior in comparison with a single time constant R-C circuit**

The idea of distributed time constants is very appealing. First, the experimental data suggests the presence of distributed time constants which suggests multiple R-C circuits. The second reason comes from the cement microstructure. As will be explain later, there are a number of chemical compounds forming during the hydration process in addition to aggregates, voids, pores and pore solution, micro cracks and regions of ITZ. Each of these elements has its own impedance depending on its geometry and composition. That is to say a void will have different impedance spectroscopy response than an aggregate etc. Clearly, concrete microstructure is random with respect to the locations of aggregate, voids etc. A conclusion that can be drawn is that the impedance spectroscopy behavior of concrete is a product of a 3D R-C network. This 3D network represents the pores and pore interconnectivity in conjunction with different cement and sand particles and grains. Vainas and Almond, and also Panteny, et al. used random RC networks explore the Universal Dielectric Response (UDR) [110, 114]. Bowen and Almond utilized R-C networks to predict the dielectric response of ceramic composites having distinct conductive and capacitive phases [115]. The experimental data obtained from testing the sensors does not

follow the UDR which stipulates that materials have the real part of the dielectric constant proportional to $1/\omega^{(n-1)}$ and their resistance proportional to ω^n [110]. However, the trends of capacitance and resistance are similar to UDR. While cement has many phases (insulating aggregate, conductive pore solution, calcium silicate hydrate etc), random R-C networks may provide some insight into sensor behavior. There are many challenges in testing this hypothesis:

1) Properties of individual particles, aggregates and chemical compounds
2) Distribution of the elements (hydration products, voids, aggregate etc) in concrete
3) Connectivity with respect to a 3D RC circuit
4) Values of individual resistors and capacitors
5) At what scale is the model to be created since concrete particle span many decades with respect to size?
6) What is a representative volume element?

Determining appropriate responses to these questions pose difficulty. The above reveals that either no information is available or information is for an element in isolation. For instance, specific properties of cement and sand particles can be obtained. A review of the ASTM C 150 standard on Type I and II cement powder shows that cement powder does not have a precise composition [19]. As an example, Type II may contain up to 6% Aluminium oxide (Al_2O_3), up to 6% Ferric Oxide (Fe_2O_3), and Magnesium Oxide (MgO). The harden cement paste will naturally reflect the composition of cement powder. Besides variability in cement powder, when cement hydrates the products vary widely from the stoichiometric predicted compounds [21]. Thus, specific properties relating to cement microstructure are not available unless a specific sample of harden cement paste is analyzed. Extending this reasoning to the connectivity of a 3D network, values of R and C and the representative volume element can be inferred that these quantities cannot be explicitly defined.

Answers to the above challenges either a) do not exist or b) there are many possibilities. As noted previously, a different approach will be used to address some of the questions raised above.

4.5 Rationale for the development of a random R-C network

Instead of seeking specific properties for each element in harden cement paste in relation to the microstructure, the microstructure properties and features will be represented with a random R-C circuit. This method will illustrate the capability of representing a wide range of resistive and capacitive properties without knowing specific information on the microstructure or composition.

The approach in creating a random RC network is based on the following assumptions. The assumptions stated below will be discussed thereafter. Note that there are three circuits that will be created; Circuit AB is built with unit circuits A and B.

Circuit AB assumptions:

1) This circuit will be 2D for simplicity
2) A parallel plate configuration
3) The experimental values of Z, R, C and Θ at 10 MHz will be used to tune the circuit without being an input to the simulation
4) Phase angle close to -90 degrees at zero moisture content (almost ideal capacitor behavior)

All other assumptions applicable to circuit AB, come from circuits A and B.

Circuit A assumptions:

1) Locations of either C or R elements is random
2) Random values of capacitance and resistance will be assigned. The specific values for C and R will have a Normal (Gaussian) distribution.

Circuit B assumptions:

1) The specific values for C and R will have a Normal (Gaussian) distribution.
2) The change in values for C and R in circuit will follow a linear change with the resistance decreasing and capacitor increasing with moisture uptake.
3) As moisture in the sensor increases, elements with ideal capacitor behavior (C) will change to real capacitor behavior (R-C). The R-C elements will be parallel (Figure 46 with Rs=0)

4.5.1 Discussion on the assumptions

4.5.2 Circuit AB

The first assumption for circuit AB is the 2D nature of the RC network. Clearly, cement microstructure is in 3D. Resistance and capacitance are extensive properties (Equation 21 and Equation 22). The area (A) in both capacitance and resistance can be assumed to be equal to 1. Units are not important here as resistance and capacitance values will not be calculated using Equation 21 and Equation 22. The other reason for using 2D is the simplicity to form the random R-C and solve the resulting circuit.

$$C = \varepsilon' \varepsilon_o A/d \qquad \text{Equation 21}$$

where
ε_o = 8.54×10−13 F/m (permittivity of free space)
ε' is the real dielectric constant of the dielectric medium in the capacitor
A – area of electrodes
d – distance between electrodes

$$R = \rho L/A \qquad \text{Equation 22}$$

where
ρ – resistivity of the material
L – length
A – cross sectional area

The parallel plate configuration is used based on the assumption that the behavior is a product of the microstructure and not the overall sensor geometry. This is supported by the experimental results where both parallel plate and concentric capacitors showed similar response.
The need for tuning the simulation arises from the fact that both resistance and capacitance are extensive properties as noted earlier. In addition, the scale between the random R-C circuit and the sensor is unknown since each R and C element is not directly related to a specific micro structural feature in cement paste. To be able to qualitatively compare the simulation and experimental results, the simulation results will be scaled using experimental values of Z, R, C

and Θ at 10 MHz. These values are not directly an input to the simulation. The input to the simulation is adjusted so that the output is of the same order of magnitude as the values mentioned above.

The phase angle requirement of nearly -90 degrees is directly related to the experimental observations. The data showed that at low moisture content, the phase angle was close to -90 degrees independent of frequency (Figure 38).

4.5.3 Circuit A

The random assignment of locations for R and C assumption is based on the random nature of cement paste. Hydration products vary depending at least on the stage of hydration, temperature and w/c ratio [27]. If aggregated, as in the case of the sensors, the sand particles have different sizes and composition and are randomly located within the cement paste. Aggregates also contribute to the formation of interfacial transition zone where, due to the wall effect, a higher water to cement ratio exists [23]. Water to cement ratio is directly related to porosity. Scivener, et al. impregnated concrete with Wood's metal and found higher porosity at the paste aggregate interface [23]. In addition, the ITZ is not a uniformly distributed or a very clearly defined zone [24]. Randomly locating C or R elements is done in an effort to capture both resistive and capacitive elements in cement paste with aggregate. The ratio of C and R elements has an effect on the overall circuit behavior [110]. As will be shown later, there are a large number of parameters that need to be defined for the model to be developed. To simplify and reduce the unknowns the ratio of C and R in will be kept constant at 1:1. The second assumption for *circuit A* is the specific values resistance and capacitors will have. As noted earlier, there is a wide variety of features and elements in cement paste. Since specific information on electrical properties of each element in a branch is not available, the values for R and C will be assigned randomly under the constraint that in each row, the values of all resistors have a Normal (Gaussian) distribution. The values are not necessarily in order with respect to the x coordinate of the branch. The same applies for the capacitors.

The distribute values of R and C allow the modeling of many feature in cement paste without knowing specific information about dimensions and properties of elements of cement microstructure. Each R and C values can be thought to be a product of the composition and dimensions of a particular grain etc. For instance, a large capacitance value can be interpreted as a particle with high dielectric constant or a particle with large area and small thickness.

4.5.4 Circuit B

For circuit B the first assumption is about the values of Resistance and capacitance. The same reasoning applies as in the second assumption for *circuit A*. A different scaling factor than in *circuit A* is used in this case.
The second assumption is that resistance and capacitance change linearly with moisture which is based on the definition of resistance and capacitance. Resistance is inversely proportional to the cross sectional area while capacitance is proportional to the cross sectional area of the electrodes. As pores in the cement microstructure fill with water only the area (increases in the case of pore filling) can change as the length between the two electrodes is fixed. The implied assumption is that the filling process is uniform. In addition, pores have some regular geometry and are aligned with the circuit elements. Other processes are not considered.

The circuit morphing, i.e., the change of elements from C to R-C in circuit B, is assumed to occur due to deviation from the ideal capacitor behavior as moisture increases. The ideal capacitor does not have any resistors in parallel or in series. As moisture increases the experimental results indicate deviation from the ideal capacitor behavior which is represented with a parallel resistor (Figure 46 with Rs = 0). The series resistor is set to zero because it only shifts the R-C behavior on the real axis without altering the radius of the semicircle.

The effort with the assumptions discussed above was not to restrict the simulation, but rather to give just enough information to create the RC network,

set up the problem mathematically and obtain solutions. Using basic definitions of resistance and capacitance the microstructure of cement can be created from the electrical point of view with the assumption stated above. The random RC network layout will be analyzed next.

4.6 Random R-C network

Using the observation that concrete is a random material two random RC circuits will be created. The reason for creating two circuits is based on the fact that aggregates absorb very little moisture. Moreover, close pores and possibly other portions of cement microstructure may not exchange moisture. Thus circuit A will not be affected by moisture whereas circuit B will change as moisture increases or decreases. Circuit A and B will be combined in parallel between nodes (Figure 49) to create the circuit AB to be analyzed. The building block, unit circuit, is shown in Figure 50. The layout of circuit AB is described in Figure 51. The AB circuit is square, i.e., it has equal number of unit circuits in the x and y directions. Each branch of a unit circuit has a box representing the total impedance between the two nodes. The impedance value depends on the element from circuit A (either C or R) and the element from circuit B that are combined in parallel in each branch. The element from circuit B will be either C or an RC parallel combination. The decision process and diagram for circuits between nodes is given in Figure 49. Subscript “c” in Figure 49 is for constant values of R and C with respect to moisture change and “cw” is for the circuit that is affected by moisture.

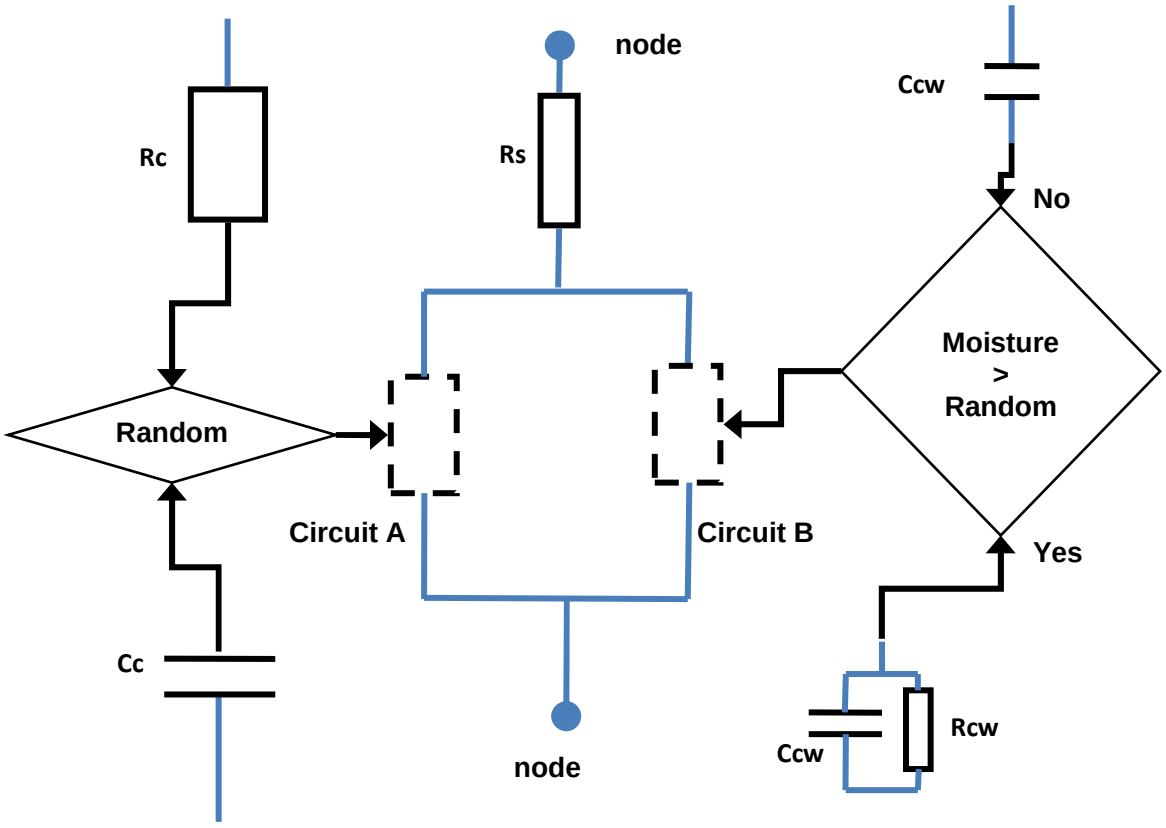

Figure 49. Branch schematic and decision process

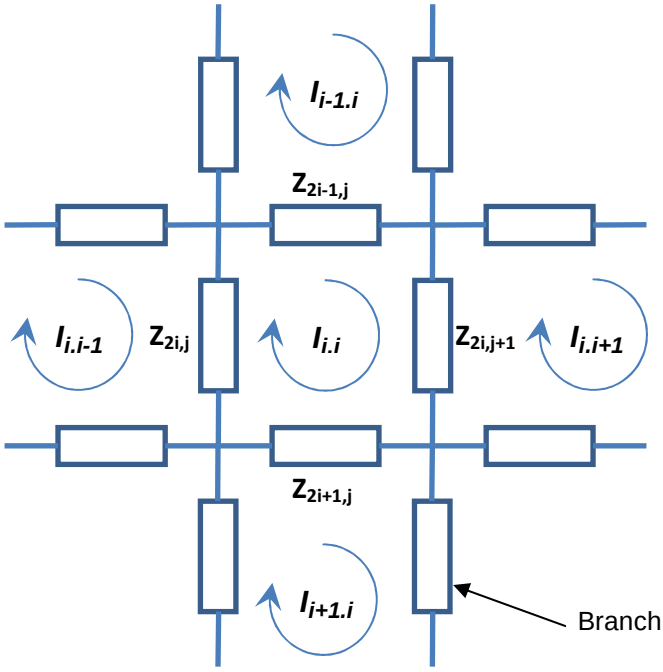

Apply Kirchhoff's voltage law

$$\Sigma V_{i,j}=0$$

```
Z[2 i - 1, j]*(I[i, j] - I[i - 1, j]) +
Z[2 i, j + 1]*(I[i, j] - I[i, j + 1]) +
Z[2 i + 1, j]*(I[i, j] - I[i + 1, j]) +
Z[2 i, j]*(I[i, j] - I[i, j - 1]) = 0
```

Figure 50. Details of unit circuit AB

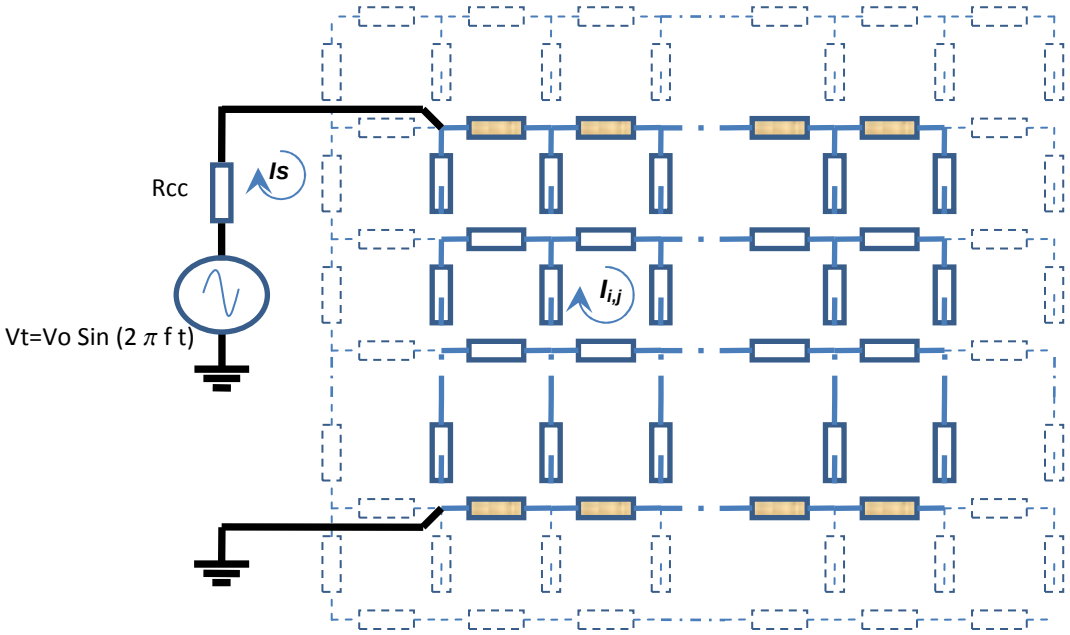

Dash lines indicate fictitious circuits used only to set up the calculations.

More unit circuits exists between nodes connected with this type of line

The impedance is set to zero to create a conductor which represents the electrodes

Figure 51. Circuit layout

In the analysis of circuit AB, the impedance of all branches was calculated based on Equation 23 through Equation 25. Kirchoff voltage law was applied to each unit circuit and also to the circuit formed in the loop of the source and the resistor R_{CC} which was probed for current measurements (Figure 51). The solution was performed using Mathematica 6.0. The random generator in this program was used in all places where a random number was required. A sample program run is included in Appendix A.

$$Z_R = R \qquad \text{Equation 23}$$

$$Z_c = \frac{1}{j\omega C} \qquad \text{Equation 24}$$

$$\omega = 2\pi f \qquad \text{Equation 25}$$

Z_R, Z_C are the impedance of resistor (R) and capacitor (C) respectively. *f* is the frequency of the excitation signal.

Based on the assumptions, Table 20 describes the parameters that are needed in setting up this simulation.

Table 20. **Parameters used to generate the RC network and run the simulation**

Symbol	Explanation of use	Value
kr	Number of rows circuit AB will have	"odd" >/=7
μ	mean value for random generators	0.5
σ	Standard deviation for random generators	0.2 - 0.5
xPc	Amplitude for resistors in circuit A (Ohms)	$10^{8} – 10^{12}$
Xc	Amplitude for capacitors in circuit A (F)	$10^{-12} – 10^{-14}$
xw	Amplitude for parallel resistors in circuit B (Ohms)	1500 - 10000
Xw	Amplitude for capacitors in circuit B (F)	$10^{-11} – 10^{-13}$
S_R	Rate of change of resistors with respect to moisture in circuit B	0.1 - 0.9
S_C	Rate of change of capacitors with respect to moisture in circuit B	0.1 - 0.5
x	Threshold for switching a "C" element to "R-C" in circuit B	0.5 - 0.9

The random R-C network created for the simulation can be visualized using color or gray scale as illustrated in Figure 52. The gray scale indicates the magnitude of impedance at each branch between notes with black indicating the largest impedance values

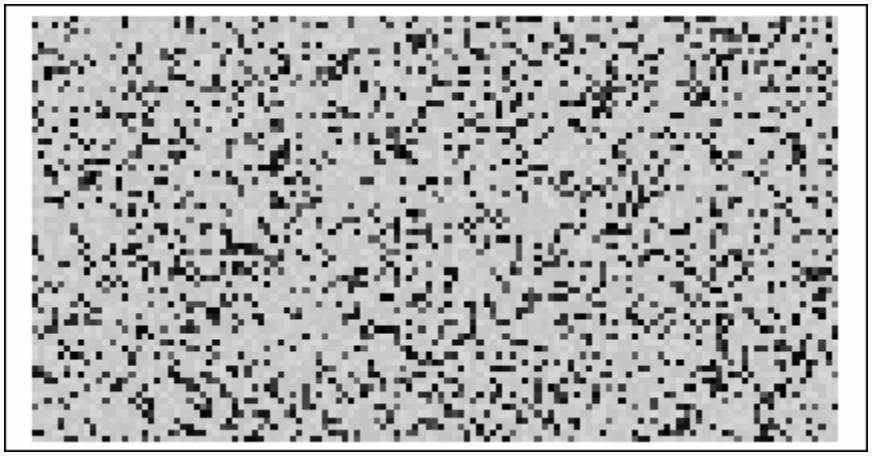

Figure 52. **Impedance random values of an R C random circuit. The darker the color the higher the impedance value (Range ~ 2650 – 50 Ohms)**

4.7 Simulation Results and qualitative comparison with experimental data

As mentioned earlier the scope of these simulations was not to validate the experimental results. Comparisons between experimental and simulation results will be on a qualitative basis. In order to facilitated comparison and given that the random RC circuit dimensions are not directly related to the microstructure both the experimental data and the simulation results have been normalized to the range of zero to one except phase angle values. Phase angle is related to the ratio of imaginary and real impedance and not to the specific value of impedance. It should be noted that among the many possible solutions the one presented here is to indicated common observations with solution that display reasonable trends. Other solution may indicate better agreement at different frequencies and/or other variables.

The following plots demonstrate phase angle results between simulation and experimental results for P1-1. In this particular case 10 MHz, the range of phase angles predicted is comparable with the experimental results but not the shape (Figure 54). If the comparison is made between 10 MHz experimental and 4 MHz simulation phase angle, both the shape and range show very good agreement (Figure 55). At 4MkHz shown in Figure 55 the range is comparable but the shape is off. Finally, at 1 MHz the experimental results show completely different trend that the simulation (Figure 56).

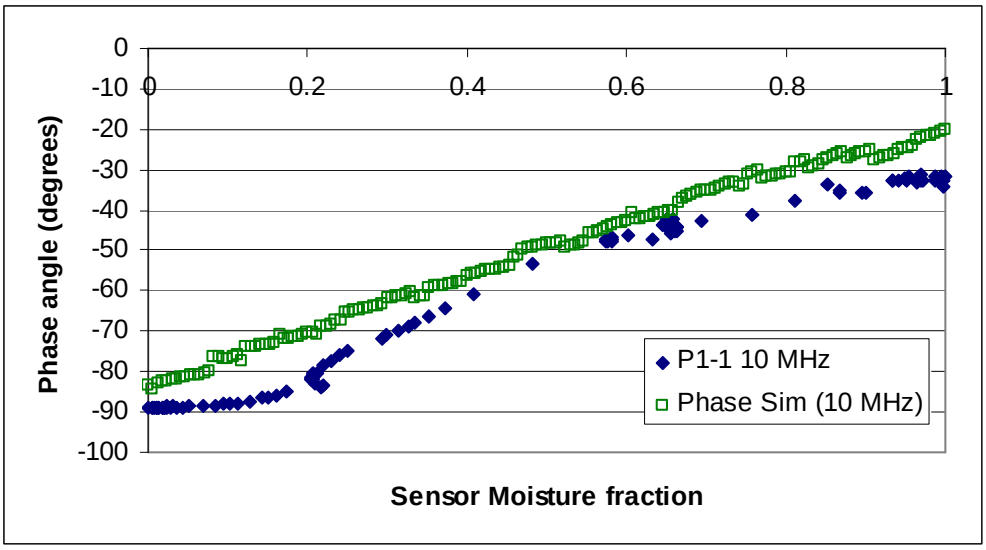

Figure 53. Phase angle comparison at 10 MHz

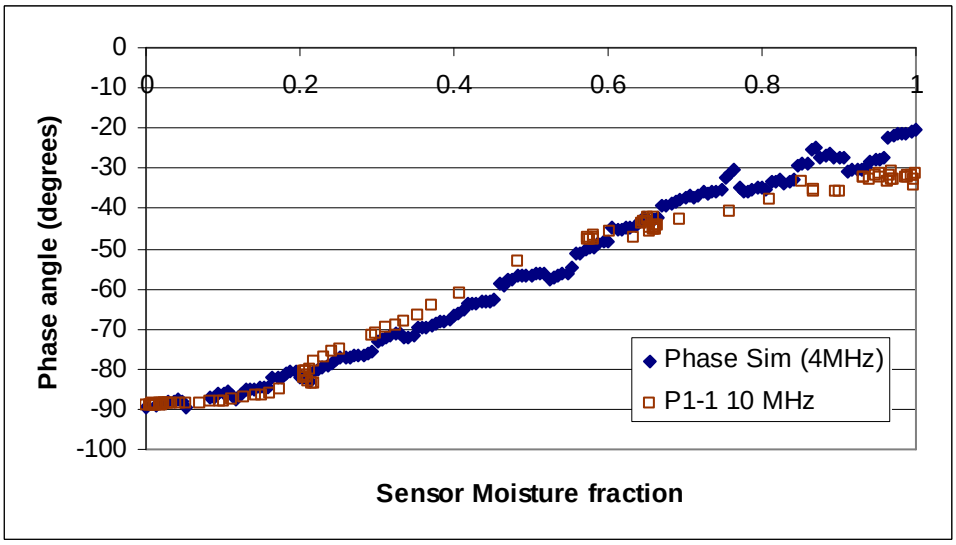

Figure 54. Phase angle comparison at 4MHz for simulation and 10 MHz for experimental results

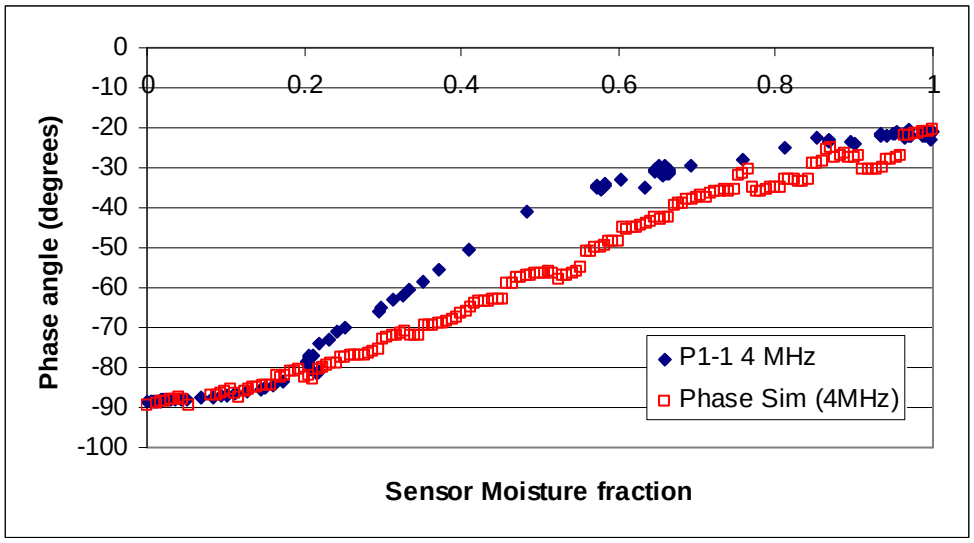

Figure 55. **Phase angle comparison at 4MHz**

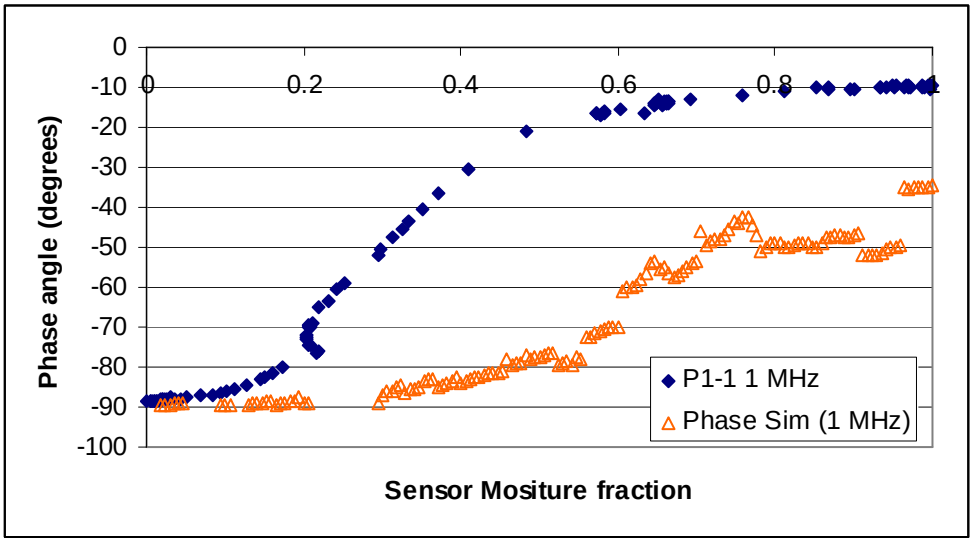

Figure 56. **Phase angle comparison at 1MHz**

Clearly, if the phase angle does not agree, other variable will also show discrepancies. The next four plots compare normalized experimental and simulation impedance values (Figure 57 - Figure 60). As in the case of phase angle, a comparison at different frequencies between experimental data and numerical, the agreement is very good. In this case the frequencies were 10 MHz and 4 MHz for the experimental and numerical data respectively (Figure 58). The simulation results do not compare favorably otherwise.

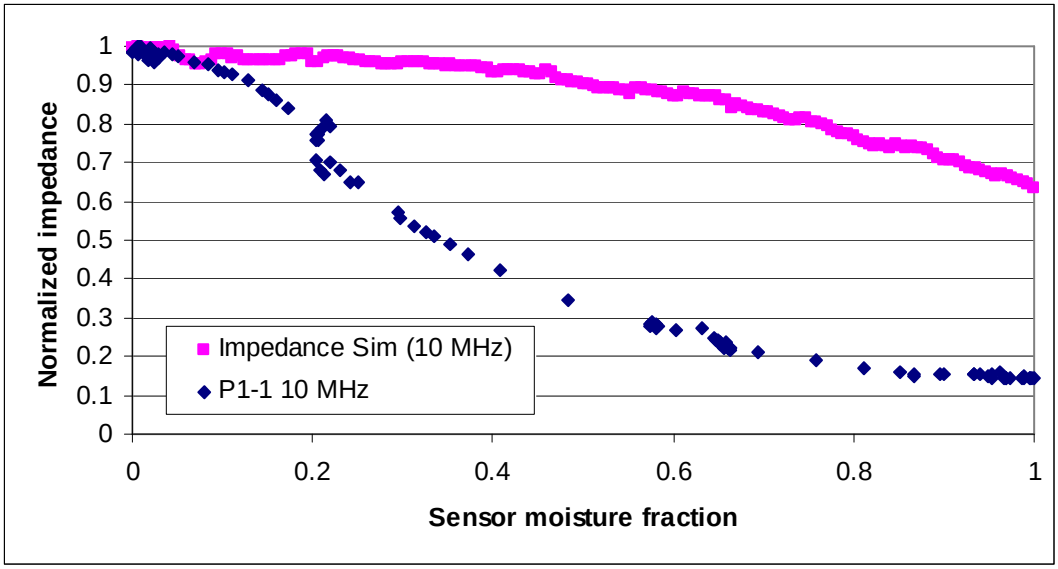

Figure 57. Normalized Impedance comparison at 10 MHz

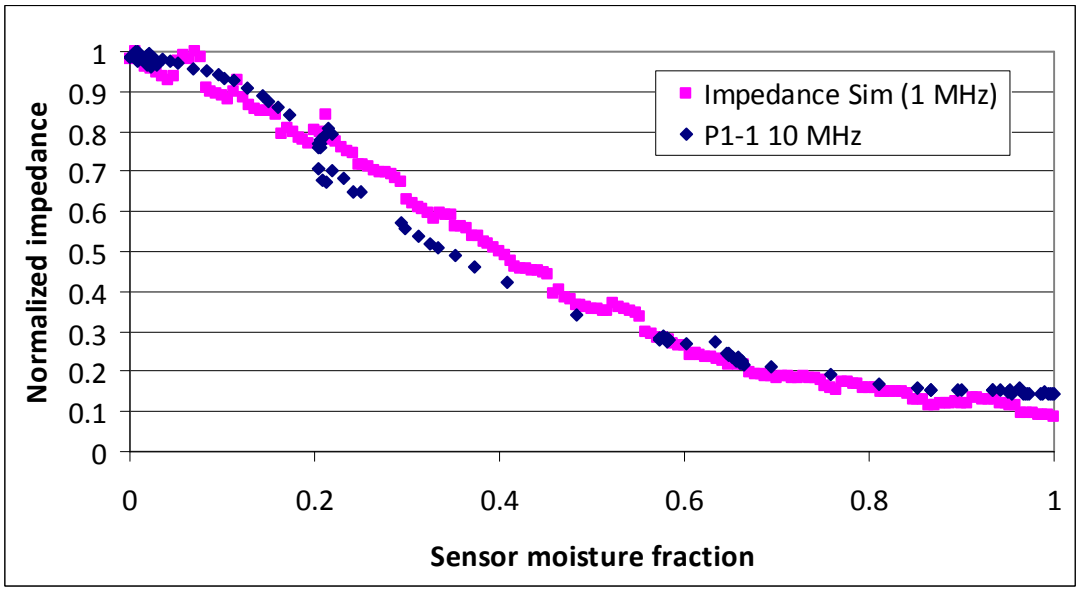

Figure 58. Normalized Impedance comparison at 1MHz for simulation and 10 MHz for experimental results

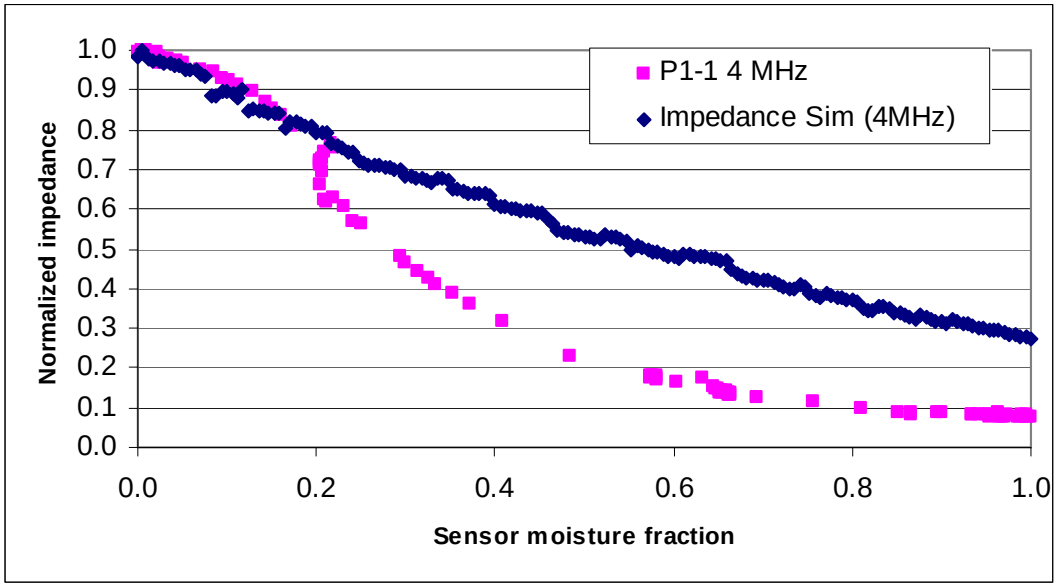

Figure 59. **Normalized Impedance comparison at 4MHz**

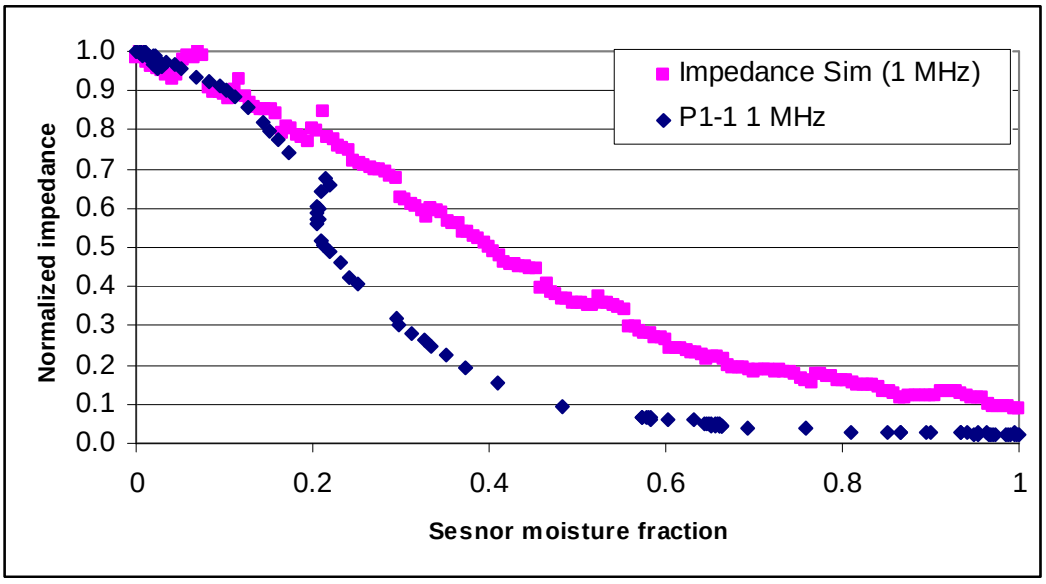

Figure 60. **Normalized Impedance comparison at 1MHz**

Of interest is the reason the effective dielectric constant obtained in experiments differs in behavior drastically from that of water and dry cement paste when tested individually. In running the simulation, it was observed that if the capacitance values are not influenced by the moisture change, i.e. all capacitors in the circuit have fixed values, effective capacitance is influenced greatly by

changes in the circuit geometry as outlined in the assumptions and the section on assembling the random R-C network.

As mentioned earlier capacitance and resistance are extensive properties which make it difficult to compare simulation and experimental results. In addition, the datum for moisture in the sensors was the 100% relative humidity environment. Clearly, the zero moisture content in the sensor is a function of the drying methodology followed. The drying method has an impact on concrete microstructure and controversy exists as of which is the best method to remove water from concrete [37-39]. The experimental results indicate a bilinear relation of capacitance to moisture. Similarly, the simulation results show a bilinear response with an extended region at low moisture (Figure 61). Assuming that the trend at low moisture content will not change, i.e. same slope, if the sensors are dried further, then the simulation might be capturing the behavior at very low moisture levels. With this assumption in mind, the experimental and simulation results can be compared as shown in Figure 62. For the comparison, the low moisture simulation results will be removed. Clearly, the simulation results show similar trends to the experimental values both in range and slope.

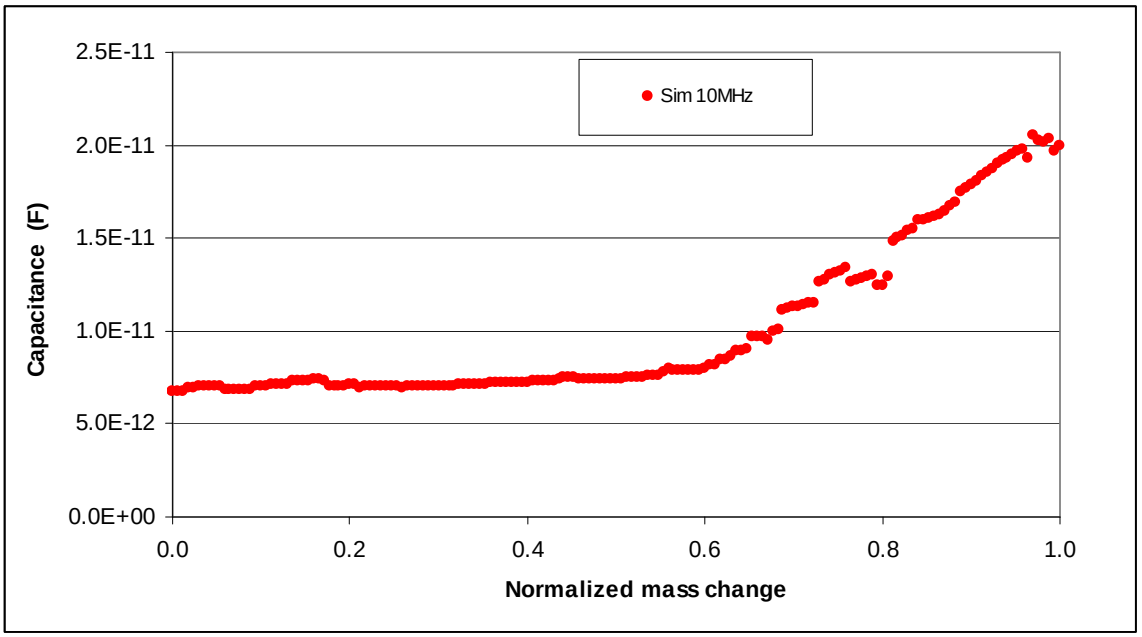

Figure 61. Simulated capacitance as function of moisture.

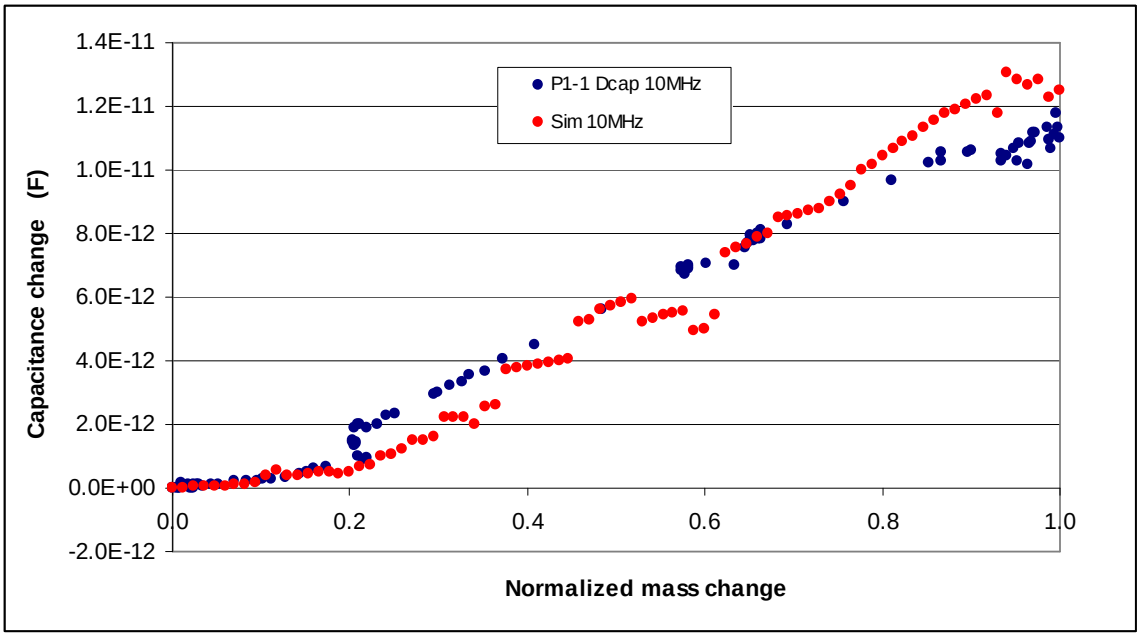

Figure 62. Comparison between simulated and experimental results for capacitance change in relation to moisture at 10 MHz

4.7.1 Effects of pore fluid resistance on effective capacitance

The simulation operated mostly unconfined with numerous possibilities as input. The idea of resistance influencing the effective capacitance can be explored using a simple model that lies on the opposite side of the spectrum when compared to random R-C networks. Figure 63 shows two configurations that will be explored. The assumptions are listed below:

- The transition line at L/2 has no influence. This is to say, if a potential is applied across the electrodes, the field varies only in the y direction. This is true if L >> d.
- Water conductivity is assumed to be either zero or infinitive.

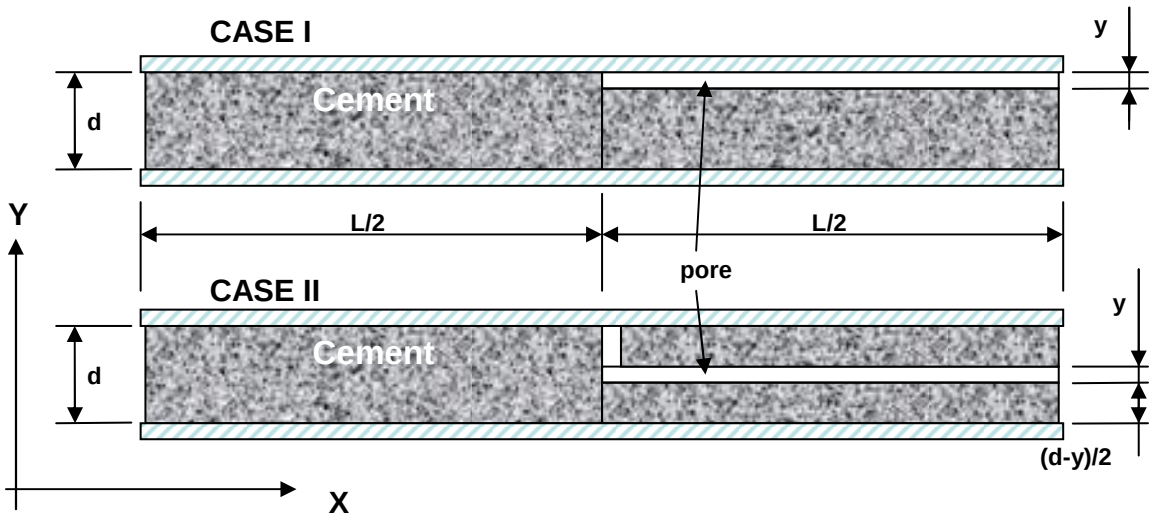

Figure 63. **Case I and II idealized geometry**

As mentioned above water conductivity will be assumed to either zero or infinitive. For each of the two configurations (case I and case II) the effective capacitance will be calculated using the two conductivities for water as mentioned above in addition to the empty pore state. The assumption of using conductivity is that a pore filled with highly conductive fluid becomes part of the electrodes. Thus, the effective distance between electrodes is altered in the area of the pore. The following dielectric constants and dimension will be used. Table 22 shows the normalized capacitance for case I and II. The empty pore state is used to normalize results.

Table 21. **Material properties and dimension for case I and II**

Material	Dielectric Constant
Air	1
Cement	3
Water	80
Dimensions	
L	1
d	L/10
y	d/10
Pore volume fraction	0.05

Table 22. **Normalized capacitance for case I and II**

Case I	Normalized Capacitance		
Pore	n/a	Water Conductivity is Zero	Water Conductivity is Infinitive
Empty	1	--	--
Full	--	1.15	1.15
Case II	Normalized Capacitance		
Pore	n/a	Water Conductivity is Zero	Water Conductivity is Infinitive
Empty	1	--	--
Full	--	1.15	1.76

Case I and II indicated that geometry alongside conductivity can give effective capacitance values that are comparable or even higher than values obtained without considering conductivity. A third case (Case III) that will be considered using a different configuration is shown in Figure 64. Two pores are considered in this case. When water is assumed to have infinite conductivity, both X and Y directions are considered. As in the two cases considered previously, if a potential is applied across the electrodes, the field varies perpendicular to the electrodes only. With infinite conductivity the pore water becomes part of the electrodes. No interaction between X and Y direction is considered. Dimensions are listed below (Table 23) and results are given in Table 24.

Table 23. **Dimensions of idealized geometry case III**

Dimensions	
L	**1**
N	**L/10**
H	**2 L**
H	**0.8 H**
Pore volume fraction	**0.16**

Table 24. **Results for simple model case III**

Case III	Normalized Capacitance		
Pore	n/a	Water Conductivity is Zero	Water Conductivity is Infinitive
Pore	n/a	Zero	Infinitive
Empty	1	--	--
Full	--	1.9	4.6

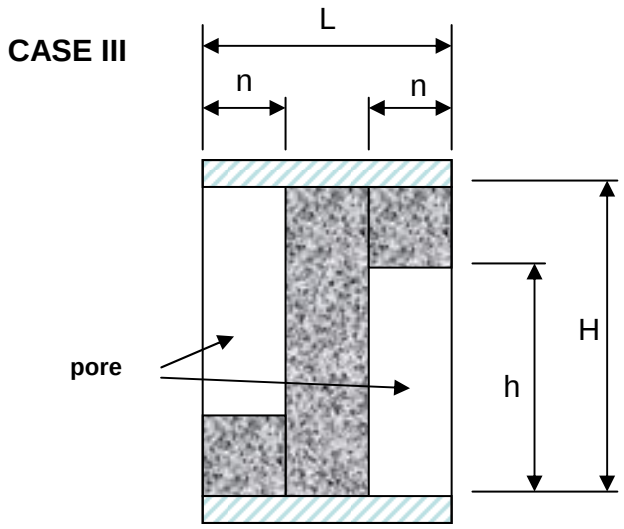

Figure 64. **Case III idealized geometry**

The three simple models considered are based on idealized geometry and behavior. The assumption of water conductivities of zero and infinitive are the extremes of the spectrum. In reality, pore solution has a finite conductivity. Rajabipour and Weiss measured extracted pores solution conductivity in the range of 2-2.5 S/m [116, 117]. On the other hand de-ionized water has conductivity in the order of 1E-6 S/m, about 6 orders of magnitude difference from cement pore solution. The finite conductivity affects the response of the pore to an AC signal. As mentioned by Taylor, et al., the depth of penetration in the pore of an applied AC signal depends on the frequency pore diameter and fluid conductivity [103].

4.8 Discussion on simulation and modeling results

Although the simulation results are not capturing the experimental data trends with fidelity, it demonstrates that a Random R-C circuit can be used to explore IS response of composites. As aforementioned, the concept of Random R-C circuits has been implemented with success on ceramic composites having distinct conductive and capacitive phases [115]. In the case of cement paste, the microstructure is multiphase and the dimension scale of elements spans many

decades. Also, water interaction with cement paste goes beyond the wetting process as chemical reactions take place. Assumptions were made to form the R-C network. For instance, the linear change in capacitance and resistance is based solely on geometry.

In many cases, the range and distribution of values chosen was not informed by specific information due to a lack thereof. The simulation is based on a random generated circuit (random locations and values of R and C) as a means to capture some of the unknown parameters. The fact that resistance and capacitance are extensive properties brings another complication to the simulation. Adding more elements affects the results in that the circuit can be viewed as modeling at a smaller scale (i.e. same volume as before adding new elements) or at the same scale but a larger volume of cement paste.

What was apparent from running this simulation is that numerous solutions are possible. Finding what is unique about circuits that produce result having common trends with the experimental results will require statistical analysis of numerous simulation results. If the random and other inputs to the simulation are seeded using information from cement paste microstructure, it may be possible to capture cement paste IS response using random R-C circuits and material related properties.

Using both the random R-C network and the simple model has demonstrated that conductivity of elements in the microstructure may affect the effective capacitance. This supports the assumption made to include resistive elements in the random R-C circuit. Lagarkov and Sarychev theoretically showed that elongated conductive sticks with high length to diameter ratio enhanced significantly the dielectric constant of composites containing the elongated conductive inclusions [118].

4.9 Conclusions

Random R-C networks have the benefit of capturing impedance response of random materials without specific geometric information on the microstructure. On the other hand, the range of values and distribution of resistor and capacitor appears to be important in successfully capturing the behavior of the material. In the case of cement paste random R-C network circuits capture impedance response trends. However, there are still many unknowns in creating circuits that fully mimic the behavior of cement paste. Assumptions utilized to create the electrical circuit were necessary due to the lag of specific information. More data relating concrete microstructure to individual material properties in needed. In this work it was assumed that R and C values change based on geometrical argument. The interaction of moisture with the cement microstructure and how the values of R and C are affected can inform the circuit evolution with moisture. Understanding of the randomness of cement paste with respect to impedance values is a must to create informed random circuits.

Chapter 5

Conclusions and Recommendations

5.1 Conclusions

Moisture and concrete are inseparable. The value of understanding moisture as a gateway to understanding degradation mechanisms for concrete itself and reinforcement is vitally important. As expected, quantifying moisture in the interior poses many challenges mainly due to the harsh concrete solution environment for sensors. Using cement paste as a sensing element and probing its impedance response for measuring moisture was developed. Since the sensing element is cement it will not be affected by the surrounding concrete. Capacitive to moisture relation is bilinear in the upper range of frequencies used in this study. Long term testing of limited variables with embedded sensors in a small concrete block proved that the sensor can perform over extended periods of time. Without a doubt, more testing is needed to establish thermal and mechanical loading effect. Optimization of the materials used in the sensors needs to be addressed to maximize performance and durability. Monitoring the sensors with a different instrument than the LCR meter used in this study has it own challenges which have not been addressed in this study.

The response of the sensor was explored with impedance spectroscopy (IS). The senor is not only useful in measurements of moisture, but it can serve as tool in the research on concrete and cement paste behavior. The IS response of the sensor is complex. A more vigorous IS study is required to validate the limited frequency range available with the instrumentation used here.

Finally, the use or R-C random networks was investigated as tool to capture, in a simulation, the IS behavior of the sensor. The complexity of the cement microstructure and the many unknowns regarding material properties and interaction of the water with pores and hydration product were the biggest obstacle in implementing R-C random networks concept.

5.2 Recommendations

The extensive data collected is not sufficient to fully understand the complex water/ cement interaction with respect to impedance measurements. Excluding the parallel plate and 1st generation sensors results, only one water/cement (w/c) ratio was conceded with two different cement/sand mixtures. Ideally a number of different w/c need to be used. This will provide information on the effects the water to cement ratio has on the impedance response. Additionally, the cement to sand ration and even the sand grading must be considered as the capacitance values measured are higher for fine sand sensors when compared to sensors utilizing coarse sand. Clearly, fine sand has more surface area and this observation must be explored further to fully understand of the reasons giving rise to the impedance behavior of cement paste.

The sensors provide a platform to investigate both moisture in concrete and also concrete itself. As indicated the response of the sensors contain any effects the embedded electrodes might have and it has not been addressed in this work.

The frequency range and distinct values considered were dictated by the multi-frequency LCR meter used in the experimental portion of this work. First the frequency range must be expanded to capture better impedance response. Second, more advanced Impedance spectroscopy instrumentation provides selection of frequency values which will help pinpoint the frequencies where drastic changes in behavior occur.

In the interest of time and in light of the events at Virginia Tech on April 16th, 2007, the sensors were transferred from 100% RH to 50% and/or 31% RH environments. Consequences from the rate of moisture change due to environmental condition changes should be evaluated over the whole spectrum of possible moisture exposure histories. This implies the use of much smaller and larger moisture step changes. Additionally, the direction of moisture change is of concern as concrete exhibits hysteresis behavior with respect to moisture uptake or loss.

REFERENSES

1. Chen, Y., J.F. Davalos, and I. Ray, *Durability Prediction for GFRP Reinforcing Bars Using Short-Term Data of Accelerated Aging Tests.* JOURNALOFCOMPOSITESFORCONSTRUCTION, 2006.
2. Tannous, F.E. and H. Saadatmanesh, *Durability of AR Glass Fiber Reinforced Plastic Bars.* Journal of Composites For Construction, 1999: p. 12-19.
3. Bhise, V.S., *Strength Degradation of GFRP Bars*, in *Civil Engineering*. 2002, Virginia Tech: Blacksburg.
4. Dejke, V., *Durability of FRP Reinforcement in Concrete –Literature Review and Experiments*. 2001, Chalmers University of Technology,Sweden.
5. Almusallam, T.H. and Y.A. Al-Salloum, *Durability of GFRP Rebars in Concrete Beams under Sustained Loads at Severe Environments.* Journal of COMPOSITE MATERIALS, 2006. **40**(7): p. 623-637.
6. Karbhari, V.M., K. Murphy, and S. Zhang, *Effect of Concrete Based Alkali Solutions on Short-Term Durability of E-Glass/Vinylester Composites.* Jounral of Composite Materials, 2002. **36**(17): p. 2101-2121.
7. Kajorncheappunngam, S., et al., *Effect of aging Environment on Degradation of Glass-Reinforced Epoxy.* Journal of Composites for Construction, 2002: p. 61-69.
8. Chu, W., L. Wu, and V.M. Karbhari, *Durability evaluation of moderate temperature cured E-glass/vinylester systems.* Composite Structures, 2004. **66**(1-4): p. 367-376.
9. Purnell, P., *Interpretation of climatic temperature variations for accelerated ageing models.* Journal of Materials Science, 2004. **39**: p. 113-118.
10. Andrade, C., J. Sarria, and C. Alonso, *Relative humidity in the interior of concrete exposed to natural and artificial weathering.* Cement and Concrete Research, 1999. **29**(8): p. 1249-1259.
11. *Standard Test Method for Determing Relative Humitity in Concrete Floor Slabs using insitu Probes*, in *Designation: F2170-02*. 2002, ASTM international.
12. Ferraris, C.F., et al. *Stress Due to Alkali-Silica Reactions in Mortars*. in *Fourth Materials Engineering Conference*. 1996. Washington, D.C: New York: ASCE.
13. Jacobsen, S., et al., *High strength concrete -- Freeze/thaw testing and cracking.* Cement and Concrete Research, 1995. **25**(8): p. 1775-1780.
14. Roy, D.M. and G.R. Gouda, *Optimization of strength in cement pastes.* Cement and Concrete Research, 1975. **5**(2): p. 153-162.
15. Jiang, L. and Y. Guan, *Pore structure and its effect on strength of high-volume fly ash paste.* Cement and Concrete Research, 1999. **29**(4): p. 631-633.
16. Nilsso, L.-O., *Long-term moisture transport in high performance concrete* Materials and Structures/Mat6riaux et Constructions, 2002. **35**: p. 641-649
17. Clark, S.M., G.R. Morrison, and W.D. Shi, *The use of scanning transmission X-ray microscopy for the real-time study of cement hydration.* Cement and Concrete Research, 1999. **29**(7): p. 1099-1102.
18. Mouret, M., A. Bascoul, and G. Escadeillas, *Microstructural features of concrete in relation to initial temperature--SEM and ESEM characterization.* Cement and Concrete Research, 1999. **29**(3): p. 369-375.
19. *Standard Specification for Portland Cement*, in *ASTM C 150*. Update year, ASTM International: West Conshohocken, PA. p. 6.

20. Kjellsen, K.O. and E.H. Atlassi, *Pore structure of cement silica fume systems Presence of hollow-shell pores.* Cement and Concrete Research, 1999. **29**(1): p. 133-142.
21. Mindess, S., J.F. Young, and D. Darwin, *Concrete*. 2nd ed. 2003, Upper Saddle River: Prentice Hall. 644.
22. Zhao, T.J., et al., *An alternating test method for concrete permeability.* Cement and Concrete Research 1998. **28**: p. 7-12.
23. Scrivener, K.L., A.K. Crumbie, and P. Laugesen, *The Interfacial Transition Zone (ITZ) Between Cement Paste and Aggregate in Concrete.* Interface Science, 2004. **V12**(4): p. 411-421.
24. Scrivener, K.L. and K.M. Nemati, *The percolation of pore space in the cement paste/aggregate interfacial zone of concrete.* Cement and Concrete Research, 1996. **26**(1): p. 35-40.
25. Powers, T.C., et al., *Permeability of Portland Cement Paste.* Journal of The American Concrete Institute, 1954. **51**: p. 285-298.
26. Khan, M.I., *Permeation of High Performance Concrete*. Journal of Materials in Civil Engineering, 2003: p. 84-92.
27. Lea, F.M., *Lea's chemistry of cement and concrete*. 4th ed, ed. P.C. Hewlett. 1998, London, Arnold, New York J. Wiley. 1053
28. Cook, R.A. and K.C. Hover, *Mercury porosimetry of hardened cement pastes.* Cement and Concrete Research, 1999. **29**(6): p. 933-943.
29. Roels, S., et al., *Characterisation of pore structure by combining mercury porosimetry and micrography* Materials and Structures, 2001. **34**: p. 76-82.
30. Leech, C., D. Lockington, and R.D. Hooton, *Estimation of Water Retention Curve from Mercury Intrusion Porosimetry and van Genuchten Model.* ACI Structural Journal, 2006: p. 291-295.
31. Washburn, E.W., *Note on a Method of Determining the Distribution of Pore Sizes in a Porous Material.* PNAS, 1921. **7**(4): p. 115-116.
32. Cook, R.A. and K.C. Hover, *Mercury Porosimetry of Cement-Based Materials and Associated Correction Factors.* ACI Materials Journal, 1993. **90**(2): p. 152-161.
33. Adolphs, J., M.J. Setzer, and P. Heine, *Changes in pore structure and mercury contact angle of hardened cement paste depending on relative humidity.* Materials and Structures/Materiaux et Constructions, 2002. **35**: p. 477-486.
34. Winslow, D. and D. Liu, *The pore structure of paste in concrete.* Cement and Concrete Research, 1990. **20**(2): p. 227-235.
35. Diamond, S., *Mercury porosimetry: An inappropriate method for the measurement of pore size distributions in cement-based materials.* Cement and Concrete Research, 2000. **30**(10): p. 1517-1525.
36. Beaudoin, J.J., *Porosity measurement of some hydrated cementitious systems by high pressure mercury intrusion-microstructural limitations.* Cement and Concrete Research, 1979. **9**(6): p. 771-781.
37. Galle, C., *Effect of drying on cement-based materials pore structure as identified by mercury intrusion porosimetry: A comparative study between oven-, vacuum-, and freeze-drying.* Cement and Concrete Research, 2001. **31**(10): p. 1467-1477.
38. Moukwa, M. and P.C. Atcin, *The effect of drying on cement pastes pore structure as determined by mercury porosimetry.* Cement and Concrete Research, 1988. **18**(5): p. 745-752.

39. Maekawa, K., R. Chaube, and T. Kishi, *Modeling of Concrete Performance. Hydration, Microstructure Formation and Mass Transport*. 1999, New York: Routledge.
40. Beaudoin, J.J., R.F. Feldman, and P.J. Tumidajski, *Pore structure of hardened portland cement pastes and its influence on properties.* Advanced Cement Based Materials, 1994. **1**(5): p. 224-236.
41. Powers, T.C., *Structure and Physical Properties of Hardened Portland Cement Paste.* Journal of the American Ceramic Society, 1958. **41**(1): p. 1-6.
42. A. P. Banta, C.F.R., *The water permeability of concrete and some factors which affect it*, in *Civil Engineering*. 1928, Caltech.
43. Martys, N.S. and C.F. Ferraris, *Capillary Transport in Mortars and Concrete.* Cement and Concrete Research, 1997. **Vol. 27**(5): p. 747-760.
44. Wilson, M.A., M.A. Carter, and W.D. Hoff, *British standard and RILEM water absorption tests: A critical evaluation.* Materials and Structures, 1999. **V32**(8): p. 571-578.
45. Lampacher, B.J. and G.E. Blight, *Permeability and Sorption Properties of Mature Near-Surface Concrete.* Journal of Materials in Civil Engineering, 1996: p. 21-25.
46. Parlange, D.A.L.a.J.-Y., *Anomalous water absorption in porous materials.* Journal of Physics D: Applied Physics, 2003. **36**(6): p. 760-767.
47. Lockington, D., J.Y. Parlange, and P. Dux, *Sorptivity and the estimation of water penetration into unsaturated concrete.* Materials and Structures, 1999. **V32**(5): p. 342-347.
48. Carmeliet, J., et al., *Determination of the Liquid Water Diffusivity from Transient Moisture Transfer Experiments.* Journal of Thermal Envelope and Building Science, 2004. **27**(4): p. 277-305.
49. Benkokrane, B., et al., *Durability of Glass Fiber-Reinfornced Polymer Reinfrocing Bars in Concrete Environment.* Journal of Composites for Construction, 2002. **6**(3): p. 143-153.
50. Rasheeduzzafar, S. Ehtesham Hussain, and A.S. Al-Gahtani, *Pore solution composition and reinforcement corrosion characteristics of microsilica blended cement concrete.* Cement and Concrete Research, 1991. **21**(6): p. 1035-1048.
51. Shehata, M.H., M.D.A. Thomas, and R.F. Bleszynski, *The effects of fly ash composition on the chemistry of pore solution in hydrated cement pastes.* Cement and Concrete Research, 1999. **29**(12): p. 1915-1920.
52. Diamond, S., *Effects of Microsilica (Silica Fume) on Pore-Solution Chemistry of Cement Pastes.* Communications of the American Ceramic Society 1983.
53. Baroghel-Bouny, V., et al., *Characterization and identification of equilibrium and transfer moisture properties for ordinary and high-performance cementitious materials.* Cement and Concrete Research, 1999. **29**(8): p. 1225-1238.
54. *Standard Test Method for ElectricalIndication of Concrete's Ability to Resist Chloride Ion Penetration*, in *ASTM C 1202-05*. 2005, ASTM International: West Conshohocken, PA. p. 6.
55. Ababneh, A., F. Benboudjema, and Y. Xi, *Chloride Penetration in Nonsaturated Concrete.* Journal of Materials in Civil Engineering, 2003: p. 183-191.
56. C. Andrade, M.A.S., A. Recuero, and O. Río, *Calculation of chloride diffusivity in concrete from migration experiments, in non-steady-state conditions.* Cement and Concrete Research, 1994. **24**: p. 1214-1228.

57. Hornain, H., et al., *Diffusion of chloride ions in limestone filler blended cement pastes and mortars.* Cement and Concrete Research, 1995. **25**(8): p. 1667-1678.
58. Nickerson, A.A.a.A.K., *The diffusion of ions through water-saturated cement.* Journal of Materials Science, 1984. **19**: p. 3068-3078.
59. R.F. Feldman, L.R.P.J., G. Chan, *Rapid chloride permeability test on blended cement and other concretes: Correlations between charge, initial current and conductivity.* Construction and Building Materials, 1999. **13**: p. 149-154.
60. Hooton, P.F.M.a.R.D., *Influence of voltage on chloride diffusion coefficients from chloride migration tests.* Cement and Concrete Research, 1996. **26**: p. 1239-1244.
61. Streicher, P.E. and M.G. Alexander, *A chloride conduction test for concrete.* Cement and Concrete Research, 1995. **25**: p. 1284-1294.
62. Al-Khaiat, H. and N. Fattuhi, *Carbonation of Concrete Exposed to Hot and Arid Climate.* Journal of Materials in Civil Engineering, 2002: p. 97-107.
63. Parrott, L.J., *Variations of water absorption rate and porosity with depth from an exposed concrete surface: Effects of exposure conditions and cement type.* Cement and Concrete Research, 1992. **22**(6): p. 1077-1088.
64. E.J. Garboczi, D.P.B., *Computer simulation of the diffusivity of cement-based materials.* Journal of Materials Science 1992. **27**(8): p. 2083-2092.
65. Olson, R.A., et al., *Interpretation of the Impedance Spectroscopy of Cement Paste Via Computer Modelling, Part III: Microstructural Analysis of Frozen Cement Paste Part III: Microstructural Analysis of Frozen Cement Paste.* Journal of Materials Science, 1995: p. 5078-5086.
66. Holly, J., D. Hampton, and M.D.A. Thomas, *Modelling relationships between permeability and cement paste pore microstructures.* Cement and Concrete Research, 1993. **23**(6): p. 1317-1330.
67. Manwart, C. and R. Hilfer, *Reconstruction of Random Media Using Monte Carlo Methods.* Physical Review E, 1999. **59**(5): p. 5596-5599.
68. Manwart, C., S. Torquato, and R. Hilfer, *Stochastic Reconstruction of Sandstones.* Physical Review E, 2000. **62**(1): p. 893-899.
69. Navi, P. and C. Pignat, *Three-dimensional characterization of the pore structure of a simulated cement paste.* Cement and Concrete Research, 1999. **29**(4): p. 507-514.
70. Zachary, C.G., A.L. David, and D.D.A. Matthew, *Internal relative humidity and drying stress gradients in concrete.* Materials and Structures, 2006. **V39**(9): p. 901-909.
71. Rajabipour, F., et al., *Procedure to Interpret Electrical Conductivity Measurements in cover concrete During Rewetting.* Journal of Materials in civil Engineering, 2005: p. 586-594.
72. Hudec, P., C. Mac Innis, and M. M., *The Capacitance Effect Method of Measuring Moisture and Salt Content of Concrete.* University of Windsor, Windsor, Ontario, Canada, 1986.
73. Paroll, H. and E. Nykänen, *Measurement Of Relative Humidity And Temperature In A New Concrete Bridge Vs. Laboratory Samples*, VTT. p. 17.
74. Heikki, K. and P. Hemming, *Nordic concrete federation mini-seminar "moisture measurement in concrete Constructions exposed to temperature and moisture variations".* Nordic Concrete research, 1998. **21**.
75. Beyea, S.D.B., B.J; Bremner, T.W; Prado, P.J; Green, D.P; Armstrong, R.L; Grattan-Bellew, P.E. , *Magnetic Resonance Imaging and Moisture Content*

Profiles of Drying Concrete. Cement and Concrete Research, 1998. **28**(3): p. 453-463.
76. Vijayakumar R, R.L., Ramamurthy N, *Determining the Moisture Content in Limestone Concrete by Gamma Scattering Method: A Feasibility Study*, in *National Seminar of ISNT*: Chennai.
77. Rocha, M.C.d.S., L.M da; Appoloni, C.R; Portezan Filho, O; Lopes, F; Melquíades, F.L; Santos, E.A. dos; Santos, A.O. dos; Moreira, A.C; Pötker, W.E; Almeida, E de; Tannous, C.Q; Kuramoto, R; Cavalcante, F.H. de M.; Barbieri, P.F; Caleffi, A.F; Carbonari, B.T; Carbonari, G. , *Moisture Profile Measurements of Concrete Samples in Vertical Water Flow by Gamma Ray Transmission Method.* Radiation Physics and Chemistry, 2001. **61**: p. 567-569.
78. Kääriäinen, H., et al., *Moisture Measurements in Building Materials with Microwaves.* NDT&E International, 2001. **34**: p. 389-394.
79. *Standard Test Method for measuring Moisture Vapor Emission Rate of Concrete Sub Floors Using Anhydrous Calcium Chlorite*, in *Designation: F1869*. 2004, ASTM international.
80. Roels, S., et al., *A Comparison of Different Techniques to Quantify Moisture Content Profiles in Porous Building Materials.* Journal of Thermal Envelope and Building Science, 2004. **27**(4): p. 261-276.
81. Chung, D.D.L., *Damage in Cement-Based Materials, Studied by Electrical Resistance Measurement.* Materials Science and Engineering, 2003.
82. Theophanous, T., et al., *Moisture Measurements in Concrete for Life Assessment of Rebars*, in *ACMBS-IV Conference, July, 2004*. 2004: Calgary, Canada.
83. Grasley, Z.C., D.A. Lange, and M.D. D'Ambrosia, *Embedded Sensors for Measuring Internal Relative Humidity in Concrete.* University of Illinois, Urbana IL.
84. Greenspan, L. and No.1, *Humidity Fixed Points of Binary Saturated Aqueous Solutions.* Journal of research of the National Bureau of Standards—A, 1997. **Vol.81A**: p. 89-96.
85. By Onkar D. Dhingra, J.B.S., *Basic Plant Pathology Methods*. 1995, CRC Press. p. 448.
86. Shi, M., Z. Chen, and J. Sun, *Determination of chloride diffusivity in concrete by AC impedance spectroscopy.* Cement and Concrete Research, 1999. **29**(7): p. 1111-1115.
87. Liu, Z. and J.J. Beaudoin, *An assessment of the relative permeability of cement systems using AC impedance techniques.* Cement and Concrete Research, 1999. **29**(7): p. 1085-1090.
88. Buenfeld, N.R., J.-Z. Zhang, and No.4, *AC Impedance Study of Sealer- and Coating- Treated Mortar Specimens.* Advances in Cement Research, 1998. **10**: p. 169-178.
89. Cormack, S.L., et al., *An AC Impedance Spectroscopy Study of Hydrated Cement Pastes.* Advances in Cement Research. **10**: p. 151-159.
90. McCarter, W.J., H. Ezirim, and N. 2, *AC Impedance Profiling Within cover Zone Concrete: Influence of Water and Ionic Ingress.* Advances in Cement Research, 1998. **10**: p. 57-66.
91. Perron, S. and J.J. Beaudoin, *Freezing of Water in Portland Cement Paste – an AC Impedance Spectroscopy Study.* Cement and Concrete Composites, 2002. **Vol. 24**: p. 467-475.

92. Tamtsia, B.T., J.J. Beaudoin, and J. Marchand, *A Coupled AC Impedance – Creep and Shrinkage Investigation of Hardened Cement Paste.* Materials and Structures, 2003. **V. 36**: p. 147-155.
93. M.R. Hansen, M.L.L., P. Zia, and S. Ahmad, *Chloride permeability and AC impedance of high performance concrete*, in *High Performance Concrete in Severe Environments*, P. Zia, Editor. 1993, American Concrete Institute. p. 121-145.
94. Hu, A., et al., *Humidity Dependence of Apparent Dielectric Constant for DSP Cement Materials at High Frequencies.* Journal of the American Ceramic Society, 1999. **82**(7): p. 1741-1747.
95. Al-Qadi, I.L., et al., *Dielectric Properties of Portland Cement Concrete at Low Radio Frequencies.* Journal of Materials in Civil Engineering, 1995. **7**(3): p. 192-198.
96. Pokkuluri, K.S., *Effect of admixtures, chlorides, and moisture on dielectric properties of portland cement concrete in the low microwave frequency range.*, in *Civil Engineering*. 1998, Virginia Polytechnic Institute and State University: Blacksburg.
97. *CRC Handbook of Chemistry and Physics*, ed. R.C. Weast. Vol. 63. 1982: CRC Press.
98. Takashima, S., et al., *Study of Bound Water of Poly-Adenine Using High Frequency Dielectric Measurements.* Biophysics Journal, 1986. **Vol. 49**: p. 1003-1008.
99. Boyarskii, D.A., V.V. Tikhonov, and N.Y. Komarova, *Model of Dielectric Constant of Bound Water in Soil for Applications of Microwave Remote Sensing.* Progress in Electromagnetics Research PIER 35, 2002: p. 251-269.
100. Marino, A.A., et al., *Dielectric Determination of Bound Water of Bone.* Phys. Med. Biol., 1967. **Vol. 12**: p. 367-378.
101. Senapati, S. and A. Chandra, *Dielectric Constant of Water Confined in a Nanocavity.* jounral of Physical Chemistry, 2001(B).
102. Fen-Chong, T. and A. Fabbri, *Freezing and thawing porous media: experimental study with a dielectric capacitive method.* Comptes Rendus Mecanique, 2005. **333**(5): p. 425-430.
103. Taylor, S.R., et al., *A Short Course on Electrochemical Impedance Spectroscopy: Theory, Applications, and Laboratory Instructions*. 2006, Materials Research Company: Madison, MS 39130.
104. McCarter, W.J. and R. Brousseau, *The A.C. response of hardened cement paste.* Cement and Concrete Research, 1990. **20**(6): p. 891-900.
105. Buck, A.L., *New Equations for Computing Vapor Pressure and Enhancement Factor*. Journal of Applied Meteorology, 1981. **20**(12): p. 1527-1532.
106. Ade Ogunsola, U.R., Leonardo Sandrolini, *Modelling shielding properties of concrete*, in *17th International Zurich Symposium on Electromagnetic Compatibility*. 2006: Zurich.
107. A. Shaari, S.G.M., J. H. Bungey, *Modelling the propagation of a radar signal through concrete as a low-pass filter.* NDT & E International, 2004. **Volume 37**(3): p. 237-242.
108. Maron, N. and O. Maron, *On the mixing rules for astrophysical inhomogeneous grains.* Monthly Notices of the Royal Astronomical Society, 2005. **357**(3): p. 873-880.

109. Jonscher, A.K., *The universal dielectric response and its physical significance.* IEEE Transactions on Electrical Insulation, 1992. **27**(3): p. 407-423.
110. Panteny, S., R. Stevens, and C.R. Bowen, *The Frequency Dependent Permittivity and AC Conductivity of Random Electrical Networks.* Ferroelectrics, 2005. **319**: p. 199 - 208.
111. Garboczi, E.J. and D.P. Bentz, *Computer Simulation of the Diffusivity of Cement-Based Materials.* Journal of Materials Science, 1992. **27**: p. 2083-2092.
112. Olson, R.A., et al., *Interpretation of the Impedance Spectroscopy of Cement Paste Via Computer Modelling, Part III: Microstructural Analysis of Frozen Cement Paste.* Journal of Materials Science, 1995: p. 5078-5086.
113. Macdonald, J., *Impedance spectroscopy.* Annals of Biomedical Engineering, 1992. **20**(3): p. 289-305.
114. Vainas, B., et al., *An evaluation of random R-C networks for modelling the bulk ac electrical response of ionic conductors.* Solid State Ionics, 1999. **126**(1-2): p. 65-80.
115. Bowen, C.R. and D.P. Almond, *Modelling the 'universal' dielectric response in heterogeneous materials using microstructural electrical networks.* Materials Science and Technology, 2006. **22**: p. 719-724.
116. Snyder, K.A., et al., *Estimating the electrical conductivity of cement paste pore solutions from OH-, K+ and Na+ concentrations.* Cement and Concrete Research, 2003. **33**(6): p. 793-798.
117. Rajabipour, F. and J. Weiss, *Electrical conductivity of drying cement paste.* Materials and Structures, 2007. **40**(10): p. 1143-1160.
118. Lagarkov, A.N. and A.K. Sarychev, *Electromagnetic properties of composites containing elongated conducting inclusions.* Physical Review B, 1996. **53**(10): p. 6318.

APPENDIX

Appendix A: Mathematica program used for the simulations and sample run

APEENDIX A

Simulations program

Circuit parameters

```
Vo = 1;
Vt = Vo ;
```

CIRCUIT SIZE

Number of Rows (kr) <MUST BE ODD> and Columns (kc) <EVEN or ODD>. The values of kr and kc control the number of elements and circuits (loops) the overall circuit will have including fictitious boundary loops.
kc is controlled by kr. This produces a square circuit i.e. equal number of branches in the x and y directions.
MINMUM value for kr is 7. Change of kr by (-2) removes ONE row of loop and change of kr by (2) adds ONE row of loops.

```
kr = 81;
kc = (kr + 1) / 2;
```

Actual loop, branch and element count

```
Nloops = ((kr - 1) / 2 - 2) * (kc - 3);
NBranch = (Nloops * 2 + (kc - 3)) + (kr - 1) / 2 - 2;
Nelm = NBranch * 4;
```

Creating matrices to set the currents in the fictitious circuits equal to zero. Additionally, the impedances on the input and output circuits are set to zero using the matrices below to create conductors

```
Izero = Append[
   Flatten[{Prepend[Flatten[{Table[j / j i / i , {i, 1, (kr - 1) / 2 - 2}, {j, 1, (kc - 1)}]}, 1],
      Table[0 * j, {j, 1, kc - 1}]]}, 1], Table[0 * j, {j, 1, kc - 1}]];
Iz = Izero * Transpose[Izero];
Iz0 = Table[0 i j , {i, 1, (kr - 1) / 2}, {j, 1, (kc - 1)}];
IzeroIs =
  Append[Flatten[{Prepend[Flatten[{Table[0 * i * j , {i, 1, (kr - 1) / 2 - 2}, {j, 1, (kc - 1)}]}, 1],
      Table[Is * i / i, {j, 1, kc - 1}]]}, 1], Table[0 * i, {j, 1, kc - 1}]];
IzIs = Transpose[IzeroIs];
Rzero =
  Append[Append[Append[Prepend[Prepend[Prepend[Table[j / j i / i , {i, 1, kr - 6}, {j, 1, kc}],
       Table[0 * j, {j, 1, kc}]], Table[0 * j, {j, 1, kc}]], Table[0 * j, {j, 1, kc}]],
     Table[0 * j, {j, 1, kc}]], Table[0 * j, {j, 1, kc}]], Table[0 * j, {j, 1, kc}]];
```

Random values to be used in calculating C, Rc, Rs and Rp for water and cement paste according to the settings given in material properties

Cement

```
σc = .2;
μc = .5;
Pkc = 1;
Pdfc = PDF[NormalDistribution[μc, σc], RandomReal[{mc, Mc}, {kc * kr}]];
RNc = Partition[Pdfc, kc] / Pkc;
RNci[i_, j_] := Extract[RNc, {i, j}]
Table[{RNci[i, j]}, {i, 1, kr}, {j, 1, kc}];
LRNC = Length[Flatten[RNc]];
ListPlot[Table[{i, Extract[Flatten[RNc], i]}, {i, 0, LRNC}]]
CRI = Table[i / i * j / j * RandomInteger[], {i, 1, kr}, {j, 1, kc}];
CRI1 = Table[i / i * j / j * Random[], {i, 1, kr}, {j, 1, kc}];
ListPlot[Table[{i, Extract[Flatten[CRI], i] + 1}, {i, 0, LRNC}]];
```

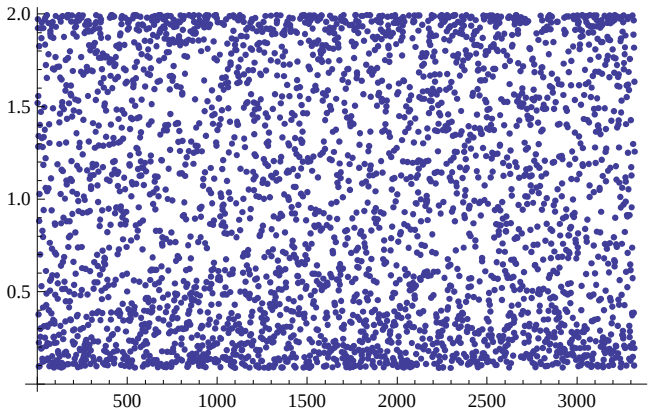


```
Max[Flatten[Pdfc]]
Min[Flatten[Pdfc]]
Max[Flatten[CRI1]]
Min[Flatten[CRI1]]
```

```
1.99471
```

```
0.087708
```

```
0.999955
```

```
0.000562226
```

```
RNcT = RNc
```

```
CRIT = CRI
```

Water

```
σw = .2;
μw = .5;
Pkw = 1;
Pdfw = PDF[NormalDistribution[μw, σw], RandomReal[{mw, Mw}, {kc * kr}]];
RNw = Partition[Pdfw, kc] / Pkw;
wmax = Max[Flatten[Pdfw]];
wmin = Min[Flatten[Pdfw]];
RNwi[i_, j_] := Extract[RNw, {i, j}]
ListPlot[Table[{i, Extract[Flatten[RNw], i]}, {i, 0, LRNC}]]
RNSP = Table[j / j i / i RandomReal[], {i, 1, kr}, {j, 1, kc}];
RNSPi[i_, j_] := Extract[RNSP, {i, j}];
WRI = Table[i / i * j / j * RandomInteger[], {i, 1, kr}, {j, 1, kc}];
ListPlot[Table[{i, Extract[Flatten[WRI], i] + 1}, {i, 0, LRNC}]]
```

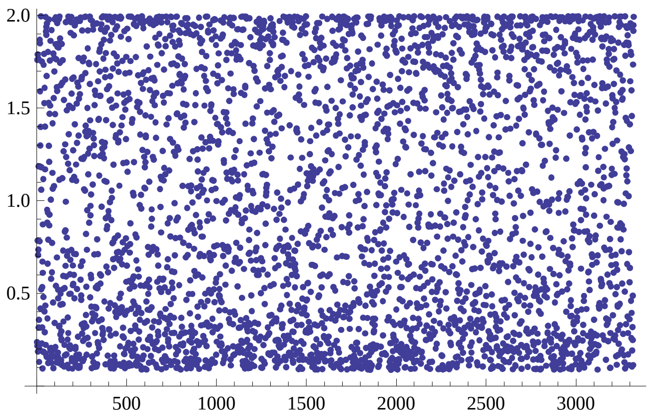


```
RNwT = RNw

RNSPT = RNSP

WRIT = WRI
```

** **

Execute section of program below this line to keep same randomness for cement and water.
Frequency and ration of water/cement/air can be changed

** **

Main Section of program Control parameters
Loop increases water or changes frequency

```
Nn = 10;
Clear[ResF, n, f, RwX, CwX]
Clear[ResF, n, f]
ResF = {};
Nns = 0.05;
Rcc = 1;
Do[
 f = 10 000 000; "Frequency";
 m = 2.3;
 xPc = 10^5; "Cement Parallel resistance Multiplier";
 Xc  = 16.5 / 10^13; "capacitor Multiplier";
 xPcs = 200; "Cement Cap Series resistance Multiplier";
 SR = 0.4;
```

```
SC = 0.5;
x = 0.9;
SR1 = 1 - 0 n/Nn;
Zcem = Table[If[Extract[CRI, {i, j}] < .55,
   -i / (2 * π * f * RNci[i, j] * Xc), -i / (2 * π * f * RNci[i, j] * Xc)], {i, 1, kr}, {j, 1, kc}];
Rinf = 10^40;
xw = 3500; "Water Parallel resistance Multiplier";
Xw = 38 / 10^13; "Water capacitance Multiplier";
RwX = 1 - (SR n/Nn);
CwX = 1 + SC n/Nn;
SR2 = 1 - 0 n/Nn;
Zw = Table[
  If[Extract[CRI1, {i, j}] < x * n/Nn, RNwi[i, j] * RwX * xw (-i * CwX / (2 * π * f * RNwi[i, j] * Xw))/(RNwi[i, j] * RwX * xw - i * CwX / (2 * π * f * RNwi[i, j] * Xw)),
   -i * CwX * RNwi[i, j] / (2 * π * f * Xw)], {i, 1, kr}, {j, 1, kc}];
Zcemw = Table[SR2 * xPcs + (Extract[Zcem, {i, j}] * Extract[Zw, {i, j}])/(Extract[Zcem, {i, j}] + Extract[Zw, {i, j}]),
   {i, 1, kr}, {j, 1, kc}] * Rzero;
Zz[i_, j_] := Extract[Zcemw, {i, j}];
TZz = Zcemw;
Ilop = Table[(i / i) (j / j) Ib_{i,j}, {i, 1, (kr - 1) / 2}, {j, 1, (kc - 1)}] * Iz + IzIs;
Iunk =
 Flatten[Append[Table[(i / i) (j / j) Ib_{i,j}, {i, 2, (kr - 1) / 2 - 1}, {j, 2, (kc - 1) - 1}], Is]];
Ibr[i_, j_] := Extract[Ilop, {i, j}];
FIunk = Flatten[Iunk];
Leqn[i_, j_] :=
 Zz[2 i - 1, j] * (Ibr[i, j] - Ibr[i - 1, j]) + Zz[2 i, j + 1] * (Ibr[i, j] - Ibr[i, j + 1]) +
  Zz[2 i + 1, j] * (Ibr[i, j] - Ibr[i + 1, j]) + Zz[2 i, j] * (Ibr[i, j] - Ibr[i, j - 1]);
Ls := Vt - Rcc Is + Plus @@ Table[Zz[i, 2] * (Ibr[i, 2] - Is), {i, 2, (kr - 1) / 2 - 1}];
{Append[Flatten[Table[Leqn[i, j] == 0, {i, 2, (kr - 1) / 2 - 1}, {j, 2, kc - 2}]], Ls == 0], Iunk};
SolI = Flatten[Solve[Append[
    Flatten[Table[Leqn[i, j] == 0, {i, 2, (kr - 1) / 2 - 1}, {j, 2, kc - 2}]], Ls == 0], Iunk]];
II = Iunk /. SolI;
ZL = Vt / Take[II, -1];
ZLmag = √(Re[ZL]^2 + Im[ZL]^2);
Θ = ArcTan[Im[ZL] / Re[ZL]] * 180 / π;
CcL = -1. / (Im[ZL] 2. π f);
Rr = -2. * (Im[ZL]);
ReZ = Re[ZL];
ImZ = Im[ZL];
Res = {{n}, {f}, {ZLmag}, ReZ, ImZ, Θ, CcL};
AppendTo[ResF, Res];
If[n == Nn, Print["END"]], {n, 1, Nn, Nns}]
ResF;
```

END

```
LResF = Length[Flatten[ResF]] - 70;
DLResF = LResF / 7;
BLResF = LResF / (DLResF);
Nyplt =
  Table[{Extract[Flatten[ResF], i + 1], Extract[Flatten[ResF], i]}, {i, 4, LResF, BLResF}];
Zplt = Table[{Extract[Flatten[ResF], i - 2], Extract[Flatten[ResF], i]},
   {i, 3, LResF, BLResF}];
Θplt = Table[{Extract[Flatten[ResF], i - 5], Extract[Flatten[ResF], i]},
   {i, 6, LResF, BLResF}];
Cplt = Table[{Extract[Flatten[ResF], i - 6], Extract[Flatten[ResF], i]},
   {i, 7, LResF, BLResF}];
Replt = Table[{Extract[Flatten[ResF], i - 3], Extract[Flatten[ResF], i]},
   {i, 4, LResF, BLResF}];
Implt = Table[{Extract[Flatten[ResF], i - 4], Extract[Flatten[ResF], i]},
   {i, 5, LResF, BLResF}];
ImReplt = Table[{Extract[Flatten[ResF], i - 4], Extract[Flatten[ResF], i]},
   {i, 5, LResF, BLResF}];
L1a = ListPlot[Zplt, PlotStyle → {Green, PointSize[Large]},
  PlotRange → Full, AxesLabel → {"H2O", "Zmag [Ω]"}]
L1b = ListPlot[Θplt, PlotStyle → {Green, PointSize[Large]},
  PlotRange → Full, AxesLabel → {"H2O", "Phase [deg]"}]
L1c = ListPlot[Cplt, PlotStyle → {Green, PointSize[Large]},
  PlotRange → Full, AxesLabel → {"H2O", "C [F]"}]
L1d = ListPlot[Replt, PlotStyle → {Green, PointSize[Large]},
  PlotRange → Full, AxesLabel → {"H2O", "ReZ [Ω]"}]
L1e = ListPlot[Implt, PlotStyle → {Red, PointSize[Large]},
  PlotRange → Full, AxesLabel → {"H2O", "ImZ [Ω]"}]
L1f = ListPlot[Nyplt, PlotStyle → {Red, PointSize[Large]},
  PlotRange → Full, AxesLabel → {"Re[Z]", "Im[Z]"}]
```

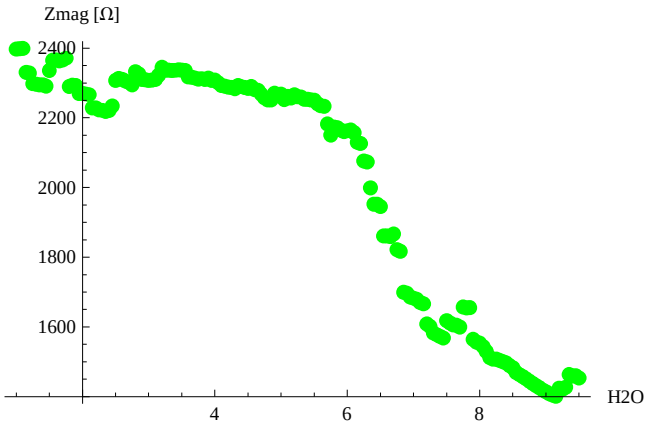

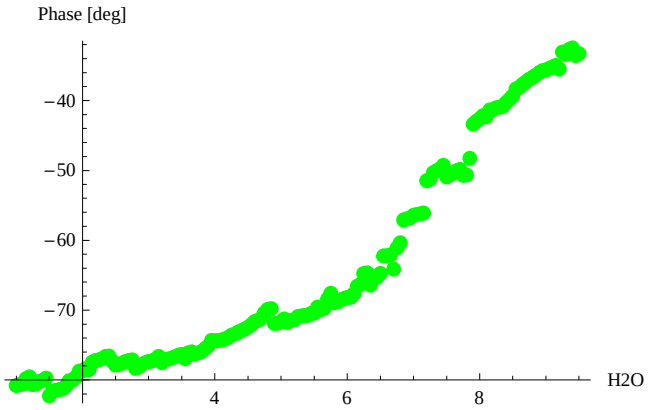
Phase [deg]
−40
−50
−60
−70
4
6
8
H2O

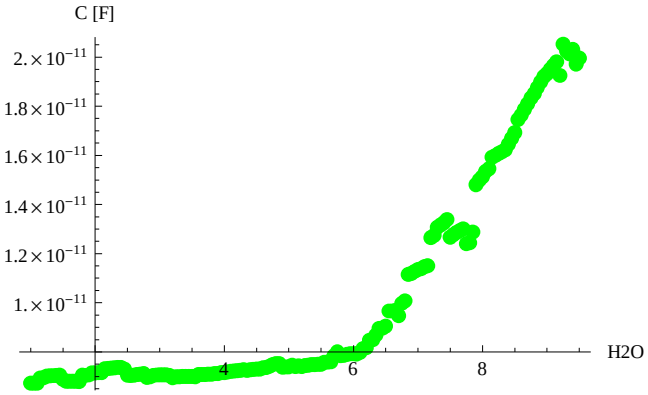
C [F]
2.×10^−11
1.8×10^−11
1.6×10^−11
1.4×10^−11
1.2×10^−11
1.×10^−11
4
6
8
H2O

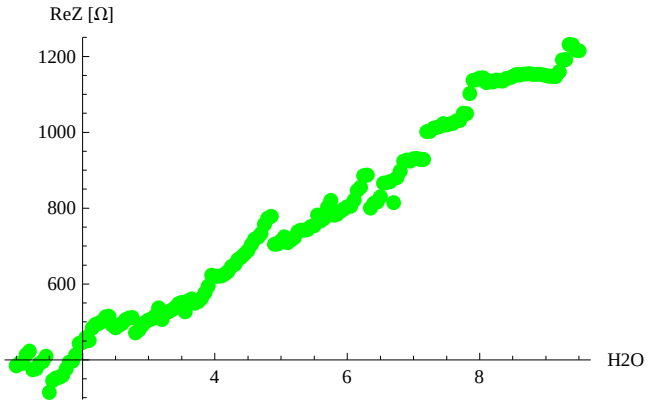
ReZ [Ω]
1200
1000
800
600
4
6
8
H2O

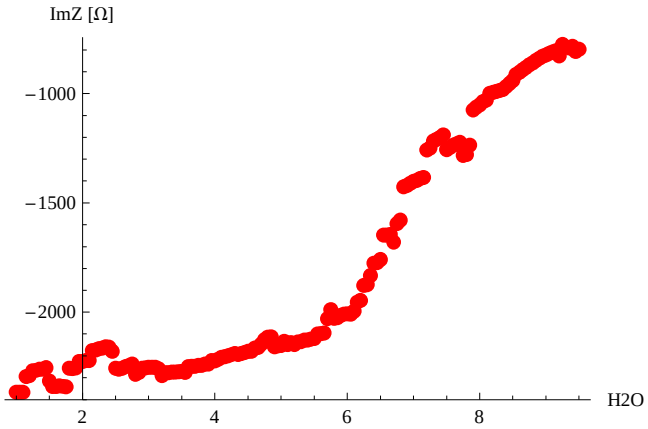

"POSTPROCESSING; Results for Current (IL), Impedance (ZL), Phase Angle (θ), Capacitance (CcL) and Resistance (RL) for the lumped circuit.";

```
{kr, kc, Nloops, Nelm, NBranch}
```

```
{81, 41, 1444, 11856, 2964}
```

Changing the format of the results (current values) to match the locations in the circuit. This adds the Zero valued currents of the fictitious circuits to the results and also creates a list of values of the current in the source loop for all the adjacent loops

```
Iv0 = Prepend[Transpose[Partition[Drop[II, -1], kc - 3]],
   Flatten[Table[j / j Take[II, -1], {j, 1, kc - 3}], 1]];
Iv1 = Append[Prepend[Transpose[Partition[Drop[II, -1], kc - 3]],
    Flatten[Table[j / j Take[II, -1], {j, 1, kc - 3}], 1]], Table[0 j, {j, 1, kc - 3}]];
Iv1o = Append[Riffle[Flatten[Iv1], 0], 0];
Transpose[Iv1];
Iv2 = Flatten[Transpose[Partition[Iv1o, 2 √Nloops]]];
IVV = Prepend[
   Prepend[Append[Append[Prepend[Partition[Append[Riffle[Flatten[Iv2], 0], 0], 2 kc - 2],
       Table[0 j, {j, 1, 2 (kc - 1)}]], Table[0 j, {j, 1, 2 (kc - 1)}]], Table[0 j,
      {j, 1, 2 (kc - 1)}]], Table[0 j, {j, 1, 2 (kc - 1)}]], Table[0 j, {j, 1, 2 (kc - 1)}]];
IZi[i_, j_] := Extract[IVV, {i, j}];
IbZi[i_, j_] := IZi[i - 1, j] - IZi[i + 1, j] + IZi[i, j - 1] - IZi[i, j + 1];
IZ = Table[IbZi[i, j], {i, 3, kr - 2}, {j, 2, kr - 2}];
MatrixForm[IZ];
MatrixForm[Partition[Drop[Drop[Flatten[IZ], kr - 3], -(kr - 3)], kr - 3]];
SolI;
MatrixForm[IZ];
IZm = Table[Abs[IbZi[i, j]], {i, 3, kr - 2}, {j, 2, kr - 2}];
FIZm = Flatten[Drop[Drop[Flatten[IZm], kr - 3], -(kr - 3)]];
IZmax = Max[FIZm];
pc = .3;
FIZmlength = Length[FIZm];
PerIZm1 = ArrayPlot[Partition[
   Table[If[Extract[FIZm, i] ≥ pc * IZmax, Extract[FIZm, i], 0], {i, 1, FIZmlength}], kr - 3]]
PerIZm2 = ArrayPlot[Partition[Table[If[Extract[FIZm, i] ≥ (pc + .1) * IZmax,
     Extract[FIZm, i], 0], {i, 1, FIZmlength}], kr - 3]]
PerIZm2 = ArrayPlot[Partition[Table[If[Extract[FIZm, i] ≥ (pc + .2) * IZmax,
     Extract[FIZm, i], 0], {i, 1, FIZmlength}], kr - 3]]
PerIZm2 = ArrayPlot[Partition[Table[If[Extract[FIZm, i] ≥ (pc + .3) * IZmax,
     Extract[FIZm, i], 0], {i, 1, FIZmlength}], kr - 3]]
PerIZm2 = ArrayPlot[Partition[Table[If[Extract[FIZm, i] ≥ (pc + .44) * IZmax,
     Extract[FIZm, i], 0], {i, 1, FIZmlength}], kr - 3]]
ArrayPlot[Partition[Drop[Drop[Flatten[IZ], kr - 3], -(kr - 3)], kr - 3]]
ArrayPlot[TZz]
```

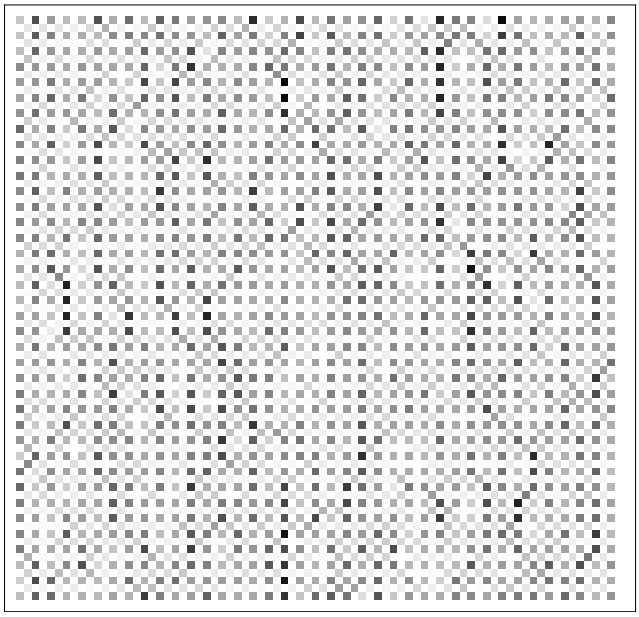

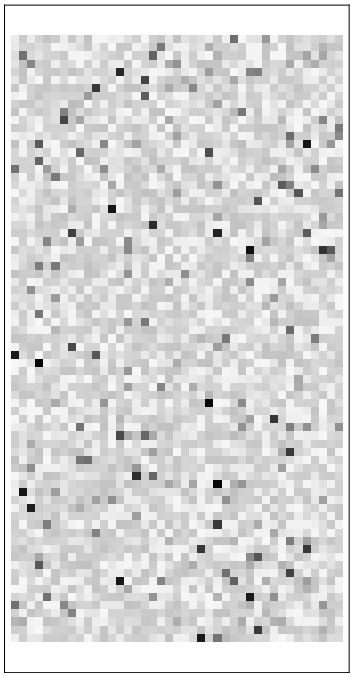

```
Dny = Table[{Extract[Flatten[ResF], i + 1], Extract[Flatten[ResF], i]}, {i, 4, LResF, BLResF}];
{f, moisture data, RCR24a 10 b}
Dx = Table[Extract[Flatten[ResF], i], {i, 1, LResF, BLResF}]
Impedance
DZ = Table[Extract[Flatten[ResF], i], {i, 3, LResF, BLResF}]
Phase
Dθ = Table[Extract[Flatten[ResF], i], {i, 6, LResF, BLResF}]
Capacitance
DC = NumberForm[Table[Extract[Flatten[ResF], i], {i, 7, LResF, BLResF}],
  NumberFormat → (Row[{#1, "e", #3}] &)]
ReImpedance
DRe = Table[Extract[Flatten[ResF], i], {i, 4, LResF, BLResF}]
ImImpedance
DIm = Table[Extract[Flatten[ResF], i], {i, 5, LResF, BLResF}]
```